https://doi.org/10.35662/unine-thesis-2824

A bi-phasic model of chloroplast biogenesis during de-etiolation in *Arabidopsis thaliana*

A dissertation submitted to the University of Neuchâtel.

For the degree of Doctor of Philosophy in Biological Sciences

Presented by

Rosa Pipitone

Plant Physiology Laboratory, Institute of Biology

University of Neuchâtel

Thesis committee

Prof. Felix Kessler (Thesis Director) – University of Neuchâtel

Dr. Emilie Demarsy (Thesis Director)– University of Geneva

Prof. Samuel C. Zeeman – ETH Zurich

Prof. Josephus Vermeer – University of Neuchâtel

April 2020

UNIVERSITÉ DE NEUCHÂTEL

Faculté des Sciences
Secrétariat-décanat de Faculté
Rue Emile-Argand 11
2000 Neuchâtel – Suisse
Tél : + 41 (0)32 718 21 00
E-mail : secretariat.sciences@unine.ch

IMPRIMATUR POUR THESE DE DOCTORAT

La Faculté des sciences de l'Université de Neuchâtel autorise l'impression de la présente thèse soutenue par

Madame Rosa PIPITONE

Titre:

"A bi-phasic model of chloroplast biogenesis during de-etiolation of *Arabidopsis thaliana*"

sur le rapport des membres du jury composé comme suit:

- Prof. Felix Kessler, directeur de thèse, Université de Neuchâtel, Suisse
- Dr Emilie Demarsy, co-directrice de thèse, Université de Genève
- Prof. Joop Vermeer, UniNE
- Prof. Sam Zeeman, ETH Zürich

Neuchâtel, le 4 juin 2020

Le Doyen, Prof. P. Felber

Keywords: Thylakoid, prolamellar body, chloroplast, etioplast, photosynthesis, de-etiolation, chloroplast division, model, plant photosystems, galactolipids, pigments, serial block face scanning electron microscopy, 3D reconstruction.

Contents

Abstract

The structure and the function of the chloroplast is unique in nature. It is the organelle in which photosynthesis and life-sustaining carbon fixation takes place. The photosynthetic light reactions occur at the internal membrane system of the chloroplast called thylakoids. A specific class of lipids (galactolipids) constitutes the majority of thylakoid membrane where photosynthetic proteins and pigments (chlorophyll and carotenoids) are assembled into photosystems. Seedlings grown in the dark develop a yellow phenotype typical of the chlorophyll deficiency, and contain the precursor of the chloroplast called etioplast. Light exposure triggers etioplast to chloroplast transition (chloroplast biogenesis) and hence the onset of photosynthesis. The chloroplast biogenesis coincides with the formation of the thylakoid membrane. Thylakoid formation is a complex process which consists of the gradual and concerted accumulation of lipids and proteins that organize into a well-defined structure within a matter of less than 100 hours. The mechanisms of thylakoid formation remain largely unknown and represent a key question in how a plant develops into a photosynthetic organism.

In my thesis, I studied thylakoid formation over a time course of chloroplast biogenesis in the *Arabidopsis thaliana* model system. Three-dimensional (3D) reconstruction of chloroplasts at specific time points was carried using serial block face-scanning electron microscopy technology (SBF-SEM). Quantitative data of chloroplast number, volume as well as envelope and thylakoid membrane surface were collected in parallel with biochemical data regarding protein and lipid components of the thylakoid membrane. Specifically, a proteomics analyses at specific time points of de-etiolation identified more than 5000 proteins of which 1112 were plastid proteins. These data combined with quantitative immunoblots, provided information on the temporal regulation of photosynthesis-associated proteins while the lipidomics analysis of the 12 major galactolipids revealed a differential regulation of the pro- and eukaryotic galactolipid biosynthetic pathways. The combination of (ultra)structural and biochemical data revealed two distinct phases of chloroplast biogenesis i.e. “Structure Establishment Phase” during which photosynthetic activity was first established followed by the “Chloroplast Proliferation Phase” which occurred in concomitance with

cell expansion. Finally, I developed a mathematical model describing the gradual expansion of the thylakoid surface during chloroplast biogenesis.

Resumé

La structure et la fonction du chloroplaste sont uniques en nature. Le chloroplaste est l'organelle dans lequel s'effectuent la photosynthèse et la fixation du carbone qui soutient la vie. Les réactions photosynthétiques dépendantes de la lumière se produisent au niveau du système interne membranaire du chloroplaste appelé thylakoïdes. Une classe spécifique de lipides (galactolipides) constitue la majorité de la membrane thylacoïdienne où des protéines et les pigments (chlorophylle et caroténoïdes) sont assemblés en photosystèmes.

Les plantules cultivées à l'obscurité développent un phénotype jaune typique de la carence en chlorophylle et contiennent le précurseur du chloroplaste appelé etioplaste. L'exposition à la lumière déclenche la transition d'étioplaste en chloroplaste (biogénèse du chloroplaste) et donc l'apparition de la photosynthèse. La biogénèse du chloroplaste coïncide avec la formation de la membrane thylacoïdienne. La formation de thylakoïdes est un processus complexe qui consiste en l'accumulation progressive et concertée de lipides et de protéines qui s'organisent dans une structure bien définie en moins de 100 heures. Les mécanismes de la formation de thylakoïdes restent largement inconnus et représentent une question clé dans la façon dont une plante se développe en organisme photosynthétique. Dans ma thèse, j'ai étudié la formation de thylakoïdes sur une période de temps de la biogénèse du chloroplaste dans le système modèle *Arabidopsis thaliana*. La reconstruction tridimensionnelle (3D) des chloroplastes à des moments précis a été réalisée à l'aide de la technologie de microscopie électronique « serial block face –scanning electron microscopy (SBF-SEM) ». Des données quantitatives sur le nombre de chloroplastes, leur volume ainsi que la surface de l'enveloppe et de la membrane thylakoïdienne ont été collectées en parallèle avec des données biochimiques concernant les composants protéiques et lipidiques de la membrane thylacoïdienne. Plus précisément, une analyse protéomique à des moments précis pendant la de-etiolation a permis d'identifier plus de 5000 protéines, dont 1112 étaient des protéines plastidiales. Ces données, combinées avec l'analyse quantitative par immunodétection, ont fourni des informations sur la régulation temporelle des protéines associées à la photosynthèse, tandis que l'analyse lipidomique des 12 principaux galactolipides a révélé une régulation différentielle des galactolipides selon leur voie de biosynthèse (voies dites

procaryotique et eucaryotique). La combinaison de données (ultra)structurales et biochimiques a révélé deux phases distinctes de la biogénèse du chloroplaste c'est-à-dire la « phase d'établissement de la structure », pendant laquelle la photosynthèse devient opérationnelle, suivie par la « phase de prolifération des chloroplastes » qui se produit en même temps que l'expansion cellulaire. Enfin, j'ai développé un modèle mathématique décrivant l'expansion de la surface thylacoïdienne pendant la dé-étiolation.

Abbreviations

ABC	activity of BC1 complex
ACP	acyl carrier protein
ARC	accumulation and replication of chloroplasts protein
ATP	adenosine triphosphate
CDP	cytidine-diphosphate
Chl *a/b*	chlorophyll a/b
CO_2	carbon dioxide
Cyt	cytochrome
Cyt b_6f	cytochrome b6 f
CZ	central zone
DAG	diaylglycerol
DEX	dexamethasone
DGDG	digalactosyldiacylglycerol
EM	electron microscopy
ER	endoplasmic retuculum
ET	electron tomography
FA	free fatty acid
FAB	fatty acid binding
FAD	fatty acid desaturase
FNR	ferredoxin-NADP(+) reductase
FtsZ	filamentous temperature sensitive
Fv/.Fm,	maximum quantum yield
G3-P	glycerol-3-Phosphate
GLs	galactolipids
GO	gene ontology
HAI	hours after imbibition
LHC(P)	light harvesting complex (protein)
LPOR	light-dependent NADPH:protochlorophyllide oxidoreductase
MGDG	monogalactosyldiacylglycerol
Min	minicell proteins
N	avogadro constant

NADP(H)	nicotinamide adenine dinucleotide phosphate
NPQ	non- photochemical quenching
PA	phosphatidic acid
PAP	plastid lipid associated protein
PC	phosphatidylcholine
PDV	plastid division
PE	phosphatidylethanolamine
PG	phosphatidylglycerol
PGP	phosphatidylgycerolphosphate
PGs	plastoglobules
PI	phosphatidylinositol
PLB	prolamellar body
PORA	protochlorophyllide oxidoreductase
PSI	photosystem I
PSII	photosystem II
PZ	peripheral zone
qP	photochemical quenching
S	thylakoid surface
SAM	shoot apical meristem
SBF-SEM	serial blockface-scanning electron microscopy
Sec	secretory pathway
SQDG	sulfoquinovosyldiacylglycerol
SrpRP	signal recognition particle
TAGs	triacylglycerols
Tat	twin-arginine translocase
TEM	transmission electron microscopy
TIC	translocon at the inner membrane complex of the chloroplast
TOC	translocon at the outer membrane complex of the chloroplast
UDP	uridine diphosphate
WT	wild type
ΦPSII	photosystem II quantum yield

Aim of the project

The aim of this PhD thesis is to provide an integrated description of the structural and molecular events taking place during chloroplast biogenesis in *Arabidopsis thaliana* cotyledons.

I will analyze the process in dark-grown, etiolated seedlings that will be exposed to light. During this so-called de-etiolation the chloroplast precursor organelle, the etioplast, is transformed into a photosynthetically active chloroplast. The characteristic prolamellar body (PLB) and tubular prothylakoids (PT) of the etioplast are replaced by the thylakoid membranes of the chloroplast that contain the newly assembled photosynthetic complexes. The extensive thylakoid membranes are formed of 80% monogalactosyldiacyglycerol (MGDG) and digalactosyldiacylglycerol (DGDG) galactolipids which are mostly synthesized during de-etiolation. A number of studies have provided information regarding isolated events during thylakoid formation in different organisms such as runner bean (Kowalevska et al., 2016), tobacco (Armarego-Mariotti et al., 2019), pea (Rudowska et a., 2012) and Arabidopsis (Fujii et a., 2019, Liang et al., 2019 and Dubreuil et al., 2018). These important studies highlight various molecular and metabolic events of thylakoid formation as well as thylakoid architecture. However, a study integrating quantitative data for these processes in one and the same organism has not been carried out so far.

Therefore, my thesis aims at a systems level study that combines quantitative information at the ultrastructural level with quantitative data of lipid and protein composition during thylakoid formation in *Arabidopsis thaliana* cotyledons.

I will pursue the following objectives:

- Analysis of photosynthetic parameters in order to determine the precise temporal onset of photosynthetic activity during the de-etiolation.
- Imaging by Serial block face – scanning electron microscopy (SBF-SEM) of de-etiolating cotyledons to generate 3D reconstuctions of chloroplasts and cells allowing to determine surface and volume of thylakoids, choroplast envelopes as well as chloroplasts and whole cells.
- Lipidomic and proteomic analyses to quantify lipid and protein compositions along the de-etiolation timeline.

- Develop a model based on quantitiatve data that describes thylakoid formation during de-etiolation.

Chapter 1 – General introduction

1.1 The evolution of plastids

1.1.1 Overview of plastid type

Plastids are cellular organelles found in algae and land plants. According to the endosymbiotic theory, plastids originate from a free-living cyanobacterium that was taken up by a eukaryotic host cell (Terry and Smith, 2013). During evolution, most bacterial genes have been transferred to the host nuclear genome. Even though plastids have a small genome which contains around 120-130 genes in higher plants, most proteins are encoded by the nuclear genome, synthesized in the cytoplasm as preproteins. At the envelope membrane, preproteins are recognized by the translocons at the outer (TOC complex) and inner envelope membrane of the chloroplast (TIC complex) which facilitate the import of preproteins into plastids. (Agne and Kessler, 2010; Jensen and Leister, 2014; Richardson et al., 2017). The organellar precursor of all plastid types is the proplastid. It can differentiate into different types of specialized, tissue specific plastids under the influence of environmental and developmental conditions. In non-photosynthetic tissues proplastids may differentiate into leucoplasts which function as lipid or starch storage organelles (Lopez-Juez and Pyke, 2005). In the absence of light, proplastids differentiate into etioplasts in photosynthetic tissues. The etioplast represents a chlorophyll-deficient plastid, which transforms into a chloroplast in the presence of light. Alternatively, the proplastid can develop directly into a chloroplast in light conditions. The chloroplast is the best-characterized plastid type present in green tissues including cotyledons, leaves, stems, fruits and flowers (Pogson and Albrecht, 2011).

1.1.2 General description of chloroplast function in photosynthesis

Chloroplasts are specialized in energy production by photosynthesis. Photosynthesis is the process transforming light energy into chemical energy that is used for carbon fixation (Lopez-Juez and Pyke, 2005). The absoprtion of light triggers electron transport through the photosystems, leading to the reduction of nicotinamide adenine

dinucleotide phosphate (NAPD) to the reduced form NADPH. Electron transport also creates a proton gradient which is used by the ATP synthase for the synthesis of adenosine triphosphate (ATP).

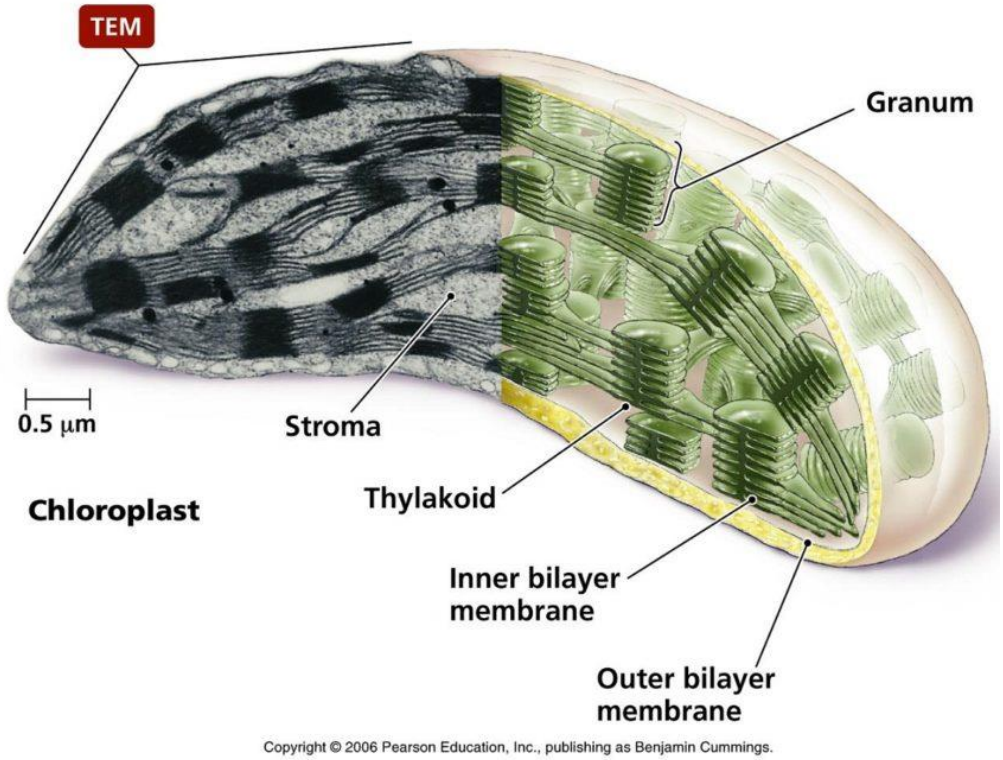

Figure 1: TEM image of chloroplast ultrastructure and schematic representation of chloroplast membranes. Stroma, grana (granum), inner and outer envelope membranes are shown. Copyright 2006 Pearson Education. Inc, publishing as Benjamin Cummings.

The inner and outer envelope membranes delimit the chloroplast while the photosynthetic light reactions take place at a third, internal membrane system called thylakoids. They are constituted of grana stacks connected by unstacked lamellae (Figure 1). The lipids that constitute the thylakoid membrane are: the galactolipids (GLs) mono - and digalactosyldiacylglycerol (MGDG and DGDG), sulfoquinovosydiacylglycerol (SQDG) and phosphatidylglycerol (PG) (Marechal et al., 1997). In addition, the thylakoid membrane contains chlorophyll *a (*Chl *a)* and *b (*Chl *b*), prenylipids such as prenylquinones (plastoquinone, phylloquinone and tocopherols) (Fritsche et al., 2017; Spicher and Kessler, 2015) and carotenoids (such

as β-carotene and lutein) (Gruszecki and Strzałka, 2005). The thylakoid membrane is the lipid matrix into which photosynthetic complexes are assembled. Photosystem II (PSII), cytochrome b_6f (cyt b_6f) and photosystem I (PSI) are the major electron carrying complexes constituted of core and more peripheral subunits. The light harvesting proteins (LHCII and LHCI) are associated with PSII and PSI. In addition, lipid droplet-like structures called plastoglobules (PGs) are attached to thylakoid membrane (Austin et al. 2006). PGs are constituted of a polar lipid monolayer which surrounds the PG core constituted of neutral lipids such as prenylquinones, carotenoids, fatty acids and triacylglycerols (TAG) (Gaude et al., 2007; Rottet et al., 2015). The most abundant plastoglobule proteins are plastid lipid associated (PAP/fibrillins), atypical activity of BC1 complex (ABC) kinases as well as enzymes implicated in structural and metabolic functions (Grennan, 2008; Kessler et al., 1999; Lundquist et al., 2012).

The thylakoid architecture emerges during chloroplast differentiation. Chloroplast transitions are accompanied by changes at the ultrastructural level and massive synthesis of photosynthetic proteins and lipids. Understanding how the thylakoid membrane is assembled is of fundamental importance and one of the remaining frontiers in chloroplast research. One long-term perspective will be the optimization of photosynthesis in crop species based on the knowledge of molecular factors regulating thylakoid biogenesis.

1.2 Chloroplast biogenesis and development

1.2.1 The proplastid-chloroplast transition

The transition from proplastid to chloroplast can take place in embryonic cells of seed cotyledons or in the in shoot apical meristem (SAM) of the vegetative shoot apex. The proplastid is an organelle which can contains either few or no thylakoid structures at all. Upon illumination, thylakoid biogenesis starts with the formation of several lamellae followed by the formation of grana bodies reviewed in Adam et al., 2011. Specifically, the proplastid – chloroplast transition has been studied in germinating Arabidopsis cotyledons (Liang et al., 2018).

A linear chloroplast biogenesis process comprising five developmental stages has been studied in germinating seeds under continuous light. Tubular and vesicular prothylakoids appeared in the proplastid 24 hours after imbibition (HAI). During the following 12 hours polysomes accumulated and then the conversion of pro-thylakoids into pre-granal thylakoids occurred (36 HAI). Grana stacks appeared concomitantly with the formation of the PSII-LHCII complexes (during which pre-granal stacks were converted in pro-granal stacks (60 HAI). The connections between grana and stroma thylakoids appeared later (84 HAI). Subunits of PSI complex were detected later than those of PSII, at 84 HAI. Finally, at the last time point (120 HAI) differentiated grana stacks were present (Liang et al., 2018).

Non-homogeneous proplastid differentiation was observed in the SAM (Charuvi et al., 2012). The SAM is constituted of stem cells of the central zone (CZ) and peripheral zone (PZ). Three different layers constitute the SAM tissue: L1, L2 and L3. L1 and L2 differentiate into epidermis and outer mesophyll respectively. Specifically, most of the photosynthetic tissue is constituted of palisade and spongy cells generated from the L2 layer. L3 constitutes the inner structure of the SAM and contributes to the formation of the inner mesophyll as well as the vascular system (Tilney-Bassett, 1986). Unexpectedly, it has been observed that in the CZ of the SAM, L1 and L3 stem cells contain proplastids that already have a thylakoid network whereas L2 stem cells (precursors of spongy and palisade cells) contain proplastids without thylakoid networks (Charuvi et al., 2012). In contrast, only plastids at the PZ in the L2 layer have thylakoid networks. A recent study on proplastid to chloroplast transition in meristematic tissue identified two phases, which controlled the establishment of photosynthesis during chloroplast development (Dubreuil et al., 2018).

1.2.2 The etioplast – chloroplast transition

Under natural growth conditions, seed germination can occur under ground leading to the development of etiolated seedlings characterized by a long hypocotyl and yellow, hook-shaped cotyledons. The etioplast is located in the embryonic cells of cotyledons where it can differentiate into a chloroplast upon illumination. Etioplasts lack thylakoids but have a system of semi-crystalline membranes called prolamellar body (PLB). PLBs

consist of tubules organized in a hexagonal structure (Solymosi and Aronsson, 2013; Williams et al., 1998) that contain protochlorophyllide (precursor of chlorophyll), photochlorophyllide reductase A (PORA) (a key enzyme required for the conversion of protochlorophyllide to chlorophyll), NADPH (the electron donor in this reaction) and galactolipids (MGDG and DGDG). Specifically, the protochlorophyillide resulting from enzymatic steps of the tetrapyrrole pathway (Brzezowski et al., 2015) forms a ternary complex with NADPH and PORA (Griffiths, 1978). However MGDG and DGDG are also required for the formation of ternary complex (Fujii et al., 2018, 2017). In the PLB fraction of wheat grains, 64 proteins were identified. The major proteins were light-dependent NADPH:protochlorophyllide oxidoreductase (LPOR) proteins. Subunits of PSII and cyt b_6f as well as proteins involved in the Calvin Cycle were also detected (Blomqvist et al., 2008). Proteomic analyses have been carried out during the de-etiolation process in rice which allowed the detection of soluble and insoluble proteins (Kleffmann et al; 2007; Reiland et al. 2011). A system to study the de-etiolation process and the maturation of the photosynthetic process have been done in tobacco leaves (*Nicotiana tabacum*). Specifically the time course of de-etiolation (from 0 to 6720 minutes of light exposure) showed that the content of PSI was unchanged in the first 240 minutes of light exposure followed by a change in abundance between 240 and 480 minutes of light exposure while the content of cyt b_6f increased after 480 minutes of light exposure. In contrast, the LHCII-PSII supercomplex started to increase earlier between 60 to 120 minutes (Armarego-Marriott et al., 2019).
However, the greening process of true leaves may differ from cotyledons. Although the different studies revealed factors (Li et al., 2015; Liang et al., 2018; Philippar et al., 2007) involved in the regulation of cotyledon greening in *Arabidopsis thaliana*, a complete proteome analysis during the greening process (as has been done for de-etiolation) has not been carried out.

In angiosperm seedlings grown in the dark, the photoreduction of protochlorophyllide to the chlorophyllide occurs upon illumination followed by the esterification step, by which chlorophyllide is converted to the chlorophyll (Schoefs and Bertrand, 2000). Simultaneously, PLBs start to disassemble, the different PLB components are rearranged into long parallel-aligned lamellae and grana structures with newly synthesized compounds (Adam et al., 2011). 3-dimensional (3D) organization of

chloroplast biogenesis has been studied in runner bean. Specifically, 3D images of paracrystalline and thylakoid structures have been acquired during the etioplast to chloroplast transition (Kowalewska et al., 2016). In dark conditions (8 day–old etiolated leaves) the PLB showed a tetrahedral structure which became irregular after just 1 hour of light exposure. Upon 8 hours of illumination stacked structures (as pre-grana) were observed first while differentiated small grana were observed on the second day of light exposure (Kowalewska et al., 2016).

Etioplast to chloroplast transition is also correlated with important variations of lipid organization. The hexagonal pattern of the prolamellar structure body is dependent on hexagonal (HII) lipid organization. During the transition dark-light, the dynamic conversion of etioplasts into chloroplasts could be operated, at least partly, via an HII-to-lamellar ($L_{\alpha)}$ lipid-phase transition (Demé et al., 2014). MGDG molecules tend to form HII structures by contrast DGDG molecules form Lα structures (Demé et al., 2014; Lee, 2000).

The reason why during the transition from dark to light, the architecture of membrane changes, could be associated with the interaction between MGDG and LHC-II (Simidjiev et al., 2000).The transmembrane alpha helices of LHC-II is presumably able to force the MGDG in order to adopt the bilayer structure. The appressed membrane structure of the grana stacks in the thylakoid membrane depends on the interaction between the LHC-II molecules, which will bring the surfaces of the appressed membrane close together followed by the interaction between MGDG headgroups. The interaction between LHC-II molecules and MGDG is crucial for the formation of appressed structures. Grana stacks are not formed when LHC-II molecules were mixed with DGDG or PG lipids (Lee, 2000).

1.2.3 Import and transport of proteins into thylakoid membrane

The thylakoid membrane is a dynamic system, which requires proteins and lipids. As mentioned previously the preproteins synthetized in the cytosol or chloroplast stroma are imported into plastids through the TOC-TIC system. Specifically, the transit peptide of the preproteins is recognized by two GTPase receptors (Toc 159 and Toc 33) at the outer envelope membrane. The import of the preprotein occurs through the Toc75

channel. To complete the translocation into plastids, the preprotein translocate through the TIC machinery constituted of: Tic40, Tic110, Tic20,Tic100 and Tic56 (Richardson et al., 2017; Richardson and Schnell, 2019). The transport of proteins into or across the thylakoid membrane is facilitated by three distinct pathways: Twin-arginine translocase (Tat), secretory (Sec) and signal recognition particle (SRP) pathways. Tat and Sec pathways are used for the transport of luminal proteins across the thylakoid membrane. Tat, Sec and SRP substrates have an additional signal peptide, which is removed after the translocation into thylakoid. The Tat pathway requires the proton gradient to provide energy for translocation while the Sec pathway requires ATP as an energy source. The SRP pathway allows the insertion of nuclear encoded proteins into the thylakoid membrane (Aldridge et al., 2009). The light harvesting complex proteins (LHCP) are known to be imported by this pathway (Klimmek et al., 2006). Substrates of the SRP pathway have a bipartite signal peptide (Viitanen et al., 1988) and require the interaction with specific proteins such as cpSRP components in order to achieve insertion into the thylakoid membrane (Aldridge et al., 2009).

1.2.4 Invagination and vesicular pathways involved on chloroplast biogenesis process

Although the import and transport of proteins into the thylakoid system have been quite well studied, one of the most important remaining questions regarding the formation of thylakoid membrane, concerns the mechanism by which lipids dynamically assemble to the form the thylakoid membrane during chloroplast biogenesis.

Two distinct pathways have been suggested:

Invagination of the inner envelope membrane: *i.e.* thylakoid membranes formed by extension and rearrangement of the chloroplast inner envelope membrane. Invaginations of the inner envelope membrane have been observed in chloroplasts of the *mgd1-2* mutant (Kobayashi et al., 2007). Whether these invaginations represent a step in the formation of thylakoid membranes or whether these structures result as a secondary effect of the *mgd1-2* mutation is not clear.

Vesicular pathway*: i.e.* vesicles budding from the inner envelope membrane and transporting lipids to the developing thylakoids.

Protrusions emanating from the inner envelope membrane to the thylakoid membrane suggested the possible formation of contact sites between the two compartments during the proplastid – chloroplast transition in SAM plastids. These connections might serve as conduit for the transfer of lipids from envelope to thylakoids (Charuvi et al., 2012). In the same study, vesicular bodies in the stroma near the inner envelope membrane were also observed in Arabidopsis SAM, providing evidence for vesicular transfer of lipids in thylakoid membrane formation. Finally, clusters of inclusions similar to plastoglobules were also observed which may be involved in lipid and metabolic processes. (Charuvi et al., 2012). The *vipp1* mutant lacks vesicles that were observed in wild type chloroplasts. Considering that *vipp1* is not able to establish photosynthesis, the vesicular structures were proposed to be involved in lipid transfer leading to the formation of the photosynthetic membrane (Kroll et al., 2001). During de-etiolation in runner bean, direct transformation of tubular PLB into lamellar structures without the formation of vesicles was reported (Kowalewska et al., 2016). Additional observations were made in Chlamydomonas (Engel et al., 2015) and *Pisum sativum* (Andersson et al. 2001). In Chlamydomonas algae, the direct connections between envelope and thylakoid membrane were rare, but 34% of envelope invaginations were found close (less than 40 nm) from the thylakoid tip, suggesting that invaginations had a role in the transfer of lipids between envelope and thylakoids (Engel et al., 2015). Synthesis and transport of galactolipids in *Pisum sativum* were studied *in vitro* by incubating intact chloroplasts with the radiolabeled lipid precursor (UDP- D-[6-^{3}H]Gal). After 20 minutes of incubation, in intact chloroplasts of still-expanding leaves (7-d-old plants), 45% and 34% of newly synthetized MGDG and DGDG respectively, were detected in thylakoid fractions. This study supported the hypothesis that galactolipid transport from envelope to thylakoids could depend partly on vesicles (Andersson et al., 2001). In an additional scenario, plastoglobules may function as a reservoir that supports lipid production for the thylakoid membrane by releasing galactolipids and/or diacylglycerol (DAG) and TAG precursors (Lichtenthaler 1968; Rottet, et al., 2015). Considering their potential role in the formation of the thylakoid membrane, number and size of plastoglobules may vary during chloroplast biogenesis, becoming small and few during thylakoid biogenesis, and then more abundant in mature chloroplasts (Lichtenthaler, 1968). This change was observed

during de-etiolation, PGs were abundant in the etioplast organelle and decreased in number during the formation of thylakoid membrane (Van Wijk and Kessler, 2017). In contrast to vesicles, plastoglobules were observed attached to thylakoid membranes exclusively, and not associated with the inner envelope membrane or localized to the chloroplast stroma as free lipoprotein particles (Austin et al., 2006).

1.3 Thylakoid architecture

1.3.1 Grana and stroma lamellae structures

Structural features of the thylakoid membrane are stacked grana interconnected by unstacked stroma lamellae (Andersson and Anderson, 1980; Arvidsson and Sundby, 1999) and reviewed by (Adam et al., 2011; Nevo et al., 2012; Pribil et al., 2014).

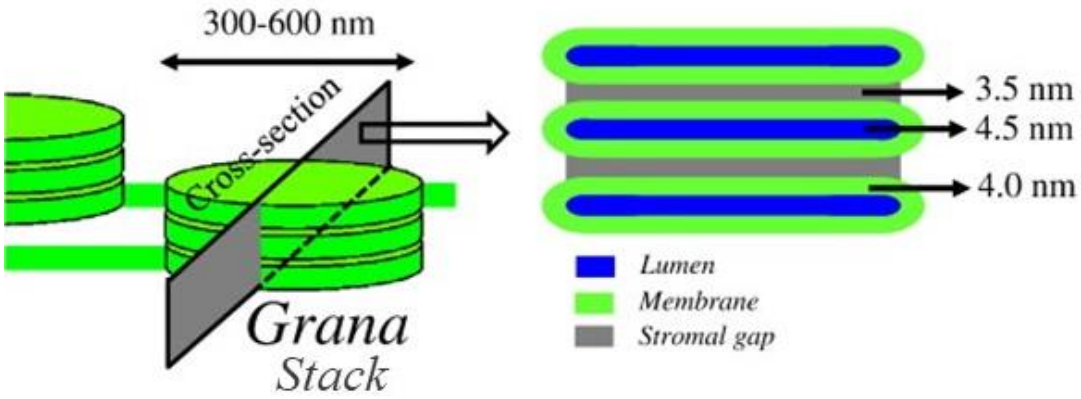

Figure 2: Schematic 3D representation of grana and their cross section. Lumen, membrane and stromal gap are shown in blue, green and grey, respectively. Figure adapted from (Kirchhoff, 2014).

As shown in figure 2, grana stacks are constituted by separate discs. Every disc is surrounded by a membrane bilayer which contains the luminal space (lumen). Discs are separated by a space called stromal gap. One single disc continues in length constituting the stroma lamellae structure. The thylakoid organization of grana and lamellae entails a specific distribution of the photosynthetic components in the thylakoid membrane (more details in the paragraph 1.4 ”Photosynthetic associated

proteins in thylakoid membrane") which allows to optimize light harvesting and energy transfer during photosynthesis (Mustardy and Garab, 2003). Electron tomographic analysis allowed to obtain quantitative information on grana structure (Daum et al., 2010; Kirchhoff et al., 2011). The lumen space has a height of 4.5 nm (Daum et al., 2010; Kirchhoff et al., 2011) which can increase up to 8.8 nm (Kirchhoff et al., 2011). While the stroma gap has a height of around 3.2 nm (Daum et al., 2010; Kirchhoff et al., 2017) which may increase up to 4.2 nm in dark conditions (Kirchhoff et al., 2017). The geometry of grana structure is correlated with the spatial organization of the photosynthetic machinery and dynamic protein diffusion (more details in the 1.4 paragraph "Photosynthetic associated proteins in thylakoid membrane").

1.3.2 Models describing thylakoid membrane organization

Three models have been proposed and discussed to describe the structures of as well as the connections between grana and stroma lamellae (Arvidsson and Sundby, 1999; Kowalewska et al., 2016; Mustardy and Garab, 2003; Mustárdy et al., 2008; Paolillo, 1970; Shimoni et al., 2005).

The first model proposed by Paolillo et al., 1970 was called the helical model. The helical model consisted of stroma lamellae surrounding the grana stack as a right-handed helix. The model is supported by other studies (Austin and Staehelin, 2011; Daum et al., 2010; Daum and Kühlbrandt, 2011; Mustárdy et al., 2008). Specifically the helical model was described as a structure which lamellae helicales surrounded the grana stack with an a specific inclination between 10 and 25 degree (Mustárdy et al., 2008). In the etioplast to chloroplast transition in runner bean they showed also helical connections between grana and stroma lamellae (Kowalewska et al., 2016). The second one, the fork model proposed by (Arvidsson and Sundby, 1999) showed that stroma lamellae bifurcated to form grana discs. Every bifurcation forms a grana structure of three layers. In a third model, the granum layers were not connected to each other by the stroma lamellae but every paired grana structure bends toward and fuses with neighbouring grana layers (Shimoni et al.,2005).

1.4 Photosynthetic associated proteins in the thylakoid membrane

Photosynthesis was described previously as the photochemical reactions in which light energy is used to convert carbon dioxide (CO_2) to produce organic compounds. The organization of photosynthetic complexes is crucial for the proper functionality of the photosynthetic machinery. PSII is only located in the appressed grana while PSI is present in the end membranes and stroma lamellae. Cyt b_6f is located in grana stacks, grana margins and in stroma lamellae while the ATP synthase is located in grana margins and stroma lamellae (Albertsson, 2001; Daum et al., 2010) as shown in the Figure 3.

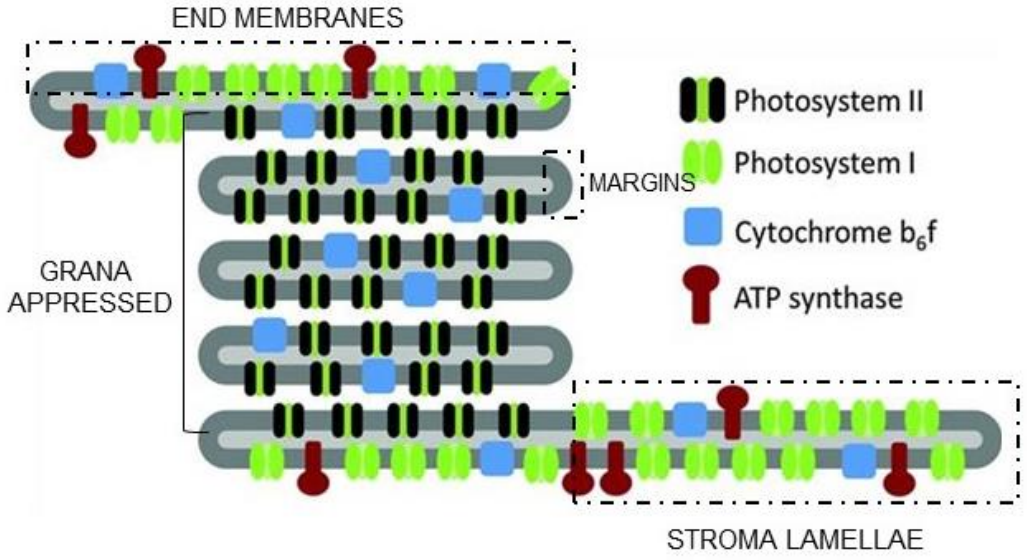

Figure 3: Differential distribution of photosynthetic complexes in the thylakoid membrane. Photosystem II is located in the appressed membranes of the grana stack. Cyt b_6f is distributed in appressed membranes of grana stack, in the end membranes and in the stroma lamellae. ATP synthase and PSI are located in the end membranes and in stroma lamellae, respectively. Figure adapted from (Rasmussen and Minteer, 2014).

The excitation of LHCII-PSII II by photons triggers electron transport through cyt b_6f to PSI finally leading to the reduction of NADP to NADPH. Intermediary molecules are also involved on the electron transport: the small molecule plastoquinone (between PSII and cyt b_6f) and the plastocyanin protein (between cytb_6f and PSI). Electron

transport is coupled to the formation of a proton gradient used by the ATP synthase to produce ATP. In this introduction, I will briefly describe the three major photosynthetic complexes (PSII, cytb_6f and PSI) as well as the light harvesting proteins associated with the photosystems.

1.4.1 Photosystem II (PSII)

Photosystem II is a large complex consisting of a core and peripheral proteins. The core is constituted of around 25-30 subunits with a surface dimension of 26 x 19 nm (Caffarri et al., 2014). Specifically, PsbA (D1), PsbB (CP47), PsbC (CP43) and PsbD (D2) subunits form the reaction center. Other small subunits (PsbE, PsbF, PsnH, PsbI-M, PsbTc, PsbX, PsbY and PsbZ) constitute the intrinsic subunits of the reaction centre. In the luminal side of the PSII, the OEC center involved on the water oxidation is made up of three subunits (PsbO, PsbP and PsbQ). OEC composition varies between species but PsbO that stabilizes the manganese ion is always present. PSII forms dimers (C_2) that form super complexes with antenna proteins also known as light harvesting complex (Lhc). The LHCII trimer is constituted of Lhcb1, Lhcb2 and Lhcb3 molecules. Minor antenna (Lhcb4-6) allow the interaction between PSII and LHCII trimer (Caffarri et al., 2014; Van Bezouwen et al., 2017). By crystallography and advanced microscopy technologies (such as cryo-electron microscopy) combined with 3D reconstruction technology, the PSII – LHCII complexes have been widely studied (Barera et al., 2012; Gao et al., 2018; Nield and Barber, 2006; Pagliano et al., 2014; Su et al., 2017; Van Bezouwen et al., 2017; Wei et al., 2016). Specifically, the $C_2S_2M_2$ supercomplex consists of two LHCII trimers bound strongly (S_2) to the PSII dimeric core (C_2) and other two LHCII trimers bounds moderately (M_2) to the C_2 complex. Other studies allowed to obtain quantitative information on the grana structure in relation to the PSII. As mentioned above the grana lumen may have a minimal thickness of 4.5nm (Daum et al. 2010; Kirchhoff et al. 2011), which corresponds to the height of the OEC complex accommodated by the grana lumen, while the stromal gap (thickness of 3.2 nm) accommodates the N-terminal LHCII peptide portions exposed on the stroma (Daum et al., 2010).

1.4.2 Cytochrome b_6f (Cyt b_6f)

Cytochrome b_6f is the intermediary complex involved in the electronic connection between PSII and PSI complexes. Cyt b_6f has a dimeric structure. Each monomer consists of 8 subunits. Specifically, there are four large subunits (cytochrome f (PetA), cytochrome b6 (PetB), the Rieske protein (PetC) and subunit IV(PetD)) and four small subunits (PetG, PetL, PetM and PetN). Each monomer carries four hememolecules, one [2Fe-2s] cluster, one chlorophyll a, one β-carotene and one plastoquinone (Kurisu et al., 2003). The crystal structure of cytb_6f has been studied in the cyanobacterium (*Mastigocladus laminosus*) and had a surface dimension of 9 x 5.5 nm (stromal side) and 12 x 7.5nm (lumen side) (Kurisu et al., 2003). The geometrical features of the thylakoid membrane strongly impact the regulation of the photosynthetic machinery (Kirchhoff et al., 2011). In fact, the variation of the stromal gap thickness during dark (4.2 +/- 1.3 nm) to light transition (3.2 +/- 0.7nm) was associated with a different localization of the cyt b_6f (Kirchhoff et al., 2017).

1.4.3 Photosystem I (PSI)

The structure of photosystem I was studied in the thermophilic cyanobacterium Synechococcus and also in plants (Jordan et al., 2001; Mazor et al., 2015). Photosystem I is constituted by the core subunits (PsaA and PsaB) surrounded by peripheral subunits (PsaF, PsaI, PsaJ, PsaK, PsaL, PsaM and PsaX). In addition, three subunits are situated on the stroma side: PsaC, PsaD and PsaE. The C-terminal of PsaC interacts with PsaA/B/D, and this is important for the correct assembly of PsaC into PSI (Jordan et al., 2001). PSI in green plants has the same structural features but contains four additional subunits (PsaG, PsaH, PsaO and PsaN instead of PsaM and PsaX (Dekker and Boekema, 2005). PSI has an oval shape (a surface dimension of around 15x20nm) discounting the association of the antenna proteins (Caffarri et al., 2014). In contrast to PSII, only four antenna proteins (LHCI) (corresponding to four Lhca proteins (Lhca 1-4)) are associated to the PSI core complex (Caffarri et al., 2014; Dekker and Boekema, 2005).

1.5 Lipids of the thylakoid membrane

The thylakoid membrane consists of a lipid bilayer formed in large part by neutral and anionic glycoglycerolipids (Kobayashi et al., 2015). Interactions between thylakoid lipids and photosynthetic complexes have been observed suggesting that these lipids are required not only as building blocks for the photosynthetic membrane but also for the photosynthetic reactions themselves (Kobayashi et al., 2007).

1.5.1 Glycerolipids

The major lipid components of the thylakoid membrane are MGDG and DGDG galactolipids (neutral lipids) constituting around 50% and 20%, respectively, of total glycerolipids making up the thylakoid membrane (Dormann, 2001). At the chemical structural level galactolipids are constituted by a glycerol backbone linking two fatty acid chains at the sn-1 and 2 positions while at the sn-3 position MGDG and DGDG carry one and two units of galactose respectively (Boudière et al., 2014). Different species of MGDG and DGDG are known according to the saturation degree of the fatty acid chains at the sn-1 and -2 positions. Saturated palmitic (16:0) and stearic (18:0) acids have no double bonds. Unsaturated α-linolenic (18:3), linoleic acid (18:2) and hexadecatrienoic acid (16:3) have 2 or more double bonds. Representative species of MGDG, DGDG, SQDG and PG are shown in figure 4.

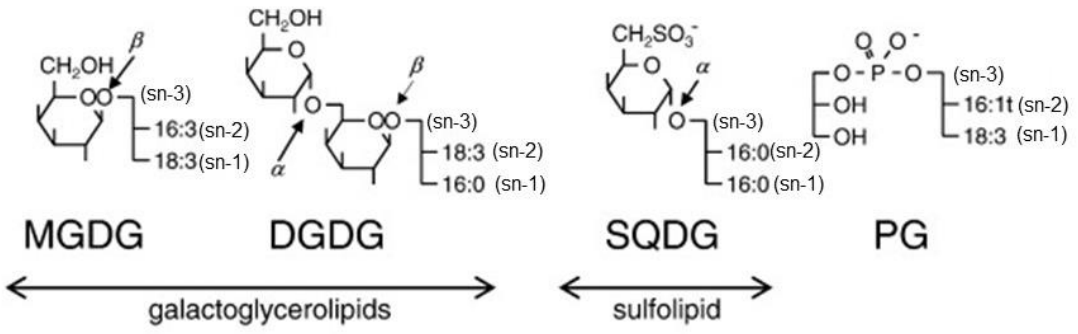

Figure 4: Representative structures of thylakoid glycerolipids. Mono-galactosyldiacyl glycerol (MGDG), di-galactosyldiacyl glycerol (DGDG), sulfoquinovosyldiacyl glycerol (SQDG) and phosphatidylglycerol (PG) molecules carry fatty acid chains at the sn-1 and sn-2 position of the glycerol molecule. In the sn-3 position one or two units of galactose are incorporated in MGDG and DGDG molecules, respectively. In contrast, SQDG and PG carry sulfoquinovose or a phosphoglycerol group, respectively, at the sn-3 position. Figure adapted from (Boudière et al., 2014).

Membrane fluidity is a function of fatty acid saturation degree: unsaturated galactolipids confer increased fluidity to the membrane when compared to more saturated galactolipids (Zheng et al., 2011). MGDG and DGDG can be synthetized by three (MGD) and two (DGD) enzymes, respectively. Mutations affecting the expression of MGD and DGD perturb the lipid composition of the thylakoid membrane causing alterations of the thylakoid ultrastructure (Dörmann et al., 1995; Kobayashi et al., 2007). This aspect will be explained in more detail in the “MGD and DGD synthases” (paragraph 1.6.2).

In addition to the before mentioned membrane components, thylakoid membranes contain other important lipids in minor percentages such as anionic lipids. Phosphatidylglycerol (PG) contains a negatively-charged polar head group (Figure 4). PG is present in all photosynthetic organisms (from cyanobacteria to higher plants). In *Arabidopsis thaliana* PG is essential for chloroplast structure (Wada and Murata, 2007). The PGP1 (phosphatidylglycerolphosphate synthase) enzyme is involved in the phosphatidylglycerol biosynthesis in Arabidopsis plastids catalyzing the synthesis of PGP (phosphatidylglycerol-phosphate) from CPD-DAG (cytidine-diphosphate

diacylglycerol) (Xu et al., 2006). PGP1 knock out mutants did not grow in the absence of sucrose and chloroplast development was affected (Hagio et al., 2002). SQDG is the only glycerolipid containing a sulfonate group conferring an anionic polar head group. SQD2 catalyzes SQDG synthesis. Under standard growth conditions, thylakoid structure in the *sqd2* mutants is not affected. SQDG is not normally a major lipid component but it can be present from about 2 to 20% in thylakoid membranes depending on the conditions (Boudière et al., 2014; Shimojima, 2011). In P_i-deprived conditions SQDG was necessary when phosphate became limiting. This may be the reason why plants maintained the sulfolipid synthetic pathway during the evolution (Yu et al., 2002). Other phosphoglycerolipids have been detected in thylakoid membranes. The *Chlamydomonas reinhardtii* thylakoid membrane contains phosphatidylinositol (PI) (2.7% of total lipid content). Phosphatidylcholine (PC) detected in *Spinacia oleracea* corresponded to the 4.5% of the total lipid mass (Boudière et al., 2014). However, treatment of intact chloroplasts with non-specific phospholipase C (an enzyme that cleaves the polar head of phospholipids), suggested that PC was not specifically associated with the thylakoid membrane but rather the result of a contamination (Andersson, et al., 2001).

MGDG/DGDG/PG/SQDG glycerolipids thus are the major components of photosynthetic membranes. Thylakoid lipids directly associate with the complexes involved in photosynthetic electron transfer. Studies of the crystal structure of photosynthetic complexes showed that three molecules of PG and one MGDG were associated with the PSI complex (Jordan et al., 2001) while six MGDG, four DGDG, three SQDG and one PG surrounded PSII (Loll et al., 2005). In addition, MGDG plays a role in the activation of the violaxanthin de-epoxidase enzyme. In high light conditions, the violaxanthin de-epoxidase is required in non-photochemical quenching by the “xanthophyll cycle” (conversion of the carotenoid violaxanthin into antheraxanthin followed by the conversion into zeaxanthin). This enzyme is localized in thylakoid membranes and is fully active *in vitro* in the presence of non-bilayer forming lipids such as MGDG (Dormann et al., 2001).

1.5.2 Prenyl lipids

The thylakoid membrane contains lipid-soluble molecules that play a direct role in photosynthetic activity and/or have an antioxidant function. Some are associated to protein-pigment complexes of the photosynthetic apparatus whereas others exist as free molecules in the thylakoid membranes. Around 30 carotenoid molecules are associated to the PSII and PSI complexes (Caffarri et al., 2014). Carotenoids - such as β-carotene, lutein, neoxanthin and xanthophylls protect plants against photodamage. Specific carotenoids such as β-carotene and lycopene are involved in the neutralization of singlet oxygen by energy transfer (Tsen et al., 2007). Upon excessive illumination, specific xanthophylls are involved in the de-excitation of singlet Chl (^{1}Chl) that accumulates in the light-harvesting complexes. This de-excitation is measured as nonphotochemical quenching of Chl fluorescence (NPQ) (Niyogi et al., 1997). Specifically, prenyl quinones (tocopherol or vitamin E, phylloquinone and plastoquinone) can prevent lipid peroxidation in thylakoid membranes (Spicher and Kessler, 2015). VTE1 (tocopherol cyclase) is the enzyme that catalyzes the penultimate step of tocopherol synthesis. Mutants deficient in VTE1 (*vte1*) are totally devoid of tocopherol and instead accumulate the pathway intermediate DMPBQ which presumably also has antioxidant capacity (Eugeni et al. 2011; 2014). VTE1 has been localized to PG and the metabolism and storage of tocopherol in part takes place in the PG (Vidi et al., 2006). In addition, segments of the phylloquinone and plastoquinone metabolic pathways have also been attributed to PG (Eugeni et al., 2011)

1.6 Synthesis and trafficking of thylakoid lipids

1.6.1 Galactolipid synthesis

Most of the plastid fatty acids are used to produce glycerolipids for plant cell membranes. In figure 5, a model of the fatty acid and glycerolipid synthesis pathways is shown.

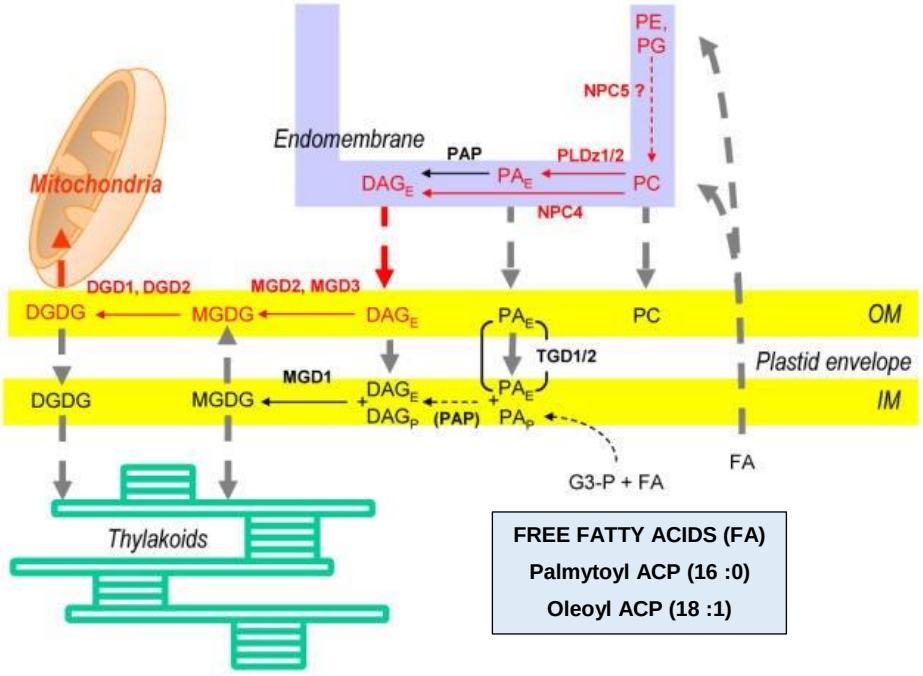

Figure 5: Schematic representation of fatty acid and galactolipid synthesis. Synthesis of fatty acids starts with the synthesis of palmitoyl-acyl carrier protein (ACP) (16:0) and oleoyl-ACP (18:1) in the plastid. They are used to synthetize phosphatidic acid (PA_E and PA_P) in the plastid and in the endomembrane system. In the both compartments the de-phosphorylation of PA leads to the formation of diacyglycerols (DAG_E and DAG_P). The DAGs are the substrate of MGD (MGD1, MGD2 and MGD3) and DGD (DGD1 and DGD2) enzymes in the synthesis of MGDG and subsequently DGDG galactolipids. Most of MGDG and DGDG are used for the formation of the thylakoid membrane. In specific growth conditions, DGDG can be also transported to and used in mitochondria. Figure adapted from (Jouhet et al; 2007).

In the plastid stroma the synthesis of fatty acids including palmitoyl-ACP(16:0) and oleoyl-ACP (18:1) takes place specifically. They can move to the inner envelope membrane and be used in the acylation of sn-glycerol-3-phosphate (G3-P) in the first

reactions of glycerolipid biosynthesis. The final product is phosphatidic acid (PA) which can be dephosphorylated to give the DAG (DAG_P). In plastids, DAG_P serves as precursor for the synthesis of galactolipids (MGDG and DGDG) (Marechal et al., 1997; Ohlrogge and Browse, 1995). The free fatty acids synthesized in the plastid can be also transported to the endoplasmic reticulum and used to synthesize DAG (DAG_E,) and (PA_E) as well as phosphatidylcholine (PC).

MGDG and DGDG synthesis involves complex pathways. Different enzymes and two different precursors are involved. MGDG biosynthesis can be catalyzed by three different MGDG synthases (MGD1 to -3), which transfer a D-Gal unit from UDP-Gal to the sn-3 position of the DAG precursor (Awai et al., 2001). DGDG can be synthetized by two different DGDG synthases that catalyze the galactosylation of MGDG (Kobayashi et al., 2004) (Figure 5).

In *Arabidopsis thaliana* two different biosynthetic pathways for galactolipids have been characterized: the eukaryotic and prokaryotic pathways (Ohlrogge and Browse, 1995). The naming of the two pathways is correlated with the DAG provenance. The DAG synthesized in the endoplasmic reticulum ("eukaryotic") and transported into the chloroplast carries an 18 C fatty acid at the sn-2 position of the glycerol backbone and becomes the precursor for all eukaryotic MGDG and DGDG. In contrast DAG synthesized inside the plastid ("prokaryotic due to the endosymbiotic origin of plastids) carries a 16 C fatty acid at the sn-2 position of the backbone and is used to synthetize prokaryotic MGDG and DGDG (Marechal et al., 1997; Ohlrogge and Browse, 1995). Two classes of MGD synthases are known according to the length of the N-terminal portion of the corresponding preproteins. Class A comprises MGD1 enzymes that have an extension of around 100 aa at the N-terminal peptide. Class B comprises the MGD2 and MGD3 enzymes with and extension of around 40 aa at the N terminus and no predicted chloroplast targeting sequence (Awai et al., 2001; Miège et al., 1999).
As shown in the Figure 5, MGD1 is located at the inner envelope membrane while MGD2 and MGD3 enzymes are at the outer envelope membrane (Awai et al., 2001). DGDG galactolipids can be synthetized by DGD-1 located in the outer and inner envelope membrane and DGD-2 in the outer envelope membrane (Klaus et al., 2002).

At the inner envelope membrane, the DAG synthesized inside the plastids is used as the precursor for 18: n/16: n MGDG in a reaction catalyzed by MGD-1. This prokaryotic MGDG may directly serve as a constituent of the thylakoid membrane or as a precursor for DGDG at the outer as well as the inner envelope membrane. In contrast, the DAG synthetized at the endoplasmic reticulum is used to produce eukaryotic 18:n/18:n MGDG at the outer (catalyzed by MGD2 and MGD3) and inner envelope membranes (catalyzed by MGD-1) which will also become the precursor for DGDG. Eukaryotic DGDG can be exported from the chloroplast or become (just like prokaryotic DGDG) a constituent of the thylakoid membrane.

1.6.2 MGD and DGD synthases

MGD-1 synthase is the most important enzyme responsible for formation of the thylakoid membranes. Two independent MGD-1 mutants have been isolated: *mgd1-1* (Jarvis et al., 2000) and *mgd1-2* (Kobayashi et al., 2007). The *mgd1-1* mutant is a knock down mutant generated by insertion of T-DNA at the -148 position (Jarvis et al., 2000). It showed a reduced mRNA level (around 75%), a chlorotic phenotype and less developed chloroplasts when compared to the wild type. At the biochemical level, in MGDG the 16:3 fatty acid at the sn-2 position (*i.e* galactolipid derived from prokaryotic pathway) decreased in the *mgd1-1* mutant compared to the wild-type while the 18:3 fatty acids (*i.e* galactolipid derived from eukaryotic pathway) content increased in the *mgd1-1* mutant (Jarvis et al., 2000). The *mgd1-2* was embryo lethal and grew only when supplemented with sucrose (Kobayashi et al., 2007). This mutant showed an overall decrease of all thylakoid membrane lipid species including MGDG, DGDG, SQDG and PG. Studies regarding the expression patterns of these enzymes allowed also to understand their importance in the formation of the thylakoid membrane. During plant development, MGD-1 was detected in cotyledons as well as rosette leaves, while MGD-3 was present only in cotyledons (3-day-old). In contrast MGD-2 was never detected in cotyledons or rosette leaves (Kobayashi et al., 2004). Besides the importance of the MGD1, it is not clear whether MGD-3 could play a role in the formation of the thylakoid membrane in the early stages of plant development in the background of MGD2 (although the severe *mgd1-2* phenotype does not appear to be compensated by the activity of MGD-3) (Kobayashi et al., 2007). Class B MGDs are

dispensable for the galactolipid biosynthesis because no strong difference in galactolipid accumulation was observed in *mgd2* and *mgd3* mutants when compared to the wild-type under standard conditions. However, under P_i deprived conditions the B-enzymes are involved in the substitution of phosphatidylcholine (PC) and phosphatidylethanolamine (PE) in the shoots and in particular in root tissues with DGDG (Kobayashi, et al., 2009).

Similar investigations have also been carried out for DGD enzymes. The DGD-1 enzyme was found to be important for photosynthetic membranes (Dörmann et al., 1995). The *dgd-1* mutant had reduced DGDG content together with reduced photosynthetic activity and chlorophyll content. At the ultrastructural level it showed a higher chloroplast volume compared to the wild-type because the lamellae were not distributed homogeneously inside the organelle but were displaced towards the envelope membrane leaving a large space of stroma in the center of the chloroplast (Dörmann et al., 1995). The *dgd1-dgd2* double mutant had only traces of DGDG indicating that the DGD-2 enzyme is also involved in DGDG synthesis (Steffen et al., 2005).

Studies of MGDG and DGDG galactolipids have been carried out during the etioplast to chloroplast transition in order to understand their function during chloroplast biogenesis from dark-grown seedlings. The activity of MGD-1 was repressed using a dexamethasone (DEX)-inducible artificial microRNA targeting MGD1 while the *dgd-1* mutant background (Dörmann et al., 1995) was used to eliminate DGD1 activity. (Fujii et al., 2014). Changes in the fatty acid composition where observed when comparing two pairs: 1) seedlings plus and minus dexamethasone treatment (- DEX , + DEX), and 2) wild type (WT) versus *dgd-1* mutant. In the presence of DEX, the 16:3 and 18:3 fatty acids decreased in MGDG while the 16:0 and 18:0 fatty acids increased during 6 to 12 hours of illumination. Globally, the total amount of MGDG was less than in the - DEX seedlings. Between – DEX and + DEX, the fatty acid composition changed also in DGDG galactolipids. The 18:3 fatty acid decreased while the 16:0 fatty acid increased in + DEX seedlings. The comparison between WT and *dgd-1* mutant showed that in the MGDG species of the mutant the proportions of 16:3 fatty acid decreased and 18:3 fatty acid increased when compared to the WT. In DGDG species

of the *dgd-1* mutant, the proportions of 18:3, 18:1 and 16:1 fatty acids were increased and 16:0, 18:2 fatty acids were decreased, with 24 hours of illumination when compared to the WT. The different fatty acid compositions observed in the controls (- DEX and WT) compared to + DEX seedlings and the *dgd1* mutant suggested a possible involvement of the alternative pathways such as those comprising MGD2 , MGD3 and DGD2 and/or a different rate of activity of some fatty acid desaturases (FAD5 and 6) (Fujii et al., 2019).

1.7 Division process in photosynthetic tissues

1.7.1 General description of chloroplast division

Chloroplast division occurs by binary fission (a single chloroplast dividing into two daughter chloroplasts followed by regeneration). Although the signals and the mechanisms of chloroplast division have not been entirely clarified, several proteins involved in plastid division and the formation of the division machinery have been identified and studied in the last 25 years. (Okazaki et al., 2009; Osteryoung and Nunnari, 2003; Yoshida et al., 2012). Filamentous temperature sensitive proteins (FtsZ) (called FtsZ-1, FtsZ2-1 and FtsZ2-2 in *Arabidopsis thaliana*) accumulate and form a polymeric ring (Z-ring) at the stromal surface of the inner envelope membrane. Accumulation and replication of chloroplasts protein (ARC) such as ARC3 and *Mini*cell proteins (MinD and MinE) are responsible for regulating the position of the Z-ring while ARC6 stabilizes it. At the outer envelope membrane ARC5 (dynamin related protein also called DRP5B) forms a second ring in order to constrict the envelope membranes. Plastid division proteins (PDV1 and PDV2) proteins are responsible to recruit ARC5 in the outer envelope membrane. Finally, constriction events are followed by the scission to generate two plastids (Yang et al., 2008; Yoshida, 2018).

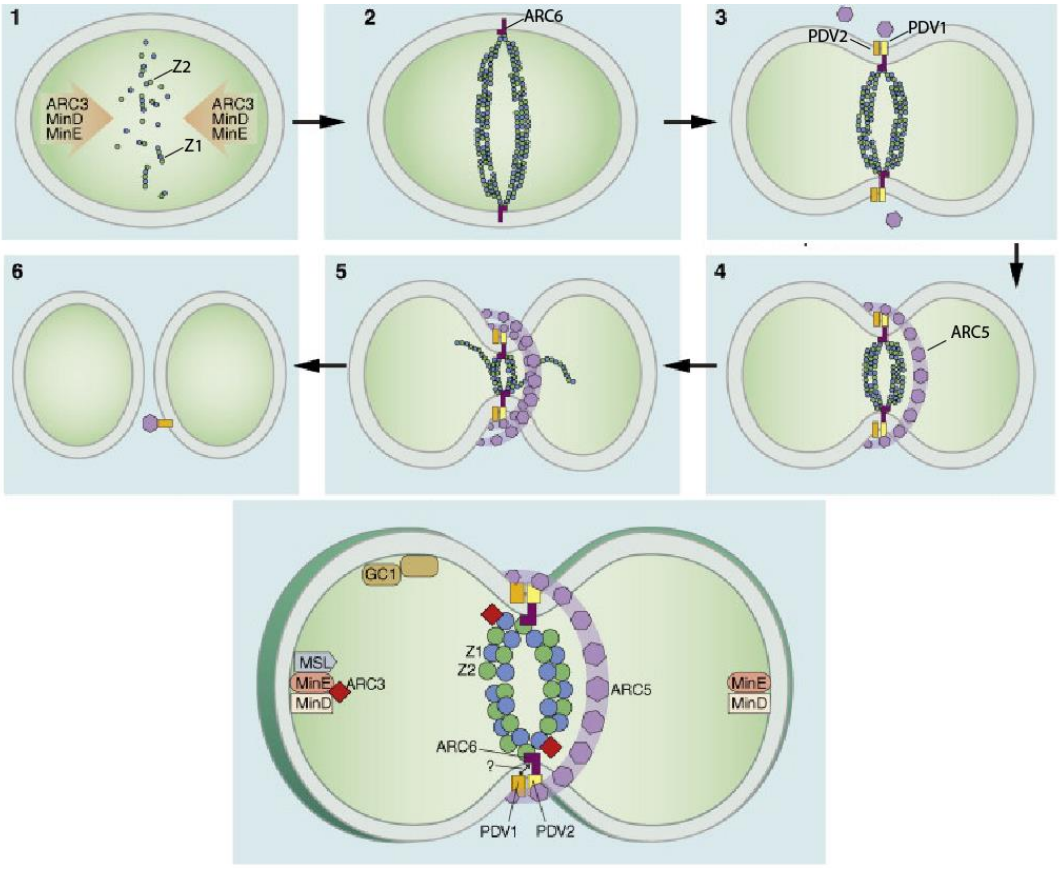

Figure 6: Simplified scheme of the plastid division mechanism. In the first two stages (1,2) accumulation and polymerization of FtsZ proteins occurs in the stroma in proximity to the inner membrane. ARC3, MinD, MinE and ARC6 are regulators of the Z-ring positioning and assembly. In stages 3 and 4, PDV1 and PDV2 are recruited and ARC5 binds to the outer envelope membrane and generate the constriction force (stage 5). The plastid machinery is disassembled after the division (stage 6). Figure adapted from (Yang et al., 2008).

Mutations of some genes involved in the plastid division activity showed alterations of chloroplast number and volume. In the L1, L2 and L3 layers of the shoot apex of Arabidopsis *ftsZ* mutants, plastids are not able to divide properly showing a larger chloroplast volume than the wild type. The number of chloroplasts per 100 um^3 of tissue analysed was also reduced compared to wild type (Swid et al., 2018) while it was reduced to one chloroplast in transgenic plants using antisense technology (Osteryoung et al., 1998).

The number of chloroplasts per cell was calculated during the greening process in Arabidopsis cell culture. Around 40 chloroplasts per cell were counted after 7 days of light. The same number was observed after 14 days of light exposure (Dubreuil et al., 2018). The relationship between chloroplast number and mesophyll cell expansion was studied in the *arc-5* mutant in which chloroplast division was affected. The number of chloroplasts did not change during the mesophyll expansion while in the wild type the relationship between number of chloroplasts and cell expansion was correlated (Pyke and Leech 1994). However, in *arc5* mutants, chloroplasts entered chloroplast division but were blocked at a late stage, before scission (Pyke and Leech 1994), while in *arc3* mutants, chloroplasts were not able to enter the chloroplast division process (Pyke and Leech 1992).

1.7.2 Division and expansion of cotyledon cells

The chloroplast division process does not seem to be correlated with cell division in land plants. In Arabidopsis cotyledons, a pronounced cellular expansion rather than cell division takes place during the early post-germinative stages. The post-germinative development of cotyledons under light exposure showed that only about 20% of the cells entered in division. This percentage remained invariable during the days of light exposure. Specifically, cell numbers in cotyledons have been estimated. In the first palisade layer the number of cells was around 1500 per cotyledon while around 300 cells were detected in the spongy layer (Stoynova-Bakalova et al., 2004). Another study counted around 4000 cells per cotyledon and this number remained constant during germination from 12 – 84 hours after imbibition (HAI) (Mansfield and Briarty, 1996).

References

Adam Z, Charuvi D, Tsabari O, Knopf RR, Reich Z. 2011. Biogenesis of thylakoid networks in angiosperms: knowns and unknowns. *Plant Mol Biol* **76**:221–234. doi:10.1007/s11103-010-9693-5

Agne B, Kessler F. 2010. Modifications at the A-domain of the chloroplast import receptor Toc159. *Plant Signal Behav* **5**:1513–6. doi:10.1104/pp.110.158048

Albertsson P-åke. 2001. A quantitative model of the domain structure of the photosynthetic membrane **1385**:349–354. doi:10.1016/S1360-1385(01)02021-0

Aldridge C, Cain P, Robinson C. 2009. Protein transport in organelles : Protein transport into and across the thylakoid membrane **276**:1177–1186. doi:10.1111/j.1742-4658.2009.06875.x

Andersson B, Anderson JM. 1980. Lateral heterogeneity in the distribution of chlorophyll-protein complexes of the thylakoid membranes of spinach chloroplasts. *Biochim Biophys Acta* **593**:427–440. doi:10.1016/0005-2728(80)90078-X

Andersson MX, Kjellberg JM, Sandelius AS. 2001. Chloroplast biogenesis. Regulation of lipid transport to the thylakoid in chloroplasts isolated from expanding and fully expanded leaves of pea. *Plant Physiol* **127**:184–93. doi:10.1104/Pp.127.1.184

Armarego-Marriott T, Kowalewska Ł, Burgos A, Fischer A, Thiele W, Erban A, Strand D, Kahlau S, Hertle A, Kopka J, Walther D, Reich Z, Schöttler MA, Bock R. 2019. Highly Resolved Systems Biology to Dissect the Etioplast-to-Chloroplast Transition in Tobacco Leaves. *Plant Physiol* **180**:654–681. doi:10.1104/pp.18.01432

Arvidsson P-O, Sundby C. 1999. A model for the topology of the chloroplast thylakoid membrane. *Funct Plant Biol* **26**:687–694. doi:10.1071/PP99072

Austin JR, Frost E, Vidi P-A, Kessler F, Staehelin LA. 2006. Plastoglobules are lipoprotein subcompartments of the chloroplast that are permanently coupled to thylakoid membranes and contain biosynthetic enzymes. *Plant Cell* **18**:1693–

1703. doi:10.1105/tpc.105.039859

Austin JR, Staehelin LA. 2011. Three-Dimensional Architecture of Grana and Stroma Thylakoids of Higher Plants as Determined by Electron Tomography. *Plant Physiol* **155**:1601–1611. doi:10.1104/pp.110.170647

Awai K, Brun D, Masuda T, Shimada H, Awai K, Mare E, Takamiya K, Ohta H, Joyard J. 2001. Two types of MGDG synthase genes , found widely in both 16 : 3 and 18 : 3 plants , differentially mediate galactolipid syntheses in photosynthetic and nonphotosynthetic tissues in Arabidopsis thaliana **98**:10960–10965. doi:10.1073/pnas.181331498

Barera S, Pagliano C, Pape T, Saracco G, Barber J. 2012. Characterization of PSII-LHCII supercomplexes isolated from pea thylakoid membrane by one-step treatment with α- and β-dodecyl-D-maltoside. *Philos Trans R Soc Lond B Biol Sci* **367**:3389–3399. doi:10.1098/rstb.2012.0056

Blomqvist LA, Ryberg M, Sundqvist C. 2008. Proteomic analysis of highly purified prolamellar bodies reveals their significance in chloroplast development. *Photosynth Res* **96**:37–50. doi:10.1007/s11120-007-9281-y

Boudière L, Michaud M, Petroutsos D, Rébeillé F, Falconet D, Bastien O, Roy S, Finazzi G, Rolland N, Jouhet J, Block MA, Maréchal E. 2014. Glycerolipids in photosynthesis: Composition, synthesis and trafficking. *Biochim Biophys Acta - Bioenerg* **1837**:470–480. doi:10.1016/j.bbabio.2013.09.007

Brzezowski P, Richter AS, Grimm B. 2015. Regulation and function of tetrapyrrole biosynthesis in plants and algae. *Biochim Biophys Acta - Bioenerg* **1847**:968–985. doi:10.1016/j.bbabio.2015.05.007

Caffarri S, Tibiletti T, Jennings R, Santabarbara S. 2014. A Comparison Between Plant Photosystem I and Photosystem II Architecture and Functioning. *Curr Protein Pept Sci* **15**:296–331. doi:10.2174/1389203715666140327102218

Charuvi D, Kiss V, Nevo R, Shimoni E, Adam Z, Reich Z. 2012. Gain and loss of photosynthetic membranes during plastid differentiation in the shoot apex of Arabidopsis. *Plant Cell* **24**:1143–57. doi:10.1105/tpc.111.094458

Daum B, Kühlbrandt W. 2011. Electron tomography of plant thylakoid membranes. *J Exp Bot* **62**:2393–2402. doi:10.1093/jxb/err034

Daum B, Nicastro D, Mcintosh JR, Ku W. 2010. Arrangement of Photosystem II and ATP Synthase in Chloroplast Membranes of Spinach and Pea 1299–1312 . doi:10.1105/tpc.109.071431

Dekker JP, Boekema EJ. 2005. Supramolecular Organization of Thylakoid Membrane Proteins in Green Plants. *Biochim Biophys Acta* **1706**:12–39 . doi:10.1016/j.bbabio.2004.09.009

Demé B, Cataye C, Block M a, Maréchal E, Jouhet J. 2014. Contribution of galactoglycerolipids to the 3-dimensional architecture of thylakoids. *FASEB J* **28**:3373–83. doi:10.1096/fj.13-247395

Dormann P. 2001. Galactolipids in plant membranes. *els* 1–7. doi:10.1002/9780470015902.a0020100.pub2

Dörmann P, Hoffmann-Benning S, Balbo I, Benning C. 1995. Isolation and characterization of an Arabidopsis mutant deficient in the thylakoid lipid digalactosyl diacylglycerol. *Plant Cell* **7**:1801–1810. doi:10.1105/tpc.7.11.1801

Dubreuil C, Jin X, Barajas-lópez JDD, Hewitt TC, Tanz SK, Dobrenel T, Schröder WP, Hanson J, Pesquet E, Grönlund A. 2018. Establishment of Photosynthesis through Chloroplast Development Is Controlled by Two Distinct Regulatory Phases 1**176**:1199–1214. doi:10.1104/pp.17.00435

Engel BD, Schaffer M, Cuellar LK, Villa E, Plitzko JM, Baumeister W. 2015. Native architecture of the chlamydomonas chloroplast revealed by in situ cryo-electron tomography. *Elife* **2015**:1–29. doi:10.7554/eLife.04889

Eugeni L, Besagni C, Ksas B, Rumeau D, Bréhélin C, Glauser G. 2011. Chloroplast lipid droplet type II NAD (P) H quinone oxidoreductase is essential for prenylquinone metabolism and vitamin K 1 accumulation **108**:14354–14359 . doi:10.1073/pnas.1104790108

Eugeni Piller L. 2014. Role of plastoglobules in metabolite repair in the tocopherol

redox cycle. *Front Plant Sci* **5**:1–10.
doi:10.3389/fpls.2014.00298

Fritsche S, Wang X, Jung C. 2017. Recent Advances in our Understanding of Tocopherol Biosynthesis in Plants: An Overview of Key Genes, Functions, and Breeding of Vitamin E Improved Crops. *Antioxidants* **6**:99.
doi:10.3390/antiox6040099

Fujii S, Kobayashi K, Nagata N, Masuda T, Wada H. 2018. Digalactosyldiacylglycerol is essential for organization of the membrane structure in etioplasts. *Plant Physiol* **177**:1487–1497.
doi:10.1104/pp.18.00227

Fujii S, Kobayashi K, Nagata N, Masuda T, Wada H. 2017. Monogalactosyldiacylglycerol facilitates synthesis of photoactive protochlorophyllide in etioplasts. *Plant Physiol* **174**:2183–2198.
doi:10.1104/pp.17.00304

Fujii S, Kobayashi K, Nakamura Y, Wada H. 2014. Inducible knockdown of MONOGALACTOSYLDIACYLGLYCEROL SYNTHASE1 reveals roles of galactolipids in organelle differentiation in Arabidopsis cotyledons. *Plant Physiol* **166**:1436–49. doi:10.1104/pp.114.250050

Fujii S, Nagata N, Masuda T, Wada H, Kobayashi K. 2019. Galactolipids Are Essential for Internal Membrane Transformation during Etioplast-to-Chloroplast Differentiation. *Plant Cell Physiol* **0**:1–15.
doi:10.1093/pcp/pcz041

Gao J, Wang H, Yuan Q, Feng Y. 2018. Structure and Function of the Photosystem Supercomplexes. *Front Plant Sci* **9**:1–7.
doi:10.3389/fpls.2018.00357

Gaude N, Bréhélin C, Tischendorf G, Kessler F, Dörmann P. 2007. Nitrogen deficiency in Arabidopsis affects galactolipid composition and gene expression and results in accumulation of fatty acid phytyl esters. *Plant J* **49**:729–39.
doi:10.1111/j.1365-313X.2006.02992.x

Grennan AK. 2008. Plastoglobule Proteome. *Plant Physiol* **147**:443–445. doi:10.1104/pp.104.900261

Griffiths WT. 1978. Reconstitution of chlorophyllide formation by isolated etioplast membranes. *Biochem J* **174**:681–692.

doi:10.1042/bj1740681

Gruszecki WI, Strzałka K. 2005. Carotenoids as modulators of lipid membrane physical properties. *Biochim Biophys Acta - Mol Basis Dis* **1740**:108–115. doi:10.1016/j.bbadis.2004.11.015

Hagio M, Sakurai I, Sato S, Kato T, Tabata S, Wada H. 2002. Phosphatidylglycerol is essential for the development of thylakoid membranes in *Arabidopsis thaliana*. *Plant Cell Physiol* **43**:1456–1464. doi:10.1093/pcp/pcf185

Jarvis P, Lutes J, Benning C, Chory J, Peto CA, Do P. 2000. Galactolipid deficiency and abnormal chloroplast development in the Arabidopsis MGD synthase 1 mutant **97**:8175–8179. doi:10.1073/pnas.100132197

Jensen PE, Leister D. 2014. Chloroplast evolution, structure and functions. *F1000Prime Rep* **6**:1–14. doi:10.12703/P6-40

Jordan P, Fromme P, Witt HT, Klukas O, Saenger W, Krauss N. 2001. Three-dimensional structure of cyanobacterial photosystem I at 2.5 A resolution. *Nature* **411**:909–917. doi:10.1038/35082000

Jouhet J, Marechal E, Block MA. 2007. Glycerolipid transfer for the building of membranes in plant cells. *Prog Lipid Res* **46**:37–55. doi:10.1016/j.plipres.2006.06.002

Kessler F, Schnell D, Blobel G. 1999. Identification of proteins associated with plastoglobules isolated from pea (Pisum sativum L.) chloroplasts. *Planta* **208**:107–113. doi:10.1007/s004250050540

Kirchhoff H. 2014. Diffusion of molecules and macromolecules in thylakoid membranes. *Biochim Biophys Acta* **1837**:495–502. doi:10.1016/j.bbabio.2013.11.003

Kirchhoff H, Hall C, Wood M, Herbstová M, Tsabari O, Nevo R, Charuvi D, Eyal S, Ziv R. 2011. Dynamic control of protein diffusion within the granal thylakoid lumen **108**:20248–20253. doi:10.1073/pnas.1104141109

Kirchhoff H, Li M, Puthiyaveetil S. 2017. Sublocalization of Cytochrome b6f Complexes in Photosynthetic Membranes. *Trends Plant Sci* **22**:574–582.

doi:10.1016/j.tplants.2017.04.004

Klaus D, Härtel H, Fitzpatrick LM, Froehlich JE, Hubert J, Benning C, Dörmann P. 2002. Digalactosyldiacylglycerol synthesis in chloroplasts of the Arabidopsis dgd1 mutant. *Plant Physiol* **128**:885–95. doi:10.1104/pp.010780

Kleffmann T, Zychlinski A Von, Russenberger D, Hirsch-hoffmann M, Gehrig P, Gruissem W, Baginsky S, Zurich H, Z A. 2007. Proteome Dynamics during Plastid Differentiation in Rice 1 **143**:912–923. doi:10.1104/pp.106.090738

Kobayashi K, Awai K, Takamiya K, Ohta H. 2004. Arabidopsis Type B Monogalactosyldiacylglycerol Synthase Genes Are Expressed during Pollen Tube Growth and Induced by Phosphate Starvation 1 **134**:640–648 . doi:10.1104/pp.103.032656

Kobayashi K, Fujii S, Sato M, Toyooka K, Wada H. 2015. Specific role of phosphatidylglycerol and functional overlaps with other thylakoid lipids in Arabidopsis chloroplast biogenesis. *Plant Cell Rep* **34**:631–42. doi:10.1007/s00299-014-1719-z

Kobayashi K, Kondo M, Fukuda H, Nishimura M, Ohta H. 2007. Galactolipid synthesis in chloroplast inner envelope is essential for proper thylakoid biogenesis, photosynthesis, and embryogenesis. *Proc Natl Acad Sci U S A* **104**:17216–17221. doi:10.1073/pnas.0704680104

Kobayashi K, Nakamura Y, Ohta H. 2009. Type A and type B monogalactosyldiacylglycerol synthases are spatially and functionally separated in the plastids of higher plants. *Plant Physiol Biochem* **47**:518–25. doi:10.1016/j.plaphy.2008.12.012

Kowalewska ŁM, Mazur R, Suski S, Garstka M, Mostowska A. 2016. Three-dimensional visualization of the internal plastid membrane network during runner bean chloroplast biogenesis. Dynamic model of the tubular-lamellar transformation. *Plant Cell* **28**:875–891. doi:10.1105/tpc.15.01053

Kroll D, Meierhoff K, Bechtold N, Kinoshita M, Westphal S, Vothknecht UC, Soll J, Westhoff P. 2001. VIPP1, a nuclear gene of Arabidopsis thaliana essential for thylakoid membrane formation. *Proc Natl Acad Sci U S A* **98**:4238–4242. doi:doi.org/10.1073/pnas.061500998

Kurisu G, Zhang H, Smith JL, Cramer WA. 2003. Structure of the Cytochrome b 6 f Complex of Oxygenic Photosynthesis : Tuning the Cavity **302**:1009–1015. doi:10.1126/science.1090165

Lee AG. 2000. Membrane lipids: It's only a phase. *Curr Biol* **10**:377–380 . doi:10.1016/S0960-9822(00)00477-2

Li L, Song Y, Wang K, Dong P, Zhang X, Li F, Li Z, Ren M. 2015. TOR-inhibitor insensitive-1 (TRIN1) regulates cotyledons greening in Arabidopsis. *Front Plant Sci* **6**:1–13. doi:10.3389/fpls.2015.00861

Liang Z, Zhu N, Mai KK, Liu Z, Tzeng D, Osteryoung KW. 2018. Thylakoid-Bound Polysomes and a Dynamin-Related Protein , FZL , Mediate Critical Stages of the Linear Chloroplast Biogenesis Program in Greening Arabidopsis Cotyledons **30**:1476–1495. doi:10.1105/tpc.17.00972

Lichtenthaler HK. 1968. Verbreitung und relative Konzentration der lipophilen Plastidenchionone in grünen Pflanzen. *Planta* **81**:140–152. doi:10.1007/BF00417443

Loll B, Kern J, Saenger W, Zouni A, Biesiadka J. 2005. Towards complete cofactor arrangement in the 3.0 A resolution structure of photosystem II. *Nature* **438**:1040–4 . doi:10.1038/nature04224

Lopez-Juez E, Pyke K a. 2005. Plastids unleashed: their development and their integration in plant development. *Int J Dev Biol* **49**:557–77. doi:10.1387/ijdb.051997el

Lundquist PK, Poliakov A, Bhuiyan NH, Zybailov B, Sun Q, van Wijk KJ. 2012. The Functional Network of the Arabidopsis Plastoglobule Proteome Based on Quantitative Proteomics and Genome-Wide Coexpression Analysis. *Plant Physiol* **158**:1172–1192. doi:10.1104/pp.111.193144

Mansfield SG, Briarty LG. 1996. The Dynamics of Seedling and Cotyledon Cell Development in Arabidopsis thaliana During Reserve Mobilization. *Int J Plant Sci* **157**:280–295. doi:jstor.org/stable/2475264

Marechal E, Block MA, Dome A, Douce R, Joyard J. 1997. Lipid synthesis and metabolism in the plastid envelope **100**:65–77. doi:10.1111/j.1399-3054.1997.tb03455.x

Mazor Y, Borovikova A, Nelson N. 2015. The structure of plant photosystem i super-complex at 2.8 Å resolution. *Elife* **4**:1–18.

doi:10.7554/eLife.07433

Miège C, Maréchal E, Shimojima M, Awai K, Block MA, Ohta H, Takamiya Kichiro, Douce R, Joyard J. 1999. Biochemical and topological properties of type A MGDG synthase, a spinach chloroplast envelope enzyme catalyzing the synthesis of both prokaryotic and eukaryotic MGDG. *Eur J Biochem* **265**:990–1001.
doi:10.1046/j.1432-1327.1999.00801.x

Mustardy and Garab C. 2003. Granum revisited . A three-dimensional model – where things fall into place **8**:117–122.
doi:10.1016/S1360-1385(03)00015-3

Mustárdy L, Buttle K, Steinbach G, Garab G. 2008. The three-dimensional network of the thylakoid membranes in plants: Quasihelical model of the granum-stroma assembly. *Plant Cell* **20**:2552–2557.
doi:10.1105/tpc.108.059147

Nevo R, Charuvi D, Tsabari O, Reich Z. 2012. Composition, architecture and dynamics of the photosynthetic apparatus in higher plants. *Plant J* **70**:157–176.
doi:10.1111/j.1365-313X.2011.04876.x

Nield J, Barber J. 2006. Refinement of the structural model for the Photosystem II supercomplex of higher plants. *Biochim Biophys Acta - Bioenerg* **1757**:353–361.
doi:10.1016/j.bbabio.2006.03.019

Niyogi KK, Björkman O, Grossman a R. 1997. The roles of specific xanthophylls in photoprotection. *Proc Natl Acad Sci U S A* **94**:14162–14167 .
doi:10.1073/pnas.94.25.14162

Noutsos C, Leister D, Jansson S, Klimmek F, Sjo A. 2006. Abundantly and Rarely Expressed Lhc Protein Genes Exhibit Distinct Regulation Patterns in Plants. *Plant Physiol* **140**:793–804.
doi:10.1104/pp.105.073304.1

Ohlrogge J, Browse J. 1995. Lipid biosynthesis. *Plant Cell* **7**:957–970.
doi:10.1105/tpc.7.7.957

Okazaki K, Kabeya Y, Suzuki K, Mori T, Ichikawa T, Matsui M, Nakanishi H, Miyagishima S -y. 2009. The PLASTID DIVISION1 and 2 Components of the Chloroplast Division Machinery Determine the Rate of Chloroplast Division in Land Plant Cell Differentiation. *Plant Cell Online* **21**:1769–1780.

doi:10.1105/tpc.109.067785

Osteryoung KW, Nunnari J. 2003. The Division of Endosymbiotic Organelles. *Science* **302**:1698–1704. doi:10.1126/science.1082192

Osteryoung KW, Stokes KD, Rutherford SM, Percival AL, Lee WY. 1998. Chloroplast division in higher plants requires members of two functionally divergent gene families with hemology to bacterial ftsZ. *Plant Cell* **10**:1991–2004. doi:10.1105/tpc.10.12.1991

Pagliano C, Nield J, Marsano F, Pape T, Barera S, Saracco G, Barber J. 2014. Proteomic characterization and three-dimensional electron microscopy study of PSII-LHCII supercomplexes from higher plants. *Biochim Biophys Acta - Bioenerg* **1837**:1454–1462. doi:10.1016/j.bbabio.2013.11.004

Paolillo DJ. 1970. The three-dimensional arrangement of intergranal lamellae in chloroplasts **255**:243–255. doi:jcs.biologists.org/content/6/1/243.article-info

Philippar K, Geis T, Ilkavets I, Oster U, Schwenkert S, Meurer J, Soll J. 2007. Chloroplast biogenesis: The use of mutants to study the etioplast-chloroplast transition. *Proc Natl Acad Sci* **104**:678–683. doi:10.1073/pnas.0610062104

Pogson BJ, Albrecht V. 2011. Genetic dissection of chloroplast biogenesis and development: an overview. *Plant Physiol* **155**:1545–1551. doi:10.1104/pp.110.170365

Pribil M, Labs M, Leister D. 2014. Structure and dynamics of thylakoids in land plants. *J Exp Bot* **65**:1955–1972. doi:10.1093/jxb/eru090

Pyke KA, Leech RM. 1994. A Genetic Analysis of Chloroplast Division and Expansion in Arabidopsis thaliana. *Plant Physiol* **104**:201–207. doi:10.1104/pp.104.1.201

Pyke KA, Leech RM. 1992. Chloroplast division and expansion is radically altered by nuclear mutations in Arabidopsis thaliana. *Plant Physiol* **99**:1005–1008. doi:10.1104/pp.99.3.1005

Rasmussen M, Minteer SD. 2014. Thylakoid direct photobioelectrocatalysis: Utilizing stroma thylakoids to improve bio-solar cell performance. *Phys Chem Chem Phys*

16:17327–17331.
doi:10.1039/c4cp02754j

Reiland S, Grossmann J, Baerenfaller K, Gehrig P, Nunes-nesi A. 2011. Integrated proteome and metabolite analysis of the de-etiolation process in plastids from rice (Oryza sativa L .) **11**:1751–1763.
doi:10.1002/pmic.201000703

Richardson LGL, Schnell DJ. 2019. Origins, function, and regulation of the TOC–TIC general protein import machinery of plastids. *J Exp Bot* **71**:1226–1238. doi:10.1093/jxb/erz517

Richardson LGL, Singhal R, Schnell DJ. 2017. The integration of chloroplast protein targeting with plant developmental and stress responses. *BMC Biol* **15**:118. doi:10.1186/s12915-017-0458-3

Rottet S, Besagni C, Kessler F. 2015. The role of plastoglobules in thylakoid lipid remodeling during plant development. *Biochim Biophys Acta* **1847**:889–899.
doi:10.1016/j.bbabio.2015.02.002

Schoefs B, Bertrand M. 2000. The formation of chlorophyll from chlorophyllide in leaves containing proplastids is a four-step process. *FEBS Lett* **486**:243–246. doi:10.1016/S0014-5793(00)02309-7

Shimojima M. 2011. Biosynthesis and functions of the plant sulfolipid. *Prog Lipid Res* **50**:234–239.
doi:10.1016/j.plipres.2011.02.003

Shimoni E, Rav-Hon O, Ohad I, Brumfeld V, Reich Z. 2005. Three-dimensional organization of higher-plant chloroplast thylakoid membranes revealed by electron tomography. *Plant Cell* **17**:2580–2586.
doi:10.1105/tpc.105.035030

Simidjiev I, Stoylova S, Amenitsch H, Javorfi T, Mustardy L, Laggner P, Holzenburg a, Garab G. 2000. Self-assembly of large, ordered lamellae from non-bilayer lipids and integral membrane proteins in vitro. *Proc Natl Acad Sci U S A* **97**:1473–1476. doi:10.1073/pnas.97.4.1473

Solymosi K, Aronsson H. 2013. Plastid Development in Leaves during Growth and Senescence **36**:39–64.
doi:10.1007/978-94-007-5724-0

Spicher L, Kessler F. 2015. Unexpected roles of plastoglobules (plastid lipid droplets)

in vitamin K1 and E metabolism. *Curr Opin Plant Biol* **25**:123–129. doi:10.1016/j.pbi.2015.05.005

Steffen R, Eckert HJ, Kelly AA, Dörmann P, Renger G. 2005. Investigations on the reaction pattern of photosystem II in leaves from Arabidopsis thaliana by time-resolved fluorometric analysis. *Biochemistry* **44**:3123–3133. doi:10.1021/bi0484668

Stoynova-Bakalova E, Karanov E, Petrov P, Hall MA. 2004. Cell division and cell expansion in cotyledons of Arabidopsis seedlings. *New Phytol* **162**:471–479. doi:10.1111/j.1469-8137.2004.01031.x

Su X, Ma J, Wei X, Cao P, Zhu D, Chang W, Liu Z, Zhang X, Li M. 2017. Structure and assembly mechanism of plant C2S2M2-type PSII-LHCII supercomplex. *Science (80-)* **357**:815–820. doi:10.1126/science.aan0327

Swid N, Nevo R, Kiss V, Kapon R, Dagan S, Snir O, Adam Z, Falconet D, Reich Z, Charuvi D. 2018. Differential impacts of FtsZ proteins on plastid division in the shoot apex of Arabidopsis. *Dev Biol* **441**:83–94. doi:10.1016/j.ydbio.2018.06.010

Terry MJ, Smith AG. 2013. A model for tetrapyrrole synthesis as the primary mechanism for plastid-to-nucleus signaling during chloroplast biogenesis. *Front Plant Sci* **4**:14. doi:10.3389/fpls.2013.00014

Tilney-Bassett RAE. 1986. Plant chimeras. London: Edward Arnold (Publishers) Ltd.

Tsen K-T, Tsen S-WD, Kiang JG. 2007. Lycopene is more potent than beta carotene in the neutralization of singlet oxygen: role of energy transfer probed by ultrafast Raman spectroscopy. *J Biomed Opt* **11**:064025. doi:10.1117/1.2398884

Van Bezouwen LS, Caffarri S, Kale R, Kouřil R, Thunnissen AMWH, Oostergetel GT, Boekema EJ. 2017. Subunit and chlorophyll organization of the plant photosystem II supercomplex. *Nat Plants* **3**:1–11. doi:10.1038/nplants.2017.80

Van Wijk KJ, Kessler F. 2017. Plastoglobuli: Plastid Microcompartments with Integrated Functions in Metabolism, Plastid Developmental Transitions, and Environmental Adaptation. *Annu Rev Plant Biol* **68**:253–289. doi:10.1146/annurev-arplant-043015-111737

Vidi PA, Kanwischer M, Baginsky S, Austin JR, Csucs G, Dörmann P, Kessler F, Bréhélin C. 2006. Tocopherol cyclase (VTE1) localization and vitamin E accumulation in chloroplast plastoglobule lipoprotein particles. *J Biol Chem* **281**:11225–11234. doi:10.1074/jbc.M511939200

Viitanen P V., Doran ER, Dunsmuir P. 1988. What is the role of the transit peptide in thylakoid integration of the light-harvesting chlorophyll a/b protein? *J Biol Chem* **263**:15000–15007.

Wada H, Murata N. 2007. The essential role of phosphatidylglycerol in photosynthesis. *Photosynth Res* **92**:205–215. doi:10.1007/s11120-007-9203-z

Wei X, Su X, Cao P, Liu X, Chang W, Li M, Zhang X, Liu Z. 2016. Structure of spinach photosystem II-LHCII supercomplex at 3.2 Å resolution. *Nature* **534**:69–74. doi:10.1038/nature18020

Williams WP, Selstam E, Brain T. 1998. X-ray diffraction studies of the structural organisation of prolamellar bodies isolated from Zea mays. *FEBS Lett* **422**:252–254. doi:10.1016/S0014-5793(98)00019-2

Xu C, Yu B, Cornish AJ, Froehlich JE, Benning C. 2006. Phosphatidylglycerol biosynthesis in chloroplasts of Arabidopsis mutants deficient in acyl-ACP glycerol-3-phosphate acyltransferase. *Plant J* **47**:296–309. doi:10.1111/j.1365-313X.2006.02790.x

Yang Y, Glynn JM, Olson BJSC, Schmitz AJ, Osteryoung KW. 2008. Plastid division: across time and space. *Curr Opin Plant Biol* **11**:577–584. doi:10.1016/j.pbi.2008.10.001

Yoshida Y. 2018. Insights into the mechanisms of chloroplast division. *Int J Mol Sci* **19**:1–13. doi:10.3390/ijms19030733

Yoshida Y, Miyagishima S ya, Kuroiwa H, Kuroiwa T. 2012. The plastid-dividing machinery: Formation, constriction and fission. *Curr Opin Plant Biol* **15**:714–721 . doi:10.1016/j.pbi.2012.07.002

Yu B, Xu C, Benning C. 2002. Arabidopsis disrupted in SQD2 encoding sulfolipid synthase is impaired in phosphate-limited growth. *Proc Natl Acad Sci U S A* **99**:5732–5737. doi:10.1073/pnas.082696499

Zheng G, Tian B, Zhang F, Tao F, Li W. 2011. Plant adaptation to frequent alterations between high and low temperatures: Remodelling of membrane lipids and

maintenance of unsaturation levels. *Plant, Cell Environ* **34**:1431–1442. ╠doi:10.1111/j.1365-3040.2011.02341.x

Chapter 2 - A bi-phasic model of chloroplast biogenesis during de-etiolation in *Arabidopsis thaliana*

Rosa Pipitone[1], Simona Eicke[2], Barbara Pfister[2], Gaetan Glauser[3], Denis Falconet[4], Thibaut Pralon[1], Samuel Zeeman[2], Felix Kessler[1,], Emilie Demarsy[1,5,*]*

R.P carried out the lipidomics and immunoblots experiments, while the proteomics and the analysis of photosynthetic parameters have been carried out together with B.P and E.D. R.P carried out the image processing and microscopy experiments together with S.E and D.F. Conceptualization: R.P., T.P., S.Z., F.K. Supervision, F.K. and E.D.

Abstract

Light triggers chloroplast differentiation in dark grown seedlings. A precursor organelle, the etioplast, transforms into a photosynthesizing chloroplast. Over the course of just a few h, an extensive photosynthetic membrane system, the thylakoid, emerges. This requires synthesis of highly abundant membrane lipids as well as specific photosynthesis-associated proteins but the sequence of events during chloroplast differentiation is still unclear. Using Serial Block Face Scanning Electron Microscopy (SBF-SEM) we generated a time course of 3D reconstructions of chloroplasts during differentiation, revealing number, volume as well as envelope and thylakoid membrane surface. The (ultra)structural data are complete with quantitative lipid and whole proteome data that together provide a time-resolved, multi-dimensional analysis of chloroplast differentiation. The superimposition of the structural and biochemical data reveals two distinct phases of chloroplast biogenesis; an initial “Structure Establishment Phase” enabling onset of photosynthesis, followed by a “Chloroplast Proliferation Phase” coinciding with cell expansion. We present a mathematical model describing the expansion of the thylakoid membrane during chloroplast differentiation. Thereby we establish a roadmap to chloroplast differentiation, a critical process towards photoautotrophic growth and survival of young plants.

2.1 Introduction

Seedling development relies on successful chloroplast biogenesis, ensuring the transition from heterotrophic to autotrophic growth. Light is a crucial factor for chloroplast differentiation. Chloroplasts may differentiate directly from proplastids present in cotyledons when seeds germinate in the light. However, seeds are most often buried in the soil where seedling development initially occurs in darkness and follow a skotomorphogenic program called etiolation, characterized by rapid hypocotyl cell elongation and pre- chloroplast development. During etiolation proplastids first differentiate into etioplasts (precursors of the photosynthetically active chloroplast). Light promotes seedling de-etiolation, a process characterized by a series of morphological such as cotyledon expansion, hypocotyl growth inhibition and greening that accompany the onset of photosynthesis in chloroplast. Etioplast to chloroplast transition is thereby triggered by light in a short time frame during de-etiolation, when the seedling emerges at the soil surface (Solymosi and Schoefs, 2010; Weier and Brown, 1970). Chloroplast differentiation is essentially characterized by the biogenesis of thylakoids, a network of internal membranes where the components of the photosynthetic electron transport chain assemble. Thylakoid biogenesis and the onset of photosynthesis rely on concerted synthesis, and for their assembly to be coordinated in space and time. In parallel, chlorophyll is synthesized and accumulates in the photosystems and associated light harvesting antennae making the chloroplast developmental process visible as “greening”. Thylakoids are organized either as stacked or non-stacked “sack”-like” compartments enclosed by a lipid bilayer, so that the inner aqueous compartment, the lumen, is isolated from the surrounding one, the stroma.

The thylakoids harbor the photosynthetic electron transport chain. It is composed of three complexes: Photosystem II (PSII), the Cytochrome b_6/f (Cyt b_6f) and Photosystem I (PSI). Mobile electron carriers transfer electron between these complexes: the low molecular weight, membrane-soluble plastoquinone (electron transfer from PSII to Cyt b_6f); and the lumenal protein plastocyanin (electron transfer from Cyt b_6f to PSI). Electron transfer leads to successive reduction and oxidation of the components of the electron transport chain. The final reduction step catalyzed by ferredoxin-NADP(+) reductase (FNR) leads to NADPH production. Oxidation of water

by PSII and of plastoquinone by Cyt b_6f releases protons into the lumen, generating a proton gradient across the thylakoid membrane that drives the activity of the thylakoid-localized chloroplast ATP synthase complex. Each of the photosynthetic complexes consists of multiple subunits encoded either by the nuclear genome and imported from the cytoplasm, or by the plastid genome. PSII and PSI have a core complex constituted of 25 to 30 and 15 proteins, respectively (Amunts and Nelson, 2009; Caffarri et al., 2014). The antenna proteins from the Light Harvesting Complexes (LHC) surround the PS cores contributing to the formation of supercomplexes. Cyt b_6f is an eight-subunit dimeric complex. Each complex of the electron transport chain has specific dimensions, orientation and location within the thylakoid membrane occupying a defined surface and their dimensions have been reported in several studies giving congruent results (Caffarri et al., 2014; Kurisu et al., 2003; Van Bezouwen et al., 2017). During de-etiolation, massive protein synthesis is required for assembly of the very abundant photosynthetic complexes embedded in the lipid bilayer membrane. The general chloroplast protein import machinery is composed of the multimeric complexes Translocon of Outer membrane Complex (TOC) and Translocon of Inner membrane Complex (TIC), and selective import is based on specific recognition of transit peptide sequences and TOC receptors (Agne and Kessler, 2010; Richardson and Schnell, 2019). Certain proteins such as protochlorophyllide oxidoreductase (PORA), controlling the light dependent step of chlorophyll synthesis, show opposite behavior, accumulating during the etiolation process (but inactive in the dark) and disappearing upon illumination e.g. (Rudowska et al., 2012). Reminiscent of their cyanobacterial origin, membranes of the chloroplast are composed mostly of glycolipids (mono and di-galactosyldiacylglycerol, MGDG and DGDG) and are poor in phospholipids when compared to other membranes in the cell (Bastien et al., 2016; Block et al., 1983; Kobayashi, 2016). Galactolipids consist of a glycerol backbone esterified to a single (MGDG) or double (DGDG) galactose molecules at the *sn*3 position, and 2 fatty acid chains at *sn*1 and *sn*2 positions of the glycerol backbone. In addition to the number of galactose molecules at *sn*3, galactolipids differ by the length and degrees of saturation of the fatty acid chains. In some species including Arabidopsis, galactolipid synthesis relies on two different pathways, defined by the organellar origin of the diacylglycerol precursor: the eukaryotic pathway requires diacyl-glycerol (DAG) synthesized in the endoplasmic reticulum (ER) and imported

into plastids; the prokaryotic pathway is entirely restricted to the chloroplast (Ohlrogge and Browse, 1995). As signatures, ER-derived galactolipids harbor a 18-carbon chain at the *sn*2 position while chloroplast-derived ones harbor a 16-carbon chain at *sn*2 position. In addition to constituting the lipid bilayer, galactolipids are integral components of photosystems and thereby contribute to photochemistry and photoprotection (Aronsson et al., 2008; Kobayashi, 2016). In addition to membrane lipids, thylakoids contain neutral lipids such as chlorophyll, carotenoids, tocopherols and plastoquinone that may exist freely or associated with the photosynthetic complexes. They may either have a direct role in photosynthesis (i.e. chlorophyll, carotenoids, plastoquinone) or participate indirectly in the optimization of light usage and/or mitigation of potentially damaging effect (i.e. tocopherols in addition to carotenoids and plastoquinone) (Hashimoto et al., 2003; Van Wijk and Kessler, 2017).

The architecture of the thylakoid membrane network was first described using conventional electron microscopy (EM). Based on these 2D observations, it was proposed that the plant thylakoid membranes are organized as single lamellae connected to appressed multi-lamellar regions called grana. How these lamellae are interconnected was revealed only later after the development of 3D electron microscopic techniques. The tremendous technological progress in the field of electron microscopy has been made recently and has led to improved descriptions of chloroplast ultrastructure (Daum et al., 2010; Daum and Kühlbrandt, 2011). Electron tomography (ET) substantially improved our comprehension of the 3D organization of thylakoid network in chloroplasts at different developmental stages and in different photosynthetic organisms, including Arabidopsis (Austin and Staehelin, 2011; Liang et al., 2018), Chlamydomonas (Engel et al., 2015), runner bean (Kowalewska et al., 2016) and *Phaeodactylum tricornutum* (Flori et al., 2017). ET also provided quantitative information on the thylakoid structure such as the number of thylakoid layers within the grana stack and thickness of the stacking repeat distance of grana membrane (Daum et al., 2010; Kirchhoff et al., 2011). These quantitative data allowed a greater understanding of the spatial organization of the thylakoid membrane in relation to the embedded photosynthetic complexes. Although ET offers an extraordinary resolution at the nanometer level, its main drawback is the limitation of the volume of the observation, enabling only a partial 3D reconstruction of a

chloroplast. SBF-SEM, technology allows a much larger volume to be studied and reconstructed in 3D to reveal cellular organization (Peddie and Collinson, 2014; Pinali and Kitmitto, 2014).

In combination with EM, biochemical fractionation of thylakoids revealed a differential lipid and protein composition of the grana and the stroma lamellae. The grana are enriched in DGDG and PSII while the stroma lamellae are enriched in MGDG, cytochrome b_6/f and PSI (Demé et al., 2014; Koochak et al., 2019; Tomizioli et al., 2014). The change in lipid and protein composition during the differentiation of chloroplast from etioplast is tightly linked to the thylakoid architecture. In particular changes in MGDG to DGDG ratio are correlated with the transition from prolamellar body and prothylakoid structures (tubular membrane) to thylakoid membrane (lamellar structure) (Bottier et al., 2007; Demé et al., 2014; Mazur et al., 2019).

Individual studies have provided precious pieces of information regarding the dynamics of the soluble chloroplast proteome, transcriptome, photosynthetic protein accumulation and photosynthetic activity, chloroplast lipids and changes of thylakoid architecture (Armarego-Marriott et al., 2019; Dubreuil et al., 2018; Kleffmann et al., 2007a; Kowalewska et al., 2016; Liang et al., 2018; Rudowska et al., 2012). However, these studies were mostly qualitative, focusing on one or two aspects and not performed in the same model organism. Therefore, chemical data related to thylakoid biogenesis remain sparse and quantitative information is rare. Here, we present a systems level study that integrates quantitative information on ultrastructural changes of the thylakoids and on lipid and protein composition during de-etiolation of *Arabidopsis thaliana* seedlings.

2.2 Results

2.2.1 Photosynthetic machinery is functional after 14h of illumination

We analysed the etioplast to chloroplast transition in 3-day-old etiolated Arabidopsis seedlings grown in absence of sucrose and illuminated continuously with white light (40 µmol/m^2/s) (Figure 1A). These experimental conditions were chosen to avoid effects of exogenous sucrose on seedling development and variations due to circadian rhythm. Dark-grown Arabidopsis seedlings displayed the characteristic closed apical hook, an elongated hypocotyl and yellow cotyledons lacking chlorophyll (Figure 1B). Upon illumination, the etiolated seedlings underwent the switch from the skotomorphogenic to the photomorphogenic developmental program, including the opening of the apical hook, greening and expansion of the cotyledons. We stopped our analysis at 96 h of illumination, before the emergence of the primary leaves. Samples were collected at different selected time points during de-etiolation depending on the following experiment (Figure 1A).

In angiosperms, chlorophyll synthesis is arrested in the dark but starts immediately upon irradiation of the seedlings (Von Wettstein et al., 1995). Chlorophyll levels in whole seedlings increased within the first 4 h of illumination and continued to increase linearly during the following days of illumination as the seedlings grew (Figure1C). In order to evaluate the photosynthetic efficiency during de-etiolation, we measured chlorophyll fluorescence and calculated the maximum quantum yield of PSII (Fv/Fm, Fig 1D and Supplemental Figure1). Under our conditions, Photosystem II maximum quantum yield increased during the first h of illumination and was near the maximal value of 0.8 at 14 h, independently of light intensity (Figure 1D and Supplemental Figure1). Other photosynthetic parameters (the Photosystem II quantum yield in the light ΦPSII and photochemical quenching qP) remained stable thereafter 14 h of de-etiolation indicating that assembly of fully functional photosynthetic machinery occurs within the first 14 h of de-etiolation, and that further biosynthesis is efficiently coordinated.

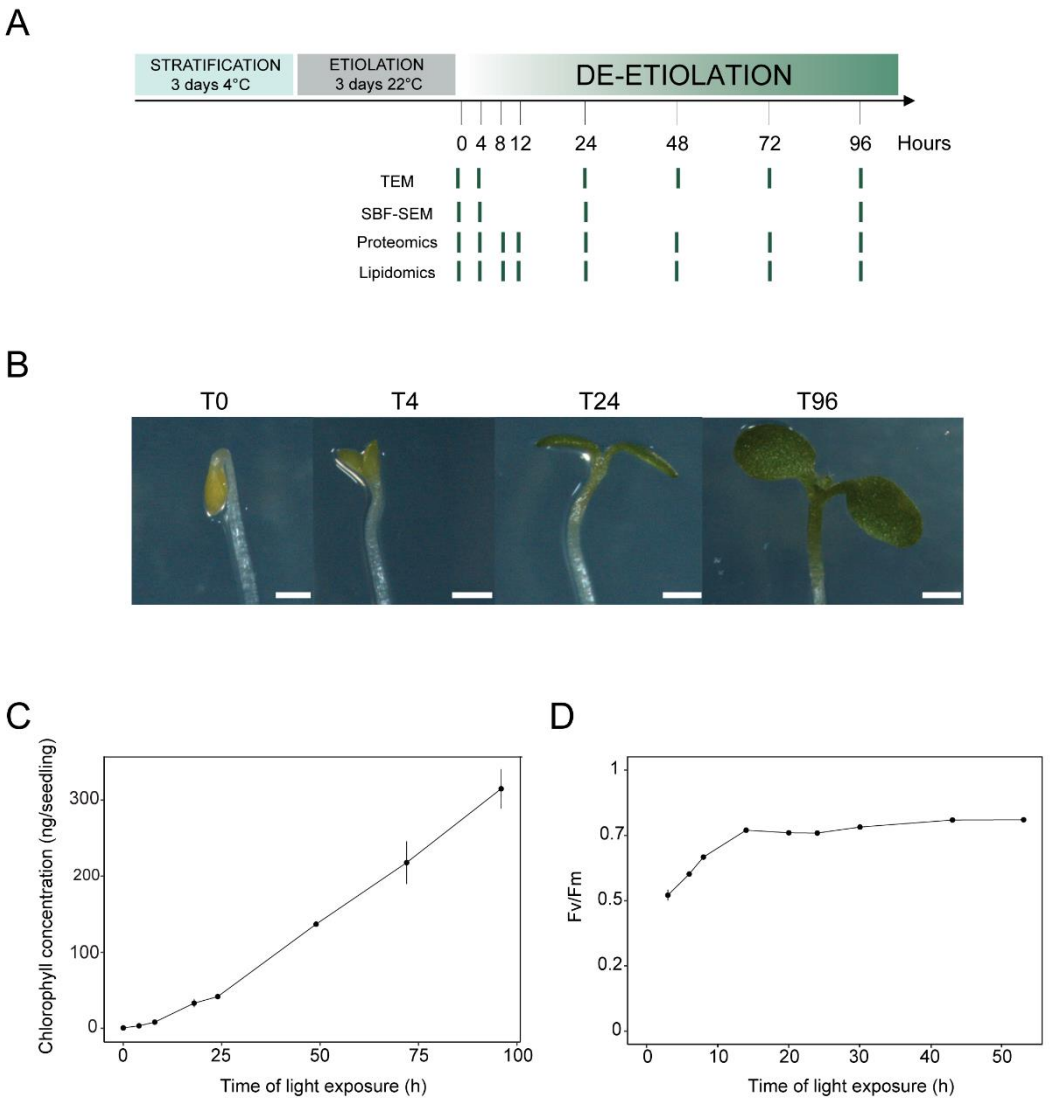

Figure 1: Photosynthesis onset during de-etiolation. (A) Scheme of the experimental design. Seeds of *Arabidopsis thaliana* (Columbia) sown on agar plates were stratified for three days at 4°C and then transferred at 22°C in the dark. After three days, etiolated seedlings were exposed in continuous white light (40 µmol/m^2/s) and harvested at different time points during de-etiolation. Selected time points used for different analyses are indicated. (B) Cotyledon phenotype of etiolated seedlings (T0) after 4 (T4), 24 (T24) and 96 (T96) h in continuous white light. Scale bars: 0.5 mm. (C) Chlorophyll quantification at different time points upon illumination. Error bars indicate ± SD (n=3). (D) Maximum quantum yield of photosystem II (Fv/Fm). Error bars indicate ± SD (n=4). Where absent, error bars could be smaller than the symbols (black dots).

2.2.2 Ultrastructural changes precede the establishment of optimal photosynthetic activity level

The photosynthetic machinery is embedded in the thylakoid membranes, which develop upon illumination from prolamellar bodies and prothylakoids present in etioplasts. We determined the dynamics of thylakoid biogenesis during etioplast to chloroplast transition by observation of chloroplast ultrastructure in cotyledons using Transmission Electron Microscopy (TEM) (Figure 2). Plastids present in cotyledons of etiolated seedlings displayed the typical etioplast ultrastructure (Figure 2A). The intra-plastidial structures of the etioplast consisted of the paracrystalline prolamellar body (PLB and tubular prothylakoids (PT) (Kowalewska et al., 2016; Liang et al., 2018; Rudowska et al., 2012). The observed PLBs constituted of hexagonal units has a diameter of 0.8 - 1 µm (Figure 2E). During the first 4 h of illumination the highly structured PLBs progressively disappeared while thylakoid lamellae were formed (Figure 2B). The lamellae were not sharply defined and their thickness varied between 15 and 70nm (Figure 2F). After 24 h the density of lamellae per chloroplast was higher than after 4 h due to an increase in lamellar length and number. In addition, appressed regions corresponding to developing granal stacks appeared (Fig 2C and G). These early granal stacks consisted of 2 to 6 lamellae with a thickness of 13 nm (Supplemental Figure 2). In addition, starch granules were present after 24h supporting the notion that these chloroplasts are photosynthetically functional and able to assimilate carbone dioxide (CO_2). After 96 h of light exposure, thylakoid membrane organization was visually similar to that seen after 24 h, but with more layers per grana (up to 10 lamellae per grana; Figure 3D and H). In addition, the thickness of the single lamellae increased by 2 to 3 nm compared to the thickness at T24 (Supplemental Figure 2). The major differences observed between T24 and T96 were increases in the size and number of starch granules and the overall chloroplast size. The average length of the etioplasts (estimated by measuring the maximum distance on individual slices) was 2 µm (+/- 0.9, n=10) in the dark (T0), while the chloroplasts were 6 µm (+/- 1.62, n=10) in length after 96h of light (T96) (Supplemental Table1). Collectively, these data show that photosynthetically functional thylakoid membranes form very rapidly during the first 24 h of illumination implying that there are efficient mechanisms for their assembly and structural organization. Subsequent changes seem to involve the

expansion of pre-existing structures (i.e. lamellae length and grana size) and the initiation of photosynthetic carbon fixation (reflected by starch content).

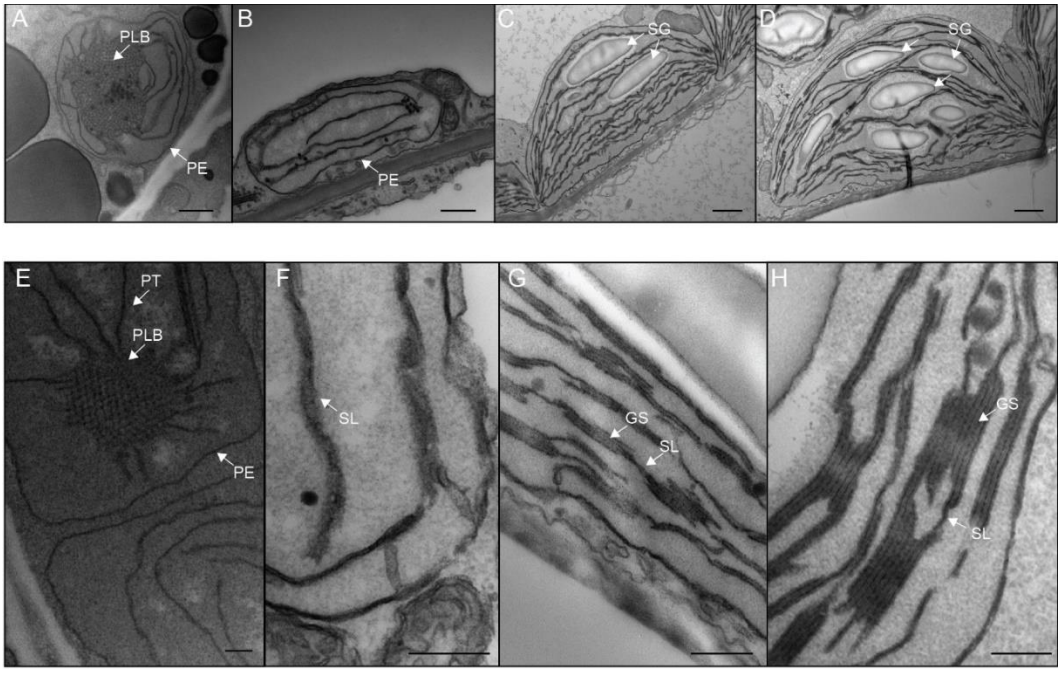

Figure 2: Qualitative analysis of chloroplast ultrastructure during de-etiolation. Transmission electron micrographs (TEM) of cotyledon cells of 3-day-old dark grown *Arabidopsis thaliana* (Columbia) seedlings illuminated for 0 (A and E), 4 (B and F), 24 (C and G) and 96 (D and H) h in continuous white light (40 µmol/m^2/s). (A-D) Scale bars: 500 nm, (E-H) Scale bars: 200 nm.

2.2.3 Quantitative analysis of total thylakoid surface dynamics during chloroplast development

In order to visualize entire chloroplasts and thylakoid networks in 3 dimensions (3D), and obtain quantitative knowledge of the total thylakoid surface during chloroplast development, we prepared and imaged cotyledons at different developmental stages by SBF-SEM. Sequential micrographs of the sample blockface were acquired after removal of a 50-nm layer via the ultramicrotome incorporated into the 3View microscope stage. This yielded a voxel size between 3 and 6 nm in the X-Y plane and 50 nm in Z plane, with total image depth of up to 200 µm. SBF-SEM image stacks were processed by 3D Amira 6.7 software (Figure 3 A-D). Prolamellar bodies, thylakoids and envelope membranes were selected using a semi-automatic tool called Segmentation Editor. From the segmented images, triangulated 3D surfaces were created (Figure 3 E-N and videos 1-4). In SEM images, the resolution was not sufficient to visualize the separation of the lamellae in the grana of the T24 and T96 chloroplasts. To improve the accuracy of the surface of thylakoid quantification, a custom-made script was run using Python in Rhinoceros 6 program (Supplemental Figure 3). Lamellae of each grana stack were segmented with a specific thickness (13 nm for 24 h chloroplasts and 16 nm for 96 h chloroplasts) corresponding to the measurements made on high-resolution TEM images (Supplemental Figures 2 and 3). Segmented images (Supplemental Figure 3) were used in Amira for 3D reconstruction and quantification.

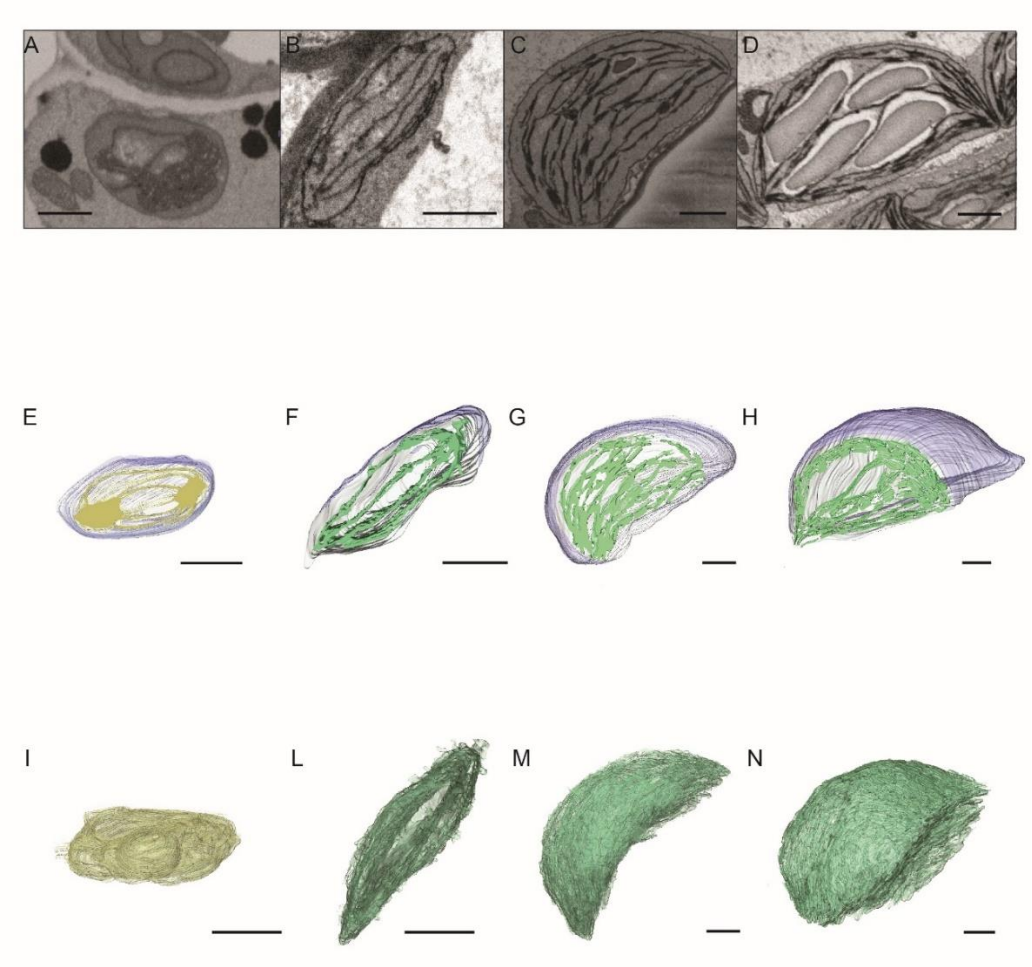

Figure 3: 3D reconstructions of chloroplast thylakoid network during de-etiolation. (A-D) Scanning electron microscopy (SEM) micrographs of representative etio- and chloroplast from 3 day-old dark grown *Arabidopsis thaliana* seedlings illuminated for 0(A), 4(B), 24(C) and 96(D) h in continuous white light (40 µmol/m^2/s). (E-H) Partial 3D reconstruction of thylakoid membranes (green) and envelope (blue) at 0(E), 4(F), 24(G) and 96(H) h. Z-depth of thylakoid membrane reconstruction corresponds to 0.3µm (E), 0.7µm (F) and 0.15µm (G and H). (I-N)Total 3D reconstruction of thylakoid membrane of an etioplast (I), or chloroplast after 4(L), 24(M) and 96(N) h in continuous white light (40µmol/m^2/s). Scale bars = 1µm.

This approach provided a complete quantification of the thylakoid surface and volume (Figure 4). Using 3D reconstruction of the thylakoid network for 3-4 developing chloroplasts for each developmental stage, quantitative data such as chloroplast volume and membrane surfaces were extracted using the Label Analysis module on Amira software (Figures 4A and B and Supplemental Table1).

The total chloroplast volume increased from T4 to T96 (Figure 4A and Supplemental Table1). Plastid shape switched from ovoid at T0 and T4 to hemispheric at T24 and T96 (Figure 3 I-N).

We observed a drastic switch from prolamellar body to thylakoid membrane in the first 4h of illumination: the typical structure of the prolamellar body connected to prothylakoids disappeared leaving only elongated lamellar structures (Figure 3E-F and videos 1 and 2). After 24 h and 96 h, thylakoid membranes showed a more organized structure and large spaces occupied by starch granules were observed (Figure 3G-H and videos 3 and 4). The chloroplast maintained the same shape while its volume doubled between 24 h and 96 h (Figure 3D and Figure 4A).

The thylakoid surface area changed from 65 μm^2 (SD +/- 24.6) to 1245 μm^2 (SD +/- 94) between 4h and 24h of illumination; an increase of 20-fold (Figure 4B and Supplemental Table 1). This thylakoid surface increased in parallel with a 7-fold increase chloroplast volume (8.21 to 57.17 μm^3) (Figure 4A and Supplemental Table 1). Between 24 h and 96 h of illumination, the thylakoid surface are increased by only 33% (Figure 4B), which could be attributed to both stroma and grana lamellae (Figure 4B). Quantification of the envelope surface area indicated that the ratio of the thylakoid to envelope surface area increased drastically from 4h to 24h of de-etiolation, but decreased slightly between 24 h and 96 h (Supplemental Table 1).

Again, our observations indicated that chloroplast development could be separated into two phases; a first phase reflected by qualitative changes (i.e structure establishment and reorganization of the thylakoid network architecture) and a second phase (starting at T24) during which thylakoid surface increased due to expansion and stacking of lamellae. In order to reveal whether these changes relied on specific temporal molecular changes, we analysed the process at the molecular level focusing on proteins and lipids that constitute the thylakoid membrane.

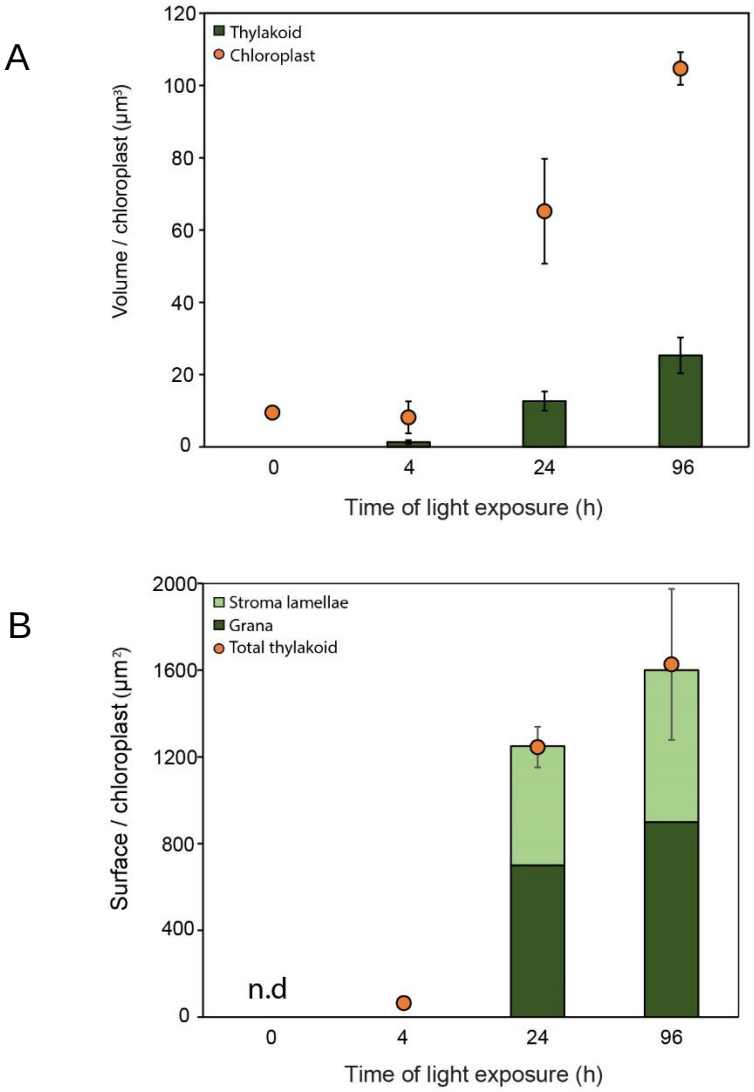

Figure 4: Quantitative analysis of chloroplast volume and thylakoid surface during de-etiolation. Quantification of total volume (A) and thylakoid surface per chloroplast (B) using 3-day-old dark grown *Arabidopsis thaliana* (Columbia) seedlings illuminated for 0, 4, 24 and 96 h in continuous white light (40 µmol/m²/s). n.d = not determined. Morphometric data were quantified by Labels analysis module of Amira software. Error bars indicate ± SD (n=3).

2.2.4 Dynamics of plastid proteins related to thylakoid biogenesis

Full proteome analysis was performed to reveal the dynamics of protein accumulation during de-etiolation. Total proteins were prepared from 3 d-old etiolated seedlings exposed to light for 0 to 96 h (eight time points; Figure 1A) and quantified by label-free shot-gun mass spectrometry. For relative quantification of protein abundances between different samples, peptide ion abundances were normalized to total protein (see Materials and Methods). We further considered only proteins that were identified with a minimum of two different peptides (with at least one being unique; see Methods for information on protein grouping), resulting in the robust identification and quantification of more than 5000 proteins. Fold changes of protein abundances between two time points were regarded significant if their adjusted p-value (i.e. the q-value) was < 0.01.

Very few changes occurred during the first 12 h of illumination (Supplemental Dataset 1). At 8 h, we observed a decrease of abundance for the photoreceptor cryptochrome 2, while accumulation of three chlorophyll a/b binding proteins increased (AT1G44575 =PSBS; AT4G10340= LHCB5; AT1G15820= LHCB6). A drastic change of proteome composition occurred within 24 h, with 467 proteins showing a significant increase (FC>2) in abundance compared with the etiolated stage, and 150 showing a significant decrease (FC<0,5). Not surprisingly, proteins related to photosynthesis were particularly common among the 100 most upregulated proteins and included proteins constituting the core and antennae of photosystems and proteins involved in carbon fixation (Supplemental Dataset 1).

In order to analyse the dynamics of the plastidial proteome, we selected proteins predicted to localize to the plastid (consensus localization from SUBA4 (Hooper et al., 2017). Global heatmap of all 1112 potential plastidial proteins revealed different accumulation patterns (Supplemental Dataset 2 and Supplemental Figure 4). Hierarchical clustering revealed a separation into 6 main clusters. Cluster 1 (purple) was constituted by proteins whose relative amounts decreased during de-etiolation. Cluster 2, 5 and 6 (pink, green, and dark green, respectively) were constituted by proteins whose relative amounts increased during de-etiolation, but differed with respect to the amplitude of variations. Proteins in cluster 2 and 6 displayed the largest amplitude of differential accumulation. Gene ontology (GO) analysis (Mi et al., 2019)

indicated a statistically significant overrepresentation of proteins related to light reaction of photosynthesis in these two clusters (Supplemental Dataset 2). Underrepresentation of organic acid metabolism and in particular carboxylic acid metabolism characterized cluster 2. Levels of proteins in cluster 3 were only moderately changed over the course of the de-etiolation and in contrast with proteins in cluster 2, overrepresentation of carboxylic acid biosynthesis and underrepresentation of photosynthesis light reactions process were clear features of this cluster. No biological processes were significant over or underrepresented in clusters 1, 4 and 5. In order to specifically analyze the dynamics of proteins related to thylakoid biogenesis we selected proteins constituting protein complexes located in thylakoids (complexes constituting the electron transport chain, ATP synthase complex), proteins involved in chloroplast lipid metabolism, chlorophyll synthesis, and protein import into the chloroplast and represented their pattern of accumulation during the de-etiolation (Figure 5). As already indicated by the global heatmap all photosynthetic related proteins increased in abundance through the course of de-etiolation. Our hierarchical clustering did not reveal any particular clustering per complex (Figure 5A). Only few chloroplast localized proteins related to lipid biosynthesis were present in our list. Among the 8 detected proteins, two separated from the others based on their abundance pattern. Fatty acid binding protein 1 (FAB1) and fatty acid desaturase 7 (FAD7) levels of expression increased only between 72 and 96 h while all the other protein selected were gradually accumulated over the de-etiolation course (Figure 5B). Synthesis of chlorophyll precursors is initiated already in the etioplast and is blocked at the level of protochlorophyllide synthesis, with PORA accumulating to high levels in the etioplast but in inactive form, and activated but downregulated at the protein level upon light exposure (Blomqvist et al., 2008; Runge et al., 1996; Von Wettstein et al., 1995). The amount of all detected proteins of this pathway was increased upon illumination, except PORA which clearly decreased and separated from other chlorophyll-related proteins (Figure 5C). We also selected proteins involved in protein import in chloroplasts, focusing on TOC-TIC machinery (Figure 5D), since this is the major route for plastid protein import and essential for chloroplast biogenesis (Kessler and Schnell, 2006). Several TOC preprotein receptors have been identified and are proposed to display differential specificities for preprotein classes (Bauer et al., 2000; Bischof et al., 2011). The composition of plastid

import complexes varies with developmental stages and in different tissues, thereby adjusting the selectivity of the import apparatus to the demands of the plastid and influencing its proteome composition (Demarsy et al., 2014; Kubis et al., 2003). Accordingly, the TOC receptors TOC120, TOC132 which are important for the import of proteins in non-photosynthetic tissues were not differentially accumulated or downregulated when comparing etioplasts and fully-developed chloroplasts (compare T0 and T96). They formed a cluster separated from other components of the plastid machinery, namely TOC159 the receptor associated with large scale import of proteins in chloroplasts. The general import channel TOC75 (TOC75 III) was expressed at the same levels throughout the de-etiolation, reflecting its general role in protein import. All other components clustered with TOC159 and displayed a gradual increase in accumulation over the course of de-etiolation. This is interesting because most of these components have not been reported to confer selectivity to the import machinery, and suggests an overall increase of chloroplast protein import capacity.

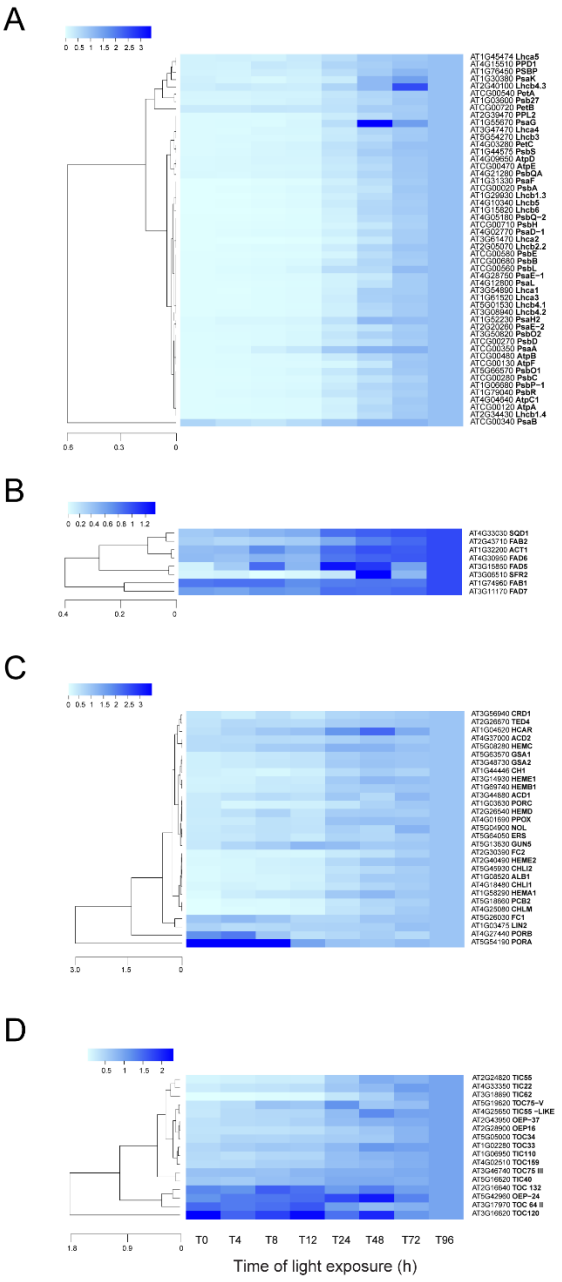

Figure 5: Dynamics of plastid proteins accumulation during de-etiolation. Hierarchical clustering (Euclidean, average linkage) of normalized protein abundance for photosynthetic related proteins (A), galactolipid metabolism (B), chlorophyll metabolism (C) and protein import related proteins during the de-etiolation (D). Protein abundance was quantified by shot-gun proteomics and heatmap colors indicate the log2 Fold change (average of 3 of 4 replicates) of each selected protein at each time point of the de-etiolation (T0 to T96), relative to the last time point (T96).

In order to validate and complement our proteomic data, immunoblots were performed to detect and quantify representative proteins of the photosynthetic complexes. Overall, immunoblot and proteomics provided similar results (Figure 6 and Supplemental Figure 5). PsbA and PsbD (PSII reaction center core), PsbO (Oxygen Evolving Complex), and Lhcb2 (outer antenna complex) proteins were not detected at time 0 but were detectable in seedlings exposed to 4 h of illumination and gradually increased. Accumulation of the PSI proteins PsaC and PsaD, as well as the Cyt b_6f complex protein, PetC, started later and were detectable only after 12h of illumination (Figure 6A). Interestingly, AtpC (ATP synthase complex) was already detected in the etioplast, as described previously (Plöscher et al., 2011). Other proteins were selected as markers of etioplast to chloroplast transition. As expected, ELIP2 (Early Light Induced Protein2) transiently accumulated upon the dark to light transition (Figure 6A) (Kimura et al., 2003). As in the proteome analysis, PORA accumulated in etiolated seedlings (T0) and disappeared progressively upon light exposure (Runge et al., 1996). Absolute quantification was carried out for PsbA, PsaC and PetC proteins using recombinant proteins as standards (Figure 6B - C and Supplemental Figure 5). Quantitative data (nmol/seedling) were obtained and normalized using the last time point (Figure 6C) to compare the dynamics of protein accumulation. In addition, the comparison of PsbA and PsaC (representative proteins of PSII and PSI, respectively) showed that after 96h of illumination, PsbA levels were about twice the PsaC levels (Figure 6B - C).

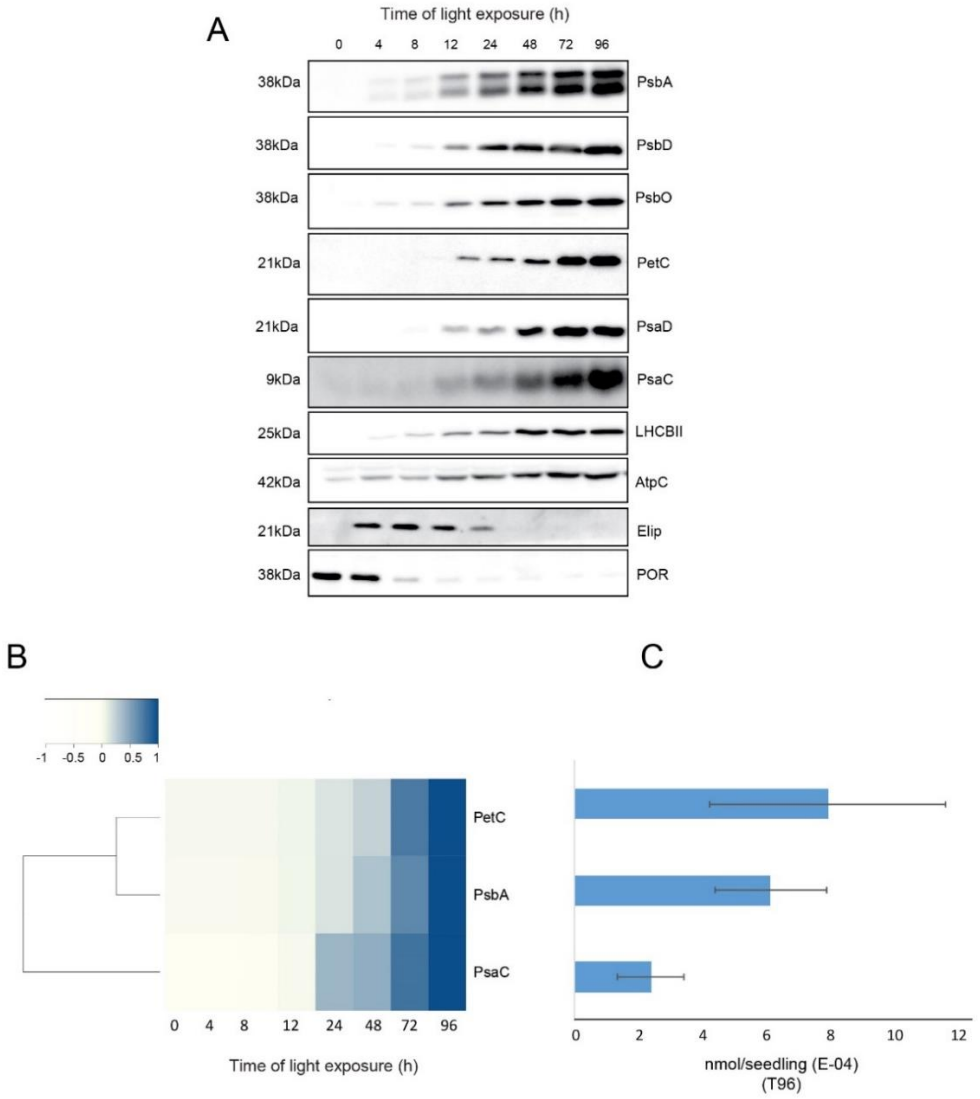

Figure 6: Dynamics of photosynthesis-related protein accumulation during de-etiolation. 3-day-old etiolated seedlings of *Arabidopsis thaliana* were illuminated for 0, 4, 8, 12, 24, 48, 72 and 96 h under white light (40 µmol/m^2/s). (A) Proteins were separated by SDS-PAGE and transferred onto nitrocellulose membrane and immunodetected with antibodies against PsbA, PsbD, PsbO, PetC, PsaD, PsaC, Lhcb2, AtpC, Elip (1 and 2) and POR (A,B and C) proteins. (B-C) Quantification of PsbA, PetC and PsaC during de-etiolation. Heatmap (left panel) was generated after normalization of the amount of each protein relative to the last time point (96). Right panel corresponds to the absolute quantification of proteins after 96 h of light exposure. Error bars indicate +/- SD (n=3).

2.2.5 Dynamics of chloroplast membrane lipids

Total lipids were extracted from seedlings collected at different time points of de-etiolation (0, 4, 8, 12, 24, 48, 72, 96 h), analysed by ultra-high pressure liquid chromatography –mass spectrometry (UHPLC-MS) and quantified against pure standards. We analyzed the quantity and kinetics of accumulation of 12 different species of galactolipids (Figure 7A - B). MGDG 18:3/16:3, MGDG 18:3/18:3, MGDG 18:3/16:1, DGDG 18:3/18:3 and DGDG 18:3/16:0 were the most abundant lipids detected at all time points. Accumulation of all galactolipids increased upon de-etiolation, however clustering analysis brought to light two distinct kinetic patterns. One group displayed a leap between 8 and 12 h, while the other group showed a more gradual increase over the time course (Figure 7C). Interestingly, the two clusters separated the lipids according to the two pathways described for galactolipid synthesis; the eukaryotic and prokaryotic pathways (ER and PL-pathway, respectively) (Figure 7A and B) (Marechal et al., 1997; Ohlrogge and Browse, 1995). During early stages of de-etiolation (from T0 to T24) we observed an incremental accumulation of MGDG and DGDG galactolipids derived from ER-pathway while galactolipids from the PL-pathway started to accumulate after one day of light exposure (T24) (Figure 7A-B). The MGDG/DGDG ratio decreased between 0 and 8 h of de-etiolation. This was associated with the transition from prolamellar body (hexagonal lipid phase) to thylakoid membrane (lamellar structure) (Bottier et al., 2007). After 8 h, the ratio started to increase gradually, becoming constant at the last two time points (T72 and T96; Figure 7D).

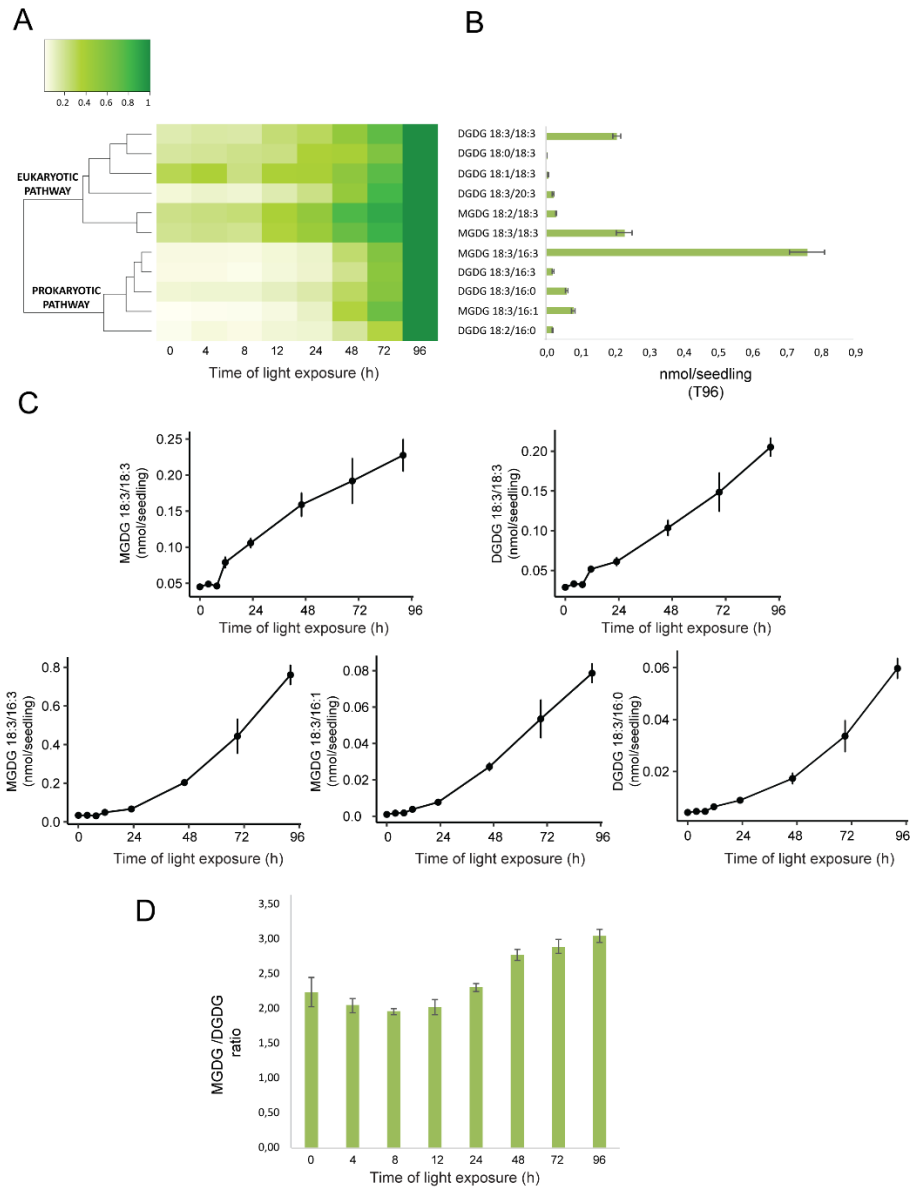

Figure 7: Dynamics of galactolipid accumulation during de-etiolation. (A) Heatmap representation of galactolipids (MGDG and DGDG) during de-etiolation. Samples were normalized to the last time point (96 h of illumination). (B) Absolute quantification expressed in nmol/seedling. (C) Absolute quantification (nmol/seedling) of the most abundant chloroplast galactolipids MGDG (MGDG 18:3/18:3, MGDG 18:3/16:3, MGDG 18:3/16:1) and DGDG (DGDG 18:3/18:3, DGDG 18:3/16:0) at different time points upon illumination of 3-day-old etiolated seedlings. Error bars indicate ± SD (n=4). (D) The MGDG/DGDG ratio was calculated using all 12 species of galactolipids detected during the de-etiolation. Error bars indicate ± SD (n=4).

2.2.6 Identification of a chloroplast division phase

We observed a massive increase of accumulation of photosynthetic proteins and galactolipids between 24 and 96 h of de-etiolation, corresponding to changes greater than 2-fold in the levels of all major chloroplast proteins and lipids between these two time points (Figures 6 and 7). Intriguingly, the total thylakoid surface per chloroplast increased only by 33 % between 24 and 96 h of de-etiolation, (Figure 4B and Supplemental Table 1). We reasoned that the increase of chloroplast proteins and lipids between 24 and 96 h of illumination could be explained by an increased number of chloroplasts (per cell and thus per seedling) and thus total thylakoid surface per seedling. We therefore determined the number of chloroplasts per cell as well as the cell number and volume for each developmental stages analyzed by SBF-SEM (0, 4, 24 and 96 h of de-etiolation) and by confocal microscopy for intermediary time points (between 24 and 96 h) (Supplemental Figure 6). The number of chloroplasts per cell was not different from 4 h (22 +/-6) to 24 h (26 +/-6) but increased sharply (4-fold increase) between 24 (26 +/-6) and 96 h (112 +/-29) of illumination, concomitantly with cell expansion (Figure 8A and B) indicating that two rounds of chloroplast division occurred between 24 and 96 h. Immunoblot analysis of FILAMENTOUS TEMPERATURE-SENSITIVE (FtsZ1, FtsZ2-1and FtsZ2-2) proteins showed that these key components of the chloroplast division machinery were already present during the early time points of de-etiolation. A strong increase of their accumulation was observed between 24 and 48 h, consistent with the idea that activation of chloroplast division takes place after 24 h of illumination, leading to an increase of the chloroplast number (Figure 8C-D). However, levels of ACCUMULATION AND REPLICATION OF CHLOROPLAST 5 (ARC5) protein, another key component of the chloroplast division machinery, clearly increased between 8 and 12 h of de-etiolation presumably reflecting the assembly of the chloroplast division machinery prior to its activation and the increase of chloroplast numbers per cell. To test whether there is a correlation between chloroplast division and volume or developmental stage, we measured the volume of chloroplasts under division at T24 and T96, using images acquired by SBF-SEM (Figure 8E) and confocal microscopy (Figure 8F). The average size of dividing chloroplasts at 24 h of illumination was higher than the median size of all chloroplasts (98 μm^3 on average compared to 55 μm^3). The volume of dividing

chloroplasts at T96 was always higher than 100 μm^3 although some of the chloroplasts in the cells were smaller (Figure 8E-F). Altogether, this indicates that division of developing chloroplasts takes place only after chloroplast had reached a certain volume.

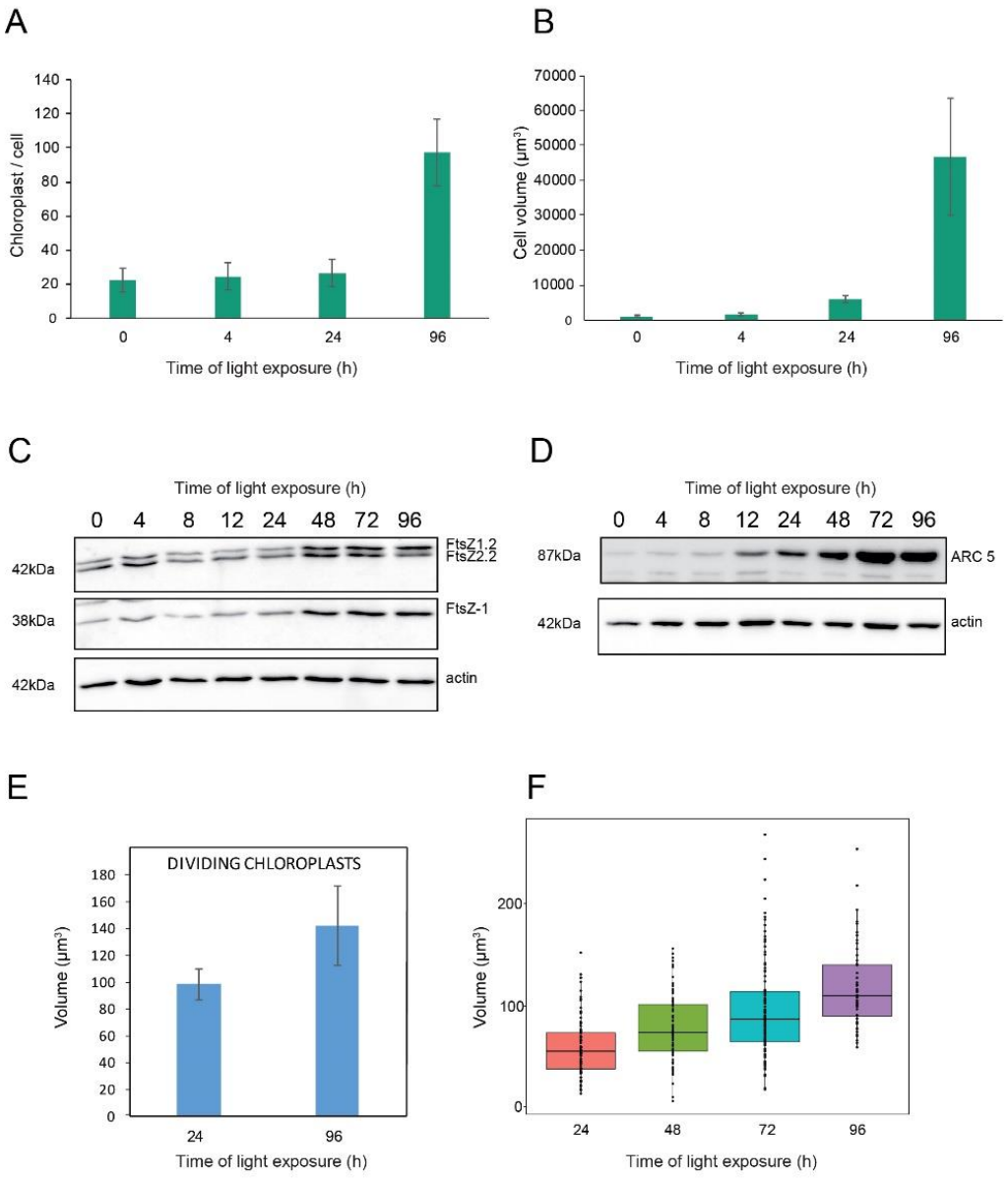
A
Chloroplast / cell
140
120
100
80
60
40
20
0
0
4
24
96
Time of light exposure (h)
B
Cell volume (µm³)
70000
60000
50000
40000
30000
20000
10000
0
0
4
24
96
Time of light exposure (h)
C
Time of light exposure (h)
0 4 8 12 24 48 72 96
42kDa
FtsZ1.2
FtsZ2.2
38kDa
FtsZ-1
42kDa
actin
D
Time of light exposure (h)
0 4 8 12 24 48 72 96
87kDa
ARC 5
42kDa
actin
E
DIVIDING CHLOROPLASTS
Volume (µm³)
180
160
140
120
100
80
60
40
20
0
24
96
Time of light exposure (h)
F
Volume (µm³)
200
100
0
24
48
72
96
Time of light exposure (h)

Figure 8: Relation between chloroplast number increase and chloroplast volume. (A-B) Chloroplast number and cell volume in cotyledons of 3-day-old dark grown *Arabidopsis thaliana* seedlings illuminated for 0, 4, 24 and 96 h in continuous white light (40 µmol/m^2/s). (A) Chloroplasts were counted in 6 cells at the time points 0 and 4 h, in 7 cells at the time point 24 h and in 5 cells at the time point 96 h. Error bars indicate SD ± (n=5 or 6 or 7). (B) Cell volume was quantified by the Labels analysis module of Amira software. Error bars indicate SD ± (n=5 or 6). (C) and (D) Total proteins were extracted from seedlings exposed to light for 0 to 96 h, separated on SDS - PAGE and transferred onto nitrocellulose. Proteins involved in plastid division (C: FtsZ and D: ARC5) and loading control (actin) were detected using specific antibodies (FtsZ2 recognizes both FtsZ2-1 and FtsZ2-2). (E) Volume of dividing chloroplast at the time points 24 and 96 h. Error bars indicate SD ± (n=4). (F) Box plot of total volume of single chloroplasts quantified at 24, 48, 72 and 96 h of de-etiolation. Each box corresponds to the distribution of a chloroplast population analyzed using confocal stacks and SBF-SEM stacks (Supplemental Figure 6). T24=88 chloroplasts, T48=69 chloroplasts, T72=107 chloroplasts and T96=51 chloroplasts.

2.2.7 Model of thylakoid surface expansion over time using the molecular data

During de-etiolation, thylakoid surface increased with the accumulation of galactolipids and photosynthetic proteins, leading to the formation of functional chloroplasts. To determine the thylakoid membrane surface area per seedling (Surface /seedling) and expansion over time, we first calculated the surface area occupied by the main galactolipids (MGDG and DGDG) and photosynthetic complexes (PSII, cyt b_6f and PSI) per seedling (Supplemental Table 3).

Equation 1:

$$Surface/seedling = nmol/seedling * N * nm^2 \ per \ molecule$$

Quantitative data of MGDG, DGDG, PsbA, PetC and PsaC (nmol/seedling) obtained from lipidomic and immunological analysis (Figures 6 and 7) were converted into number of molecules/seedling using the Avogadro constant (*N*). In order to calculate the surface exposed to the stroma and account for the lipid double layer of the membrane, corresponding values of lipids (Figure 4B) were divided by 2. In addition, the lipid values were corrected by subtracting the portion of lipids incorporated in the envelope and not in the thylakoids (Supplemental Table 3 and Supplemental Dataset 3).The surface occupied by molecule of MGDG and DGDG as well as the surface of PSII, Cyt b_6f and PSI photosynthetic complexes (nm^2 per molecule, corresponding to surface exposed to the stroma) were retrieved from literature (Supplemental Table 2). Specifically, we used the minimal molecular area of MGDG and DGDG (Bottier et al., 2007). To quantify the surface occupied by the galactolipids and photosynthetic complexes in thylakoids per seedling, the number of molecules/seedling of galactolipids was multiplied by the corresponding molecule surface area while the number of molecules per seedling of PsbA, PetC and PsaC, which are subunits of PSII, Cyt b_6f and PSI respectively, were multiplied by the surface of the corresponding complex (see Supplemental Table 2).

Finally, thylakoid surface (S) per seedling was the sum of the surface occupied by MGDG, DGDG and photosynthetic complexes (PS) per seedling plus an ε term, corresponding to compounds such as other lipids (e.g. sulfoquinovosyldiacylglycerol,

plastoquinone), or protein complexes (ATP synthase and NDH) that were not quantified

Equation 2:

$$\boldsymbol{S}\_thylakoid(t)/seedling = (\boldsymbol{S}\_MGDG(t) + \boldsymbol{S}\_DGDG(t) + \boldsymbol{S}\_PS\,(t) + \varepsilon)/seedling$$

Omitting the unknown ε factor, we plotted the surface of thylakoid calculated for each time point where quantitative molecular data were available (0, 4, 8, 12, 24, 48, 72 and 96 h) as a function of the time of light exposure (Supplemental Figure 7). The best fitting curve corresponded to a S-shaped logistic function, characterized by a lag phase at early time points (0-8 h), followed by a phase of near-linear increase, and a final plateau at the latest time points (72-96 h). To model this relation, a four-parameter logistic non-linear regression equation was used to describe the dynamics of the total thylakoid surface over time (Supplemental Figure 7).

2.2.8 Superimposition of molecular and morphometric data

We compared the values of thylakoid surface obtained with the model based on molecular data, with the values obtained from the morphometric analysis (Figure 9). The total thylakoid surface per seedling (S_thylakoid_morpho) was calculated by multiplying the thylakoid surface (S_thylakoid) per chloroplast obtained by morphometrics (Figure 4B) by the number of chloroplasts (nb. cp) per cell (Figure 8A) and the number of cells (nb. cells) per seedlings for each time point (t)

Equation 3:

$$\boldsymbol{S}\_thylakoid\_morpho(t)/seedling = \boldsymbol{S}\_thylakoid(t)/chloroplast * nb.cp(t)/cell * nb.cells(t)/seedling$$

We estimated the number of cells per seedling by measuring the total volume occupied by palisade and spongy cells cotyledon (that corresponded to the 50% of the total cotyledon volume) (Supplemental Figure 8 and Supplemental Dataset 4) and dividing

by the average cell volume quantified by Amira software (Figure 8B). As reported previously (Pyke and Leech, 1994), cell number was constant during cotyledon development. We estimated this number at 3200 mesophyll and palisade cells per seedling at T24 and T96 (Supplemental Figure 8 and Supplemental Dataset 4). The surface of the thylakoid membrane quantified by the morphometric approach was also estimated at time point T4 assuming that the number of cells per cotyledon remained similar between 4 and 24 h. We compared the thylakoid surface predicted by our mathematical model to the surface estimated experimentally with our 3D thylakoid reconstruction and morphometric measurements (Figure 9 and Supplemental Table 1). As shown in Figure 9, total surface area of thylakoid per seedling determined by the two approaches were very similar for the 4, 24 h time points while showed an important difference at the last time point 96 h.

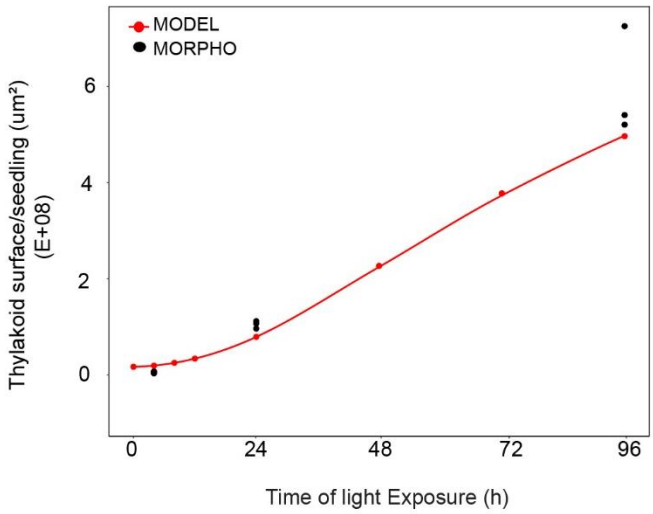

Figure 9: Superimposition of thylakoid surface per seedling obtained from morphometric analysis and mathematical model. Thylakoid surface per seedling was estimated using quantitative data from 3View analysis ("MORPHO" black dots at 4, 24 and 96 h of light exposure; and see Figure 4 and Supplemental Table 1) and model generated using the quantitative data from proteomics and lipidomics ("MODEL" red line at 0, 4, 8,12, 24, 48, 72, and 96 h of light exposure and Supplemental Table 1).

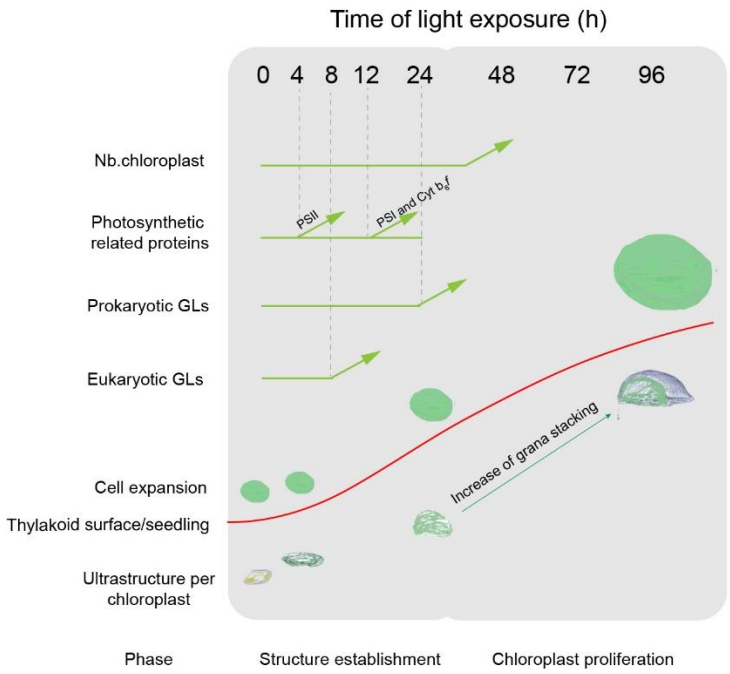

Figure 10: Summary of the changes occurred during the de-etiolation process in *Arabidopsis thaliana* seedlings. The timing is divided in two phases «Structure Establishment Phase» which is correlated with the disassembly of the PLB and the gradual formation of the thylakoid membrane as well as the initial increase of eukaryotic (after 8 h) and prokaryotic (after 24 h) galactolipids and photosynthetic related proteins (PSII subunits at 4 h, PSI and cyt b_6f at 12 h). The second phase called «Chloroplast Proliferation Phase» is associated with the increase of the chloroplasts in concomitance with cell expansion and linear increase of prokaryotic and eukaryotic galactolpids and photosynthetic proteins. An increase of the grana stacking is observed in the chloroplast ultrastructure. The red curve (retrieved from the Figure 9) shows the dynamism of the thylakoid surface /seedling during the de-etiolation process.

2.3 Discussion

Here an overview of thylakoid biogenesis has been obtained through the analysis of 3D structures of entire chloroplasts in combination with proteomic and lipidomic analyses. A summary of the changes that occur during the de-etiolation process is shown in the Figure 10. The de-etiolation can be divided into two phases identified in our study. Structural changes (disassembly of the PLB and the gradual formation of thylakoid lamellae) as well as the initial increase of eukaryotic and prokaryotic galactolipids and photosynthetic proteins (PSII, PSI and cyt b_6f) occurred during the "Structure Establishment Phase" while the increase of the number of chloroplasts in concomitance with cell expansion were observed in the "Chloroplast Proliferation Phase". Collection of quantitative data allowed us to create a mathematical model of the expansion of the thylakoid membrane and describe this process during de-etiolation.

2.3.1 A set of 3D reconstructions of whole chloroplasts by SBF-SEM

In contrast to electron tomography, which is limited in the volume of observation, SBF-SEM allows us to acquire ultrastructural data from large volumes of mesophyll tissue, and generate 3D reconstructions of entire cells and chloroplasts (Figure 3 and Supplemental Figure 6). SEM image resolution was sufficient to visualize stromal lamellae and contours of grana, while the segmentation of the grana in different lamellae was simulated according to our own TEM analysis and literature data (Supplemental Figure 2 and 3). This previously untried approach allowed us to obtain quantitative data of chloroplast and thylakoid structure at different developmental stages during de-etiolation of Arabidopsis. At the latest time point of our analysis (96 h of illumination), the total surface area of thylakoids present in the seedling cotyledons was 582 mm^2 (see values in Supplemental Table 1 for calculation) representing about 300 times the surface area of the cotyledons at this developmental stage (surface area of adaxial side of two cotyledons estimated at 2 mm^2). This is consistent with the estimation made previously regarding the surface area of the thylakoids relative to the surface area of a leaf (Bastien et al., 2016; Demé et al., 2014). This emphasizes how

fast and efficient thylakoid biogenesis is during plant development, allowing plants to optimize their capacity to absorb light -their primary source of energy.

2.3.2 “Structure Establishment Phase”

The observation of TEM images and quantification of 3D chloroplast ultrastructure by SBF-SEM analysis indicated the importance of the first h of light exposure for the transformation of the etioplast into a chloroplast. The typical structure of the prolamellar body (PLB) connected with tubular prothylakoids (PTs) was replaced by lamellar thylakoids during the first 4 h. Measurements of PLB diameter and thylakoid length as well as thickness were comparable with literature values (Daum et al., 2010; Kirchhoff et al., 2011; Solymosi and Aronsson, 2013) indicating that these morphometric values are conserved between various model organisms. Thylakoid surface increased 20-fold between 4 and 24 h. Remarkably, photosystem II maximum quantum yield reached the optimal value (0.8) after 14 h of illumination, independently of the light intensity (Figure 1D and Supplemental Figure 1). This shows that photosystem II assembly occurs within the same period as thylakoid membrane formation and that photosynthesis is operational almost immediately upon greening.

Our proteomic and lipidomic analyses suggest that the ultrastructural changes rely on specific temporal molecular changes. The proteomic approach revealed the accumulation pattern of more than 5000 unique proteins over 8 time points covering de-etiolation. These data provide information not only for plastid development but also more widely on the light-regulated developmental processes (Supplemental Dataset 1). Our dataset is more exhaustive in terms of the temporal resolution and the number of unique proteins detected than previous reports on chloroplast differentiation and de-etiolation (Bräutigam and Weber, 2009; Plöscher et al., 2011; Reiland et al., 2011; Wang et al., 2006).

Here, we focused on chloroplast localized proteins and specifically proteins of the thylakoid membrane. According to the SUBA4 localization consensus, 1112 proteins were assigned to the plastid compartment, which covers about a third of the total plastid proteome (Ferro et al., 2003; Hooper et al., 2017; Kleffmann et al., 2007a). Our data suggest that the major ultrastructural changes that occur between 0 and 4h were probably mostly due to reorganization of pre-existing molecules rather than *de novo*

synthesis. These results are consistent with other studies reporting only minor increases in protein accumulation and translation during the initial steps of chloroplast differentiation (Dubreuil et al., 2018; Kleffmann et al., 2007a; Reiland et al., 2011). Gene Ontology analysis (GO) combined with expression pattern based hierarchical clustering highlighted that most photosynthesis-related proteins are globally coregulated (Supplemental Figure 4, clusters 2 and 6). However, targeted immunoblot analysis revealed different patterns of accumulation for specific photosystem subunits: PSI subunits were detected at later time point than PSII subunits, but thereafter PSI subunit accumulation was faster (Figure 6). Photosynthetic parameters kinetics were consistent with the sequential activation of PSII and PSI, with photochemical quenching indicating an increase of oxidation of the plastoquinone pool during the first 14 h (Supplemental Figure 1). This is consistent with data obtained in other systems used to study chloroplast development: in Arabidopsis cell cultures, during germination and development of Arabidopsis seedlings in the light, and in tobacco leaves upon reillumination after dark adaptation, PSI accumulation kinetics and activity differed from those of PSII (Armarego-Marriott et al., 2019; Dubreuil et al., 2018; Liang et al., 2018) . The molecular mechanisms underlying this differential accumulation are currently unknown. However it may be correlated with preferential localization of these protein complexes in specific thylakoid membrane domains (lamellae and grana, respectively) and the time taken to establish these domains during chloroplast development (i.e. with the grana appearing later than the stromal lamellae).

Chloroplast membranes have a specific composition that differs from the composition of other cell membranes. Galactolipids constituting the bulk of the thylakoid membranes, but are mostly absent from other membrane systems under growth conditions where phosphorus nutrient is not limited (Jouhet et al., 2007). MGDG and DGDG represent around 80% of the thylakoid membrane lipids. The absolute quantification of 12 types of MGDG and DGDG galactolipids (representing the major forms) revealed specific patterns of accumulation (Figure 7). Specifically, from T8 to T24 a gradual accumulation of MGDG and DGDG galactolipids derived from the ER-pathway (eukaryotic) was observed, while galactolipids from the PL- pathway (prokaryotic) started to accumulate after one day of light exposure (T24). These results reveal the different galactolipid compositions of etioplast and chloroplast: galactolipids from the ER-pathway are dominant in the etioplast, and those from the PL-pathway

are predominant in the chloroplast. As no significant changes in the lipid pattern was observed after 4 h of illumination, it appears likely that the emergence of prothylakoids relies on the existing lipids in the prolamellar body of the etioplast, as suggested also by (Armarego-Marriott et al., 2019). At later time points, galactolipids from both the ER and PL pathways constitute the lipid matrix of the thylakoid membrane. How the two galactolipid biosynthesis pathways are regulated during development and/or upon light treatment remains to be elucidated but we hypothesize that the PL -pathway gains traction after T24 when photosynthetic capacity has become fully established.

2.3.3 “Chloroplast Proliferation Phase”

Between 24 and 96 h of illumination, the thylakoid surface increased only by 33%. During this period, the thylakoid membranes acquired a more clearly defined organization of grana stacks (Figure 2). Although thylakoid surface was increased only by 33%, the chloroplast continued to enlarge at the same rate as the previous stages (0-24 h). This expansion of chloroplast volume may be due to the enlargement of extrathylakoidal spaces occupied by the emerging starch granules. These results suggest that large amounts of lipids and proteins are necessary to build up the thylakoid membrane during the first 24 h, while the increase of lipids and proteins between 24 and 96 h enables the expansion of already functional thylakoid membranes in preparation for chloroplast division. Indeed, chloroplast number per cell increased during de-etiolation and this increase depends on the division of pre-existing chloroplasts.

Both chloroplasts and mitochondria divide through the activity of supramolecular complexes that constitute the organelle division machineries (Yoshida, 2018). As the increase of chloroplast number was observed between 24 and 96 h of illumination, chloroplast division may correlate with developmental stage of the organelle. Components of the chloroplast division machinery (e.g. FtsZ and ARC5) were detectable in etioplasts but accumulated significantly during de-etiolation, as the number of chloroplasts per cell increased (Figure 8C and D). Interestingly, the capacity to divide appeared to correlate with a minimum chloroplast volume of about 100 μm^3 even at 24 h of illumination when the majority of the chloroplast were smaller (Figure 8E). Whether and how the size of chloroplast and the developmental stage can be

sensed in order to activate the chloroplast division machinery is unknown and requires further study.

2.3.4 A model of thylakoid expansion

Our mathematical model describing the expansion of the thylakoid area per seedling over time took into account the surface area occupied by the membrane lipids MGDG and DGDG as well as the major photosynthetic complexes (PSII, PSI and Cyt b_6f). We omitted some components that contribute to the total surface of the thylakoid membrane (e.g. protein complexes ATP synthase and NDH; the lipid sulfoquinovosyl diacyl glycerol; together grouped as "ε" in Equation 2), the predictions made by our model fits the surface estimated by SBF-SEM at 4-, 24 h while it doesn't fit the last time point at 96 h. This means that compounds used to generate the mathematical model appear to contribute most to the surface changes of thylakoid during de-etiolation in the very early biogenesis step (the structure establishment phase). In contrast, during the later stages of the de-etiolation (during the expansion phase), the contribution of other compounds omitted in our model is obviously required to build up thylakoid surface.

In our proteomics data (Supplemental Figure 4 and Supplemental Dataset 2) we revealed some proteins that increased between 24 and 96 h. We identified the FtsH protease (AT2G30950). FtsH proteases have a critical role during thylakoid biogenesis. In *Arabidopsis thaliana* they constitute a hetero-hexameric complex of four FtsH subunits, which is integrated in the thylakoid membrane (Kato and Sakamoto, 2018). Although the surface area of the FtsH complex is unknown in *Arabidopsis thaliana*, it can be considered one of the potential compounds that contribute to the thylakoid surface changes which were omitted from our mathematical model. Other proteins, such as the ones involved in carotenoid biosynthesis (AT3G10230) or fatty acid metabolism (AT1G08640) also increased significantly after 24 h suggesting a contribution on the "ε" factor.

One of the next challenges would be to test the model under different conditions in order to test how this biological system responds to internal (perturbing hormone concentrations, genetic modification of thylakoid lipid and protein composition) or

external factors (such as different quality of light). This could be instrumental to reveal new potential regulatory mechanism of thylakoid biogenesis and maintenance.

Upon de-etiolation, acquisition and increase of photosynthetic capacity relies on successful chloroplast biogenesis. At the cell level, this process is expected to be highly coordinated with metabolism and development of other organelles. Lipid synthesis involves lipid exchanges between chloroplast and Endoplasmic Reticulum. How do lipid trafficking is organized is not yet solved, but could require membrane contact sites between these two organelles (Michaud and Jouhet, 2019). Physical interaction between mitochondria and chloroplasts have been reported previously in diatoms (Bailleul et al., 2015; Flori et al., 2017). Whether such contact sites occur and is functional in plants has not been reported. However, this is expected e.g. based on the necessity of the chloroplast to exchange metabolites with mitochondria and peroxisomes to ensure activation of photorespiration concomitantly with photosynthesis. Study of membrane contact sites is an emerging field in cell biology (Scorrano et al., 2019). Analyzing the dynamics and functionality of contact sites between chloroplast membrane and other organelles, and general coordination of metabolism in plant cell during de-etiolation would be a next big question, that could be further addressed using the SBF-SEM stacks and our proteomic resource.

2.4 Materials and methods

Plant material and Growth conditions

Arabidopsis thaliana seeds (Columbia ecotype) were surface-sterilized with 70% ethanol/ 0.05% (v/v) Triton, then washed with 100% ethanol. Seeds were sown on agar plates containing 0.5 Murashige and Skoog salt mixture (MS, Duchefa) without sucrose. Following stratification in the dark for 3 days at 4°C, seeds were irradiated with 40 µmol.$m^{-2}s^{-1}$ for 2 h at 21 °C and then transferred to the dark for three days at 21°C. Etiolated seedlings were collected in the dark (0 h of light) and at selected time points (4, 8, 12, 24, 48, 72, 96 h) upon continuous white light exposure (40 µmol.m^{-2} s^{-1} at 21°C).

Photosynthetic parameters

Maximum quantum yield of photosystem II ($\Phi_{MAX}= F_V/F_M$) was determined using a Fluorcam (Photon Systems Instruments) with blue light LEDs (470 nm). Plants were dark-adapted for a minimum of 5 min before measurement.

Chlorophyll concentration

Chlorophylls were extracted in 4 volumes of dimethylformamide (DMF) (v/w) over-night at 4°C. After centrifugation, chlorophylls were measured using a NanoDrop™ instrument at 647 and 664nm. Chlorophyll contents were calculated according to Porra et al. (1989).

Transmission electron microscopy

Samples were fixed under vacuum (200 mBar) in 0.1 M cacodylate buffer (pH 7.4) containing 2.5% (w/v) glutaraldehyde, 2% (w/v) formaldehyde (fresh from paraformaldehyde) for 4h and left in the fixation solution until the next morning at 4 °C. The samples were then incubated in a metal solution containing 3% (w/v) potassium ferrocyanide and 4 mM calcium chloride in 0.1 M cacodylate buffer combined with an equal volume of 4% (w/v) aqueous osmium tetroxide (OsO_4) for 1 h, on ice. After the first heavy metal incubation, samples were rinsed with ddH2O and treated with 1% (w/v) thiocarbohydrazide solution for 1 h at 60° C. Samples were rinsed (ddH2O for 15 min) before the second exposure to 2% (w/v) aqueous solution of OsO_4 for 30 min,

at room temperature. Following this second exposure to osmium, tissues were placed in 1% (w/v) uranyl acetate (aqueous) and left overnight at 4°C. The samples were rinsed with H2O for 15 min, and placed in the lead aspartate solution for 30 min at 60°C. Samples were dehydrated in a series of aqueous ethanol solutions from 50% (v/v) to 100% and embedded in Durcupan resin by successive changes of Durcupan resin/acetone mixes, with the last imbibition in 100% Durcupan resin. Polymerization of the resin was conducted for 48 h at 60 °C (Deerinck et al., 2010). Ultrathin sections (70 nm) were cut using Ultrathin-E microtome (Reichert-Jung) equipped with a diamond knife. The sections were observed with Philips CM-100 electron microscopy operating at Sigma 60 kV.

Confocal analysis

To derive the chloroplast and cell volumes, 1-5 µm thick-sections of cotyledon cells were acquired with X10 and X40 oil immersion objectives using a LEICA TCS SP5 confocal laser scanning microscope. Chlorophyll was excited using a red laser (33%) and spectral detection channel was PMT3.

SBF-SEM

SBF-SEM was performed on Durcupan-resin embedded cotyledons for four time points of the de-etiolation T0, T4, T24 and T96. Overview of the mesophyll tissue and (≈600 images) zoomed stacks of the chloroplasts (≈300 images) have been acquired. Voxel size of zoomed stacks of T4 were 3.9 x 3.9 x 50nm, T24: 4.7 x 4.7 x 50nm, and T96: 5.6 x 5.6 x 50nm. Voxel size for overview of T0: 9.5 x 9.5 x 100 nm, T4: 19.3 x 19.3 x100 nm, T24: 4 x 4 x 200 nm and T96: 4.3 x 4.3 x 200 nm.

Segmentation, 3D reconstruction and surface and volume quantification

Segmentation and 3D reconstruction of 3View and confocal images were performed using Amira software (FEI Visualization Sciences Group). Specifically, prolamellar body, thylakoids and envelope membranes as well as the cells were selected using a semi-automatic tool called Segmentation Editor. From the segmented images, triangulated 3D surfaces were created using Generate Surface package. Quantification of morphometric data (Area 3D and volume 3D) was acquired using Label Analysis package.

Grana segmentation in Rhino

Grana structures acquired from SBF-SEM were selected in Amira. The grana selections were converted in line set view in Amira software using the Generate Contour line package. In order to complete the grana segmentation, the line set views were imported into the Rhinoceros program. Every grana was segmented in layers with a specific thickness and distance according to quantitative data collected (Supplemental Figure 2). After segmentation images were re-imported in Amira software in order to quantify surface area using the Label Analysis package.

Chloroplast number determination

Chloroplasts per cell were counted manually using the Image J software. From the same SBF-SEM stack, 5 and/or 6 cells were cropped at each time point (T0, T4, T24 and T96) to count the number of chloroplast per cell. From TEM images the number of chloroplasts / cell was determined at T24 (17 cells), T48 (12 cells), T72 (12 cells) and T96 (17 cells). TEM images were acquired from two independent experiments.

Liquid chromatography-mass spectrometry analysis and protein quantification

Preparation of peptides, liquid chromatography-mass spectrometry analysis and protein quantification

Etiolated seedlings were grown as described in section “Plant material and growth conditions”. At each time point, ca. 80 seedlings were pooled, frozen in liquid nitrogen and stored at -80°C until use. Frozen material was ground with mortar and pestle, and 40 – 80 mg of plant material used for protein and peptide preparation using the iST kit for plant tissues (PreOmics, Germany). Briefly, each sample was resuspended in 100 µl provided “Lysis” buffer and processes with High Intensity Focused Ultrasound (HIFU) for 1 min setting the ultrasonic amplitude to 65% to enhance solubilization. For each sample, 100 µg of protein were transferred to the cartridge and digested by adding 50 µl of the provided “Digest” solution. After 180 min of incubation at 37 °C, the digestion was stopped with 100 µl “Stop” solution. The solutions in the cartridge were removed by centrifugation at 3800 g, while the peptides were retained on the iST filter. Finally, the peptides were washed, eluted, dried and re-solubilized in 18.7 µL of solvent (3% (v/v) acetonitrile, 0.1% (v/v) formic acid).

Mass spectrometry (MS) analysis was performed on a Q Exactive HF-X mass spectrometer (Thermo Scientific) equipped with a Digital PicoView source (New Objective) and coupled to a M-Class UPLC (Waters). Solvent composition at the two channels was 0.1% (v/v) formic acid for channel A and 0.1% formic acid, 99.9% (v/v) acetonitrile for channel B. For each sample, 2 µL of peptides were loaded on a commercial MZ Symmetry C18 Trap Column (100 Å, 5 µm, 180 µm x 20 mm, Waters) followed by nanoEase MZ C18 HSS T3 Column (100 Å, 1.8 µm, 75 µm x 250 mm, Waters). The peptides were eluted at a flow rate of 300 nL/min by a gradient from 8 to 27% B in 85 min, 35% B in 5 min and 80% B in 1 min. Samples were acquired in a randomized order. The mass spectrometer was operated in data-dependent mode (DDA), acquiring a full-scan MS spectra (350−1400 m/z) at a resolution of 120 000 at 200 m/z after accumulation to a target value of 3 000 000, followed by HCD (higher-energy collision dissociation) fragmentation on the twenty most intense signals per cycle. HCD spectra were acquired at a resolution of 15 000 using a normalized collision energy of 25 and a maximum injection time of 22 ms. The automatic gain control (AGC) was set to 100 000 ions. Charge state screening was enabled. Singly, unassigned, and charge states higher than seven were rejected. Only precursors with intensity above 250 000 were selected for MS/MS. Precursor masses previously selected for MS/MS measurement were excluded from further selection for 30 s, and the exclusion window was set at 10 ppm. The samples were acquired using internal lock mass calibration on m/z 371.1012 and 445.1200. The mass spectrometry proteomics data were handled using the local laboratory information management system (LIMS) [Turker et al 2010], and all relevant data have been deposited to the ProteomeXchange Consortium via the PRIDE (http://www.ebi.ac.uk/pride) partner repository with the data set identifier PXDXXXX.

Protein quantification based on precursor signal intensity was performed using ProgenesisQI for Proteomics (v4.0.6403.35451; nonlinear dynamics, Waters). Raw MS files were loaded into ProgenesisQI and converted to mzln files. To select the alignment reference, a group of samples that had been measured in the middle of the run (to account for drifts in retention times) and derived from harvest time point 12h or later (to account for increasing sample complexity) was preselected, from which replicate 3 of time point 48h was then automatically chosen as best alignment reference. After automatic peak picking, precursor ions with charges other than 2+, 3+

or 4+ were discarded. The five highest-ranked MS/MS spectra, at most, for each peptide ion were exported, using the deisotoping and charge deconvolution option and limiting the fragment ion count to 200 peaks per MS/MS. The resulting Mascot generic file (.mgf) was searched with Mascot Server version 2.6.2 (www.matrixsicence.com) using the following settings: trypsin digest with up to two missed cleavages allowed; carbamidomethylation of cysteine as fixed modification; acetylation at the protein's N terminus and oxidation of methionine residue as variable modification; precursor ion mass tolerance 10 ppm; fragment ion (MS/MS) tolerance 0.04 kDa. This search was performed against a forward and reverse (decoy) Araport11 database that included common MS contaminants and iRT peptides. The mascot result was imported into Scaffold Q+S (v4.8.9; Proteome Software Inc), where a spectrum report was created using a false discovery rate (FDR) of 10% and 0.5% at the protein and peptide level, respectively, and a minimum of one identified peptide per protein. After loading the spectrum report into ProgenesisQI, samples were normalized according to the abundance of iRT peptides that showed a correlation score of >0.5 (i.e. whose abundance profiles correlated well with those from the other iRT peptides). Samples were grouped according to harvest time point in a between-group analysis with 4 replicates for each condition, except for time point 0h, where n = 3. For this time point, replicate 4 was excluded since it had a relatively high normalization factor of 7.8 and a low alignment score of 29.5% (values of all other samples ranged between 0.8 and 1.5 for normalization factors and 45.2% and 95.1% for alignment scores). Quantification employed the Hi-N method, measuring the three most abundant peptides for each protein (Grossmann et al., 2010). Quantification also used protein grouping, which assigns proteins for which only shared but no unique peptides were identified to a "lead" identifier containing all these shared peptides and thus having the greatest coverage among all grouped identifiers or highest score where coverage is equal. Quantification was restricted to protein (groups) with at least two identified peptides among which at least one is unique to the protein (group). Since in no case a decoy protein was the single associated protein under these conditions, the false-discovery rate at the protein level over the whole experiment is estimated to be 0.

Immunoblot analysis

Proteins were extracted from whole seedlings in 4 volume (w/v) of SDS-PAGE – sample buffer (0.2 M Tris/HCL pH 6.8, 0.4 M Dithiothreitol, 8% (w/v) SDS, 0.4% (w/v) Bromophenol blue and 40% (v/v) glycerol).

Proteins were denatured for 15 min at 65°C and cell debris were removed by centrifugation for 5 min at 16000 g. Proteins were separated on SDS-PAGE (10 to 15% (w/v) polyacrylamide concentrations depending on the molecular weight of the protein of interest) and transferred onto a nitrocellulose membrane for western blotting (overnight at 4°C) in Dunn buffer (10 mM $NaHCO_3$, 3 mM Na_2CO_3, 0.01% (w/v) SDS and 20% ethanol).

Absolute quantification of PsbA, PetC and PsaC was performed according to Agrisera instructions and using recombinant proteins (PsbA AS01 0116S, PetC AS08 330S and PsaC AS04 042S; Agrisera). Three calibration curves respectively for the three recombinant proteins have been created. Concentrations used to generate PsbA and PetC calibration curve were 1.75, 2.5, 5, and 10 (ng/µl), Concentrations used to generate PsaC curve were 0.375, 0.75, 1.5 and 3 (ng/µl). Immunodetections were performed using: anti-Actin (Sigma, A0 480) at 1/3000 dilution in 5% (w/v) milk in Tris-buffered saline (TBS); anti-Lhcb2 (Agrisera, AS01 003), anti-D1(PsbA) (Agrisera, AS05 084), anti-PsbO (Agrisera, AS14 2825), anti-PsbD (Agrisera, AS06 146), anti-PetC (Agrisera, AS08 330), anti-AtpC (Agrisera, AS08 312) at 1/5000 dilution in 5% milk/TBS; Anti-PsaD (Agrisera, AS09 461) at 1/2000 in 5% milk/TBS; anti-PsaC (Agrisera, AS042P) and anti-ARC5 (Agrisera, AS13 2676) at 1/2000 in 3% (w/v) bovine serum albumin (BSA) inTBS. Anti-FtsZ-1 and anti-FtsZ2-1 / FtsZ 2-2 (El-Shami et al., 2002 ; Karamoko et al., 2011) and were used at 1/2000 dilution in 5% milk (w/v) in TBS. After incubation with primary antibodies overnight at 4°C , blots were washed 3 times in TBS containing 0.1% (v/v) Tween without antibodies for 10 minutes and incubated for 1 h at RT with horseradish peroxidase-conjugated secondary antibodies (1/3000 (v/v) anti-rabbit or anti-mouse secondary antibodies, Agrisera) .

Chemioluminescence signals were generated with Enhanced ChemioLuminescence homemade reagent (1 M Tris/HCl pH 8.5, 90 mM Coomaric acid and 250 mM luminol) and detected with a Fujifilm Image - Quant LAS 4000 mini CCD (GE Healthcare) . Quantifications were performed with ImageQuant TL software (GE Healthcare).

Lipid profiling

Lipids were extracted from whole seedlings ground in mortar with a pestle under liquid nitrogen. Ground plant material corresponding to 40 to 80 mg fresh weight was suspended in tetrahydrofuran:methanol (THF/MeOH) 50:50 (v/v). 10-15 glass beads (1mm in diameter) were added followed by homogenization (3 min, 30Hz,) and centrifugation (3 min, 14000 g, at 4°C). The supernatant was removed and transferred to an HPLC vial. Lipid profiling was carried out by ultra-high pressure liquid chromatography coupled with atmospheric pressure chemical ionization-quadrupole time-of-flight mass spectrometry (UHPLC-APCI-QTOF-MS) (Martinis et al., 2011). Reverse-phase separation was performed on an Acquity BEH C18 column (50 × 2.1mm, 1.7µm). The conditions were the following: solvent A = water; solvent B = methanol; 80– 100% B in 3 min, 100% B for 2min, re-equilibration at 80% B for 0.5 min. Flow rate was 0.8ml min−1 and the injection volume 2.5µl. Data were acquired using MassLynx version 4.1 (Waters), and processed with MarkerLynx XS (Waters). Peak lists consisting of variables described by mass-to-charge ratio and retention time were generated. Absolute quantification of mono (MGDG) and di-galactosyldiacylglycerol (DGDG) was conducted creating calibration curves of MGDG (reference number 840523) and DGDG (reference number 840523) products of Avanti Company. Calibration curves were prepared using the following concentrations: 0.08, 0.4, 2, 10, 50 ug ml^{-1} of MGDG or DGDG.

Mathematical Model

A non-linear mixed effects model (with fixed effect of time and random effect of replicates on 3 of the parameters), built on a 4-parameter logistic function, have been implemented in R, following the examples in (Pinheiro and Bates, 2000). The R-packages used are: nlme (Pinheiro and Bates, 2000), effects, lattice and car (Fox and Weisberg, 2018).

Supplemental Figures

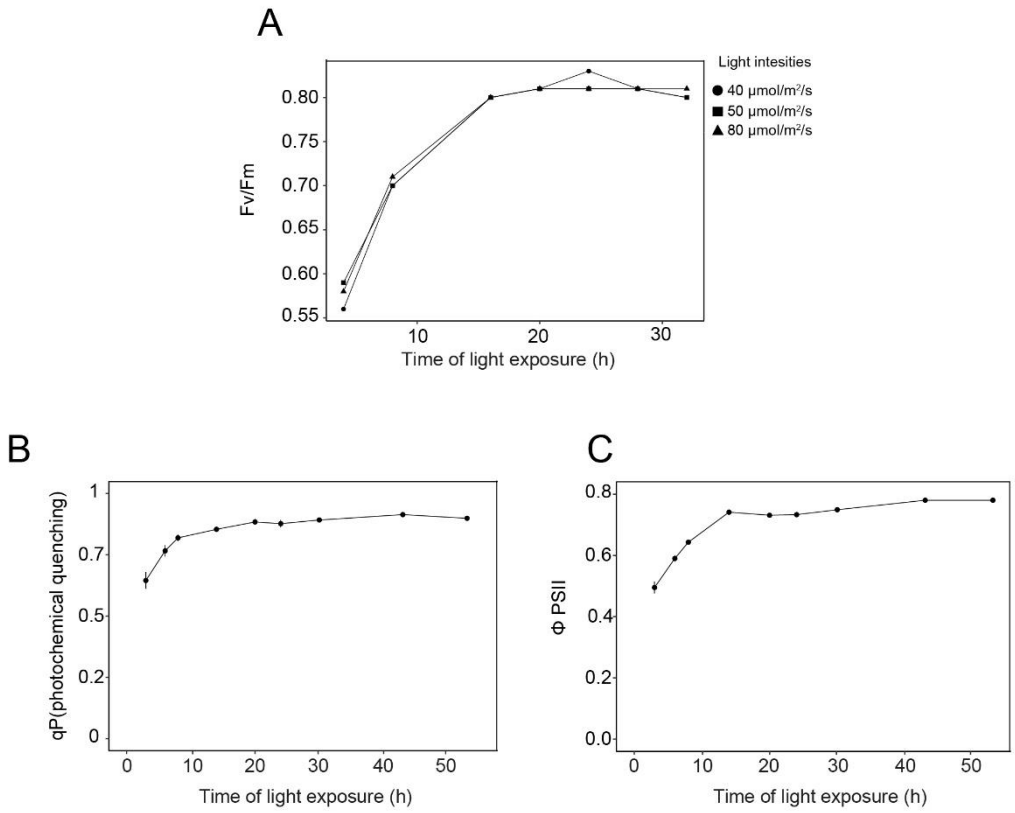

Supplemental figure 1: (A) 3-day-old etiolated seedlings were de-etiolated under different light intensities (40, 50 and 80 µmol/m^2/s). Maximum photosynthetic quantum yield of PSII (Fv/Fm) of plant (dark-adapted for 5 minutes) was calculated at different time points of illumination. (B-C) 3-day-old etiolated seedlings were de-etiolated under light intensity 40 µmol/m^2/s. Photochemical quenching (qP) (B) and efficiency of PSII (Φ PSII) (C) were calculated at different time points of illumination. Error bars indicate ± SD (n= 3 or 4). Where absent, error bars could be smaller than the symbols black dots.

A

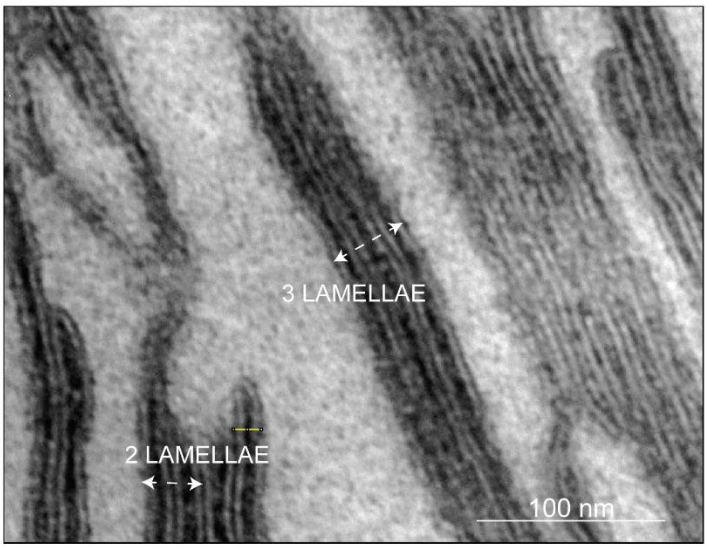

B

$$\frac{\textit{Thickness of 2 or 3 lamellae - (Stromal gap thickness * nb)}}{\textit{nb.lamellae measured}} = \textit{one lamellae thickness}$$

C

	Thickness 2 lamellae (nm)	Thickness 3 lamellae (nm)	Stromal gap thickness *(Daum et al.,2010)*
T24	29.7 + / - 1.9	48.3 + / - 4.8	
one lamellae thickness (T24)	$\frac{29.7-3.2}{2} = 13.2$	$\frac{48.3-(3.2*2)}{3} = 13.9$	
T96	34.7 + / - 0.71	56 + / - 2.1	3.2 nm +/- 0.7
one lamellae thickness (T96)	$\frac{34.7-3.2}{2} = 15.7$	$\frac{56-(3.2*2)}{3} = 16.5$	

Supplemental Figure 2: Measurements of lamellae thickness. (A)TEM chloroplast micrographs of 3-day-old dark grown *Arabidopsis thaliana* (Columbia) seedlings illuminated for 96 h in continuous white light (40 µmol/m^2/s) used to measure the thickness of lamellae that constitute the grana stack. Measurements have been carried out using ImageJ. (B) Equation used to calculate the thickness of one lamellae. (C) Data indicate mean +/- standard deviation (n=10 for 2 lamellae and n=7 for 3 lamellae).

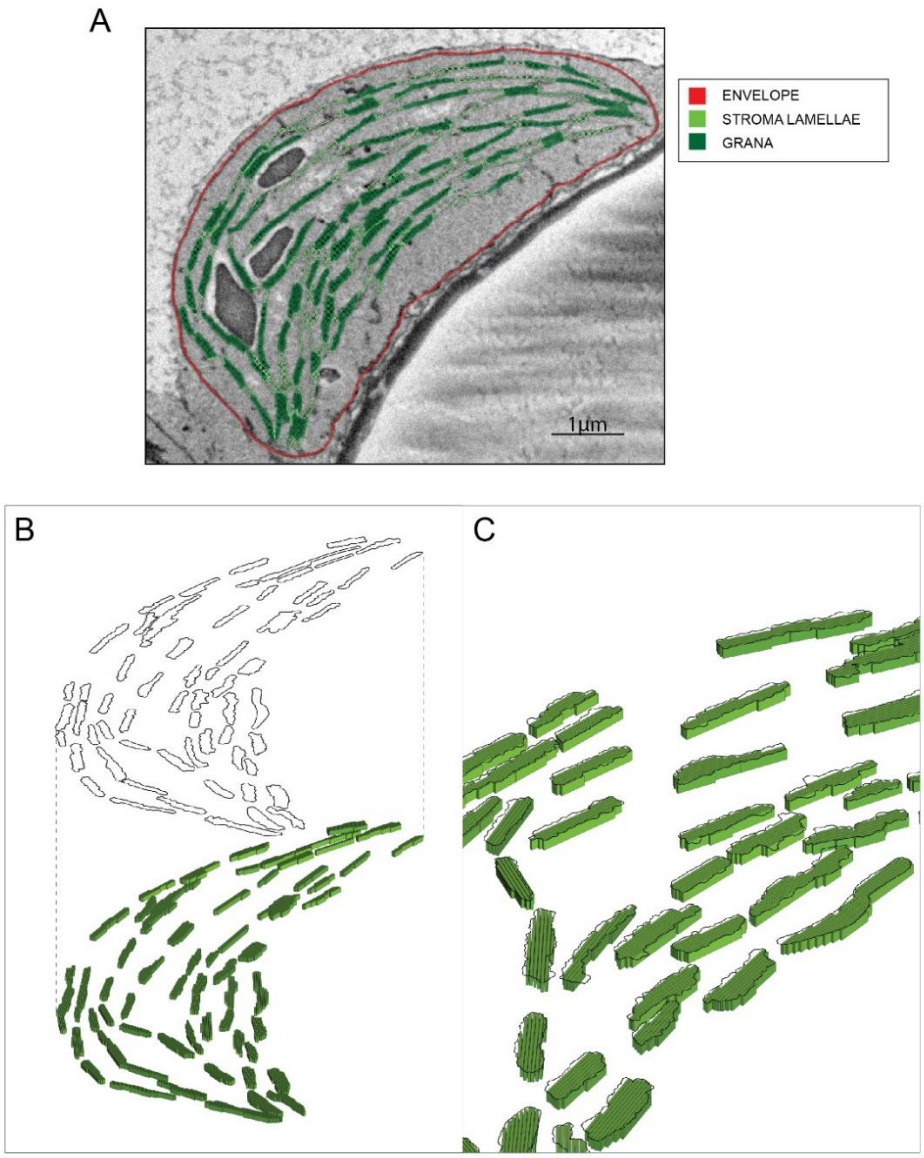

Supplemental Figure 3: Grana segmentation (T24). (A) Segmentation of the envelope (red), stroma lamellae (green) and grana (forestgreen) exposed to the stroma was selected in Amira software. (B-C) The grana surface was converted in line set (black line) and segmented in layers (3D structure in green) at a specific thickness and distance using Rhino software, with the corresponding thickness (lamellae and stromal gap) measured and calculated as described in supplemental Figure 2C. Grana segmentation have been carried out in thylakoid membrane of de-etiolating seedlings exposed 24 and 96 h under continuous white light (40µmol/m^2/s), representative example of a T24 replicate is illustrated here.

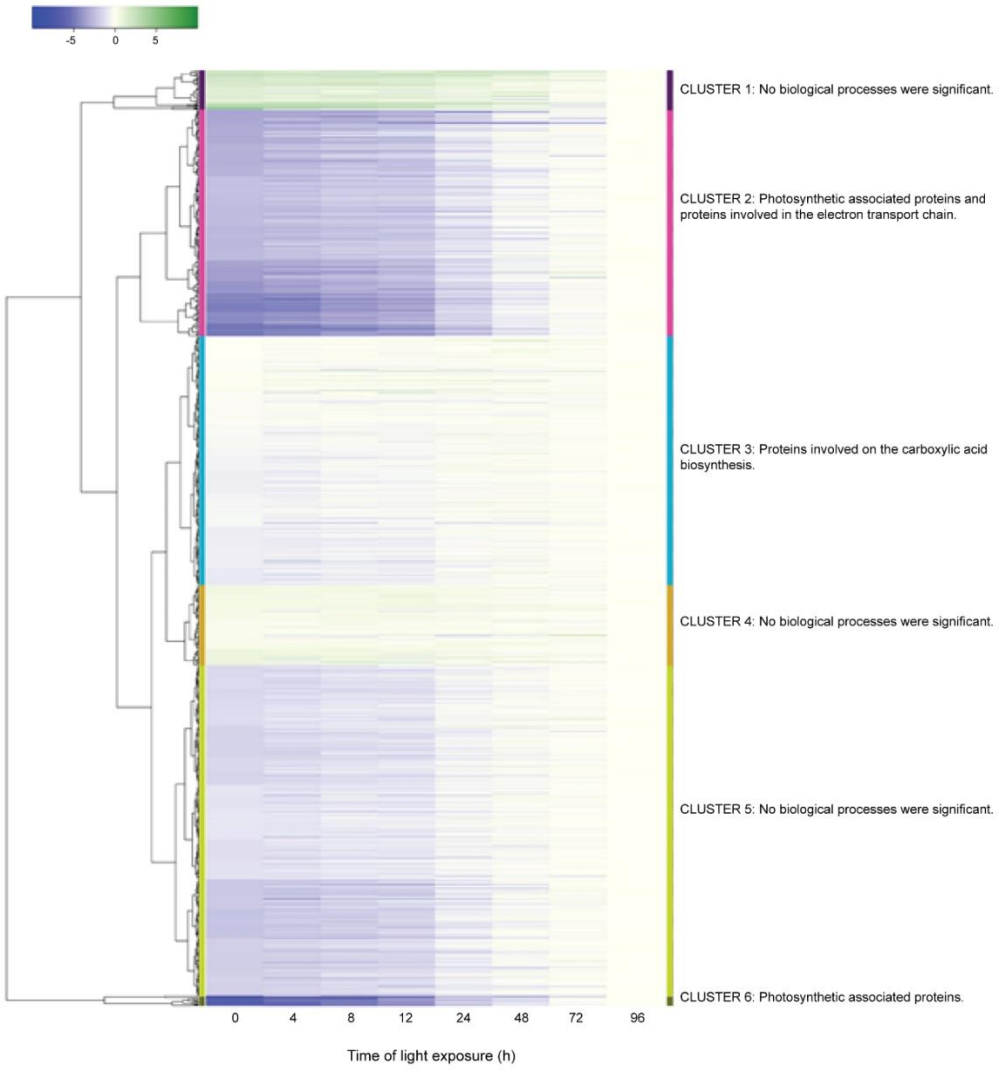

Supplemental Figure 4: Dynamics of plastid protein accumulation during de-etiolation. Proteins assigned to chloroplast localization (SUBA4, Hooper et al., 2017) were selected for hierarchical clustering analysis (Euclidean, average linkage), based on their abundance relative to the last time point (T96). T0 to T96 indicates the time of light exposure (in hours). Defined clusters are indicated with different colours (1= purple; 2= pink; 3= turquoise ; 4= brown ; 5= green ; 6= dark green). Protein IDs (AGI) and common names are readable in the Supplemental Dataset 2.

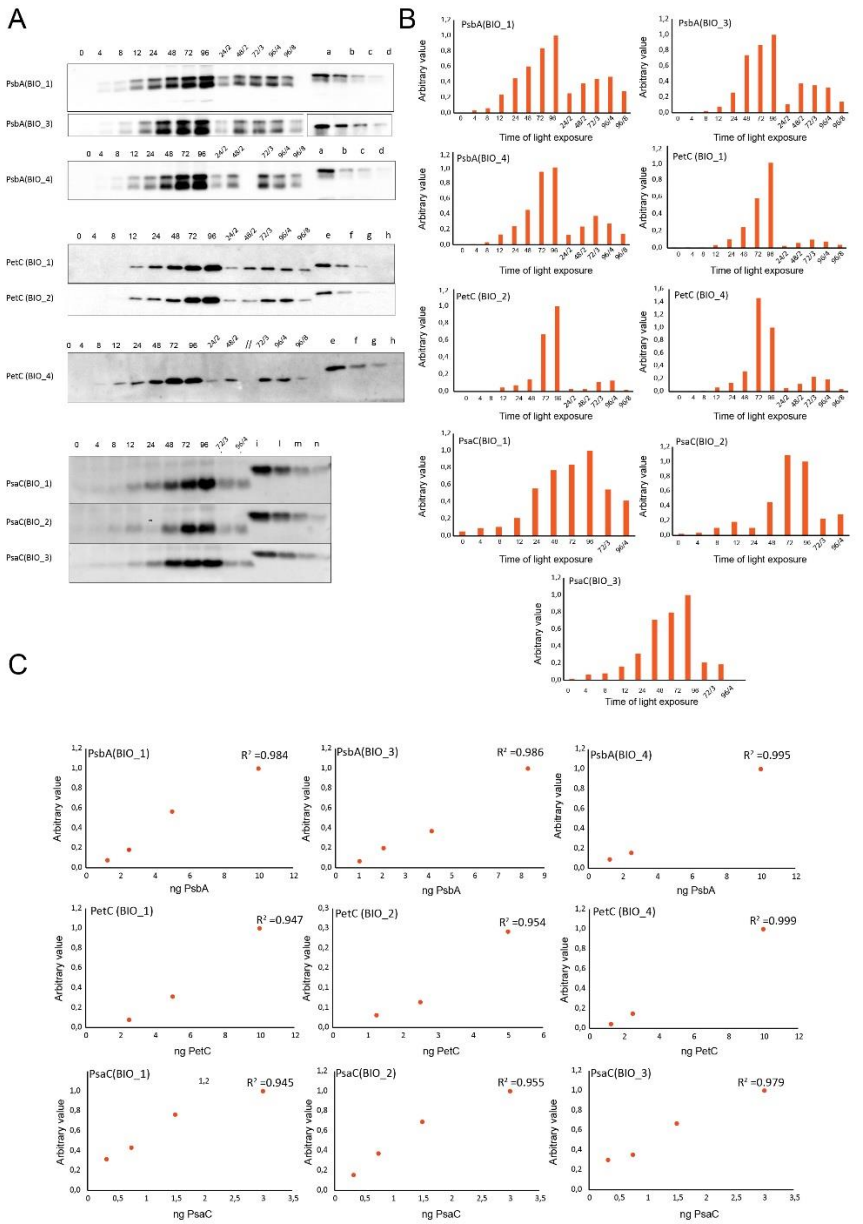

Supplemental Figure 5: Quantification of photosystem related proteins. (A) Immunodetection of PsbA, PetC and PsaC during de-etiolation. Dilutions were used for the latest time point to avoid saturation of the signal. (B) The different bands were detected by Amersham Imager program and quantified by Image QuantTL (Amersham). (C) Calibration curves were created using recombinant proteins (Agrisera). Calibration curve composition: PsbA 10ng(a), 5ng(b), 2.5 ng(c), 1.25ng (d), PetC 10ng(e), 5ng(f), 2.5ng(g), 1,25ng(h), PsaC 3ng(i), 1.5ng(l), 0.75ng(m), 0.325ng(n). The analysis was carried out for three or four independent experiments (BIO1 - 4).

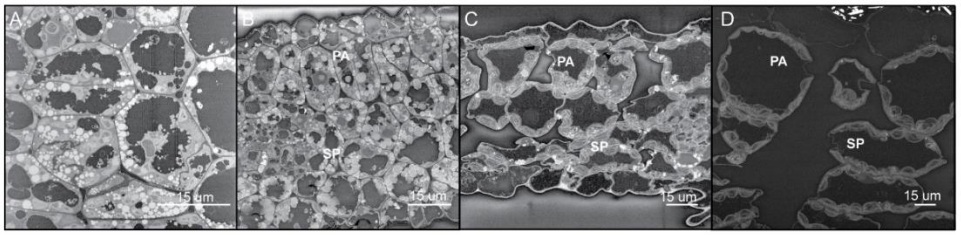
A
B
PA
SP
15 µm
C
PA
SP
15 µm
D
PA
SP
15 µm

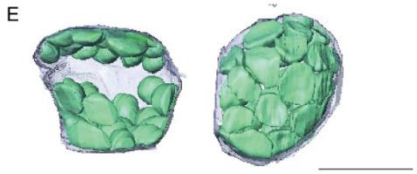
E

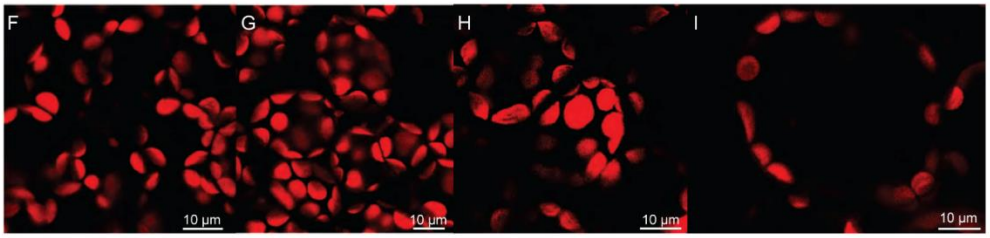
F
G
10 µm
10 µm
H
10 µm
I
10 µm

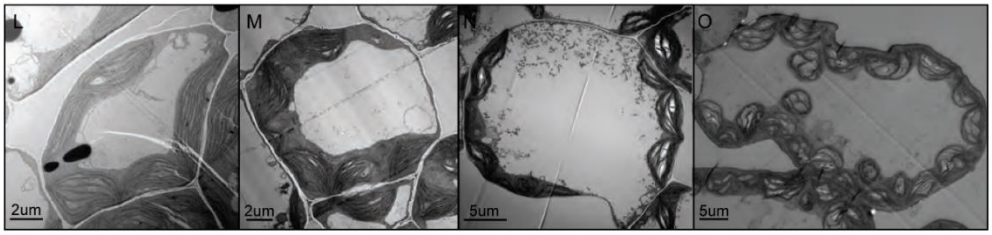
L
2um
M
2um
N
5um
O
5um

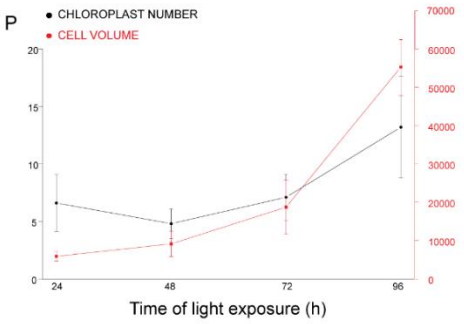
P
CHLOROPLAST NUMBER
CELL VOLUME
20
15
10
5
0
70000
60000
50000
40000
30000
20000
10000
0
24
48
72
96
Time of light exposure (h)

Supplemental Figure 6: Changes of chloroplast number in concomitance with cell expansion. SEM micrographs of 3 day-old dark grown *Arabidopsis thaliana* (Columbia) seedlings illuminated for 0(A), 4(B), 24(C) and 96(D) h in continuous white light (40µmol/m^2/s). Palisade (PA) and spongy (SP) cells are indicated. Scale bars: 15 µm. (E) 3D reconstruction of a palisade cell (24 hours after light exposure), after segmentation of chloroplasts and cell plasma membrane. (F-I) Confocal images of dark- grown seedlings illuminated for 24(F), 48(G), 72(H) and 96(I) h in continuous white light (40µmol/m^2/s). The Z-depth of each stack corresponds to 1µm. (L-O) TEM micrographs of dark- grown seedlings illuminated for 24(L), 48(M), 72(N) and 96(O) h in continuous white light (40µmol/m^2/s). (P) Cell volume were quantified by Amira software using confocal stacks (red line). Relative chloroplast number per cell was counted using 2D TEM images (black line). Red error bars indicate ± SD (n=12 or 17). Black error bars indicate ± SD (n= 3 or 4).

A

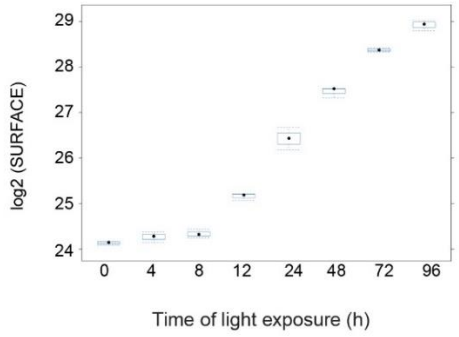

B

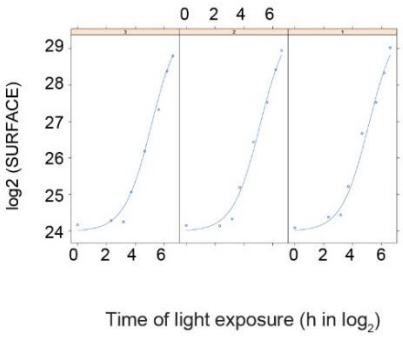

C

Coefficient	Value	± SE	t-Value	P value
a	23.99	± 0.12	196.67	0
b	29.79	± 0.47	62.11	0
c	0.9	± 0.12	7.50	0
d	5.1	± 0.18	26.96	0

Equation.4 $$y = a + \frac{b - a}{1 + e^{(d - x) / c}}$$

Supplemental Figure 7: Non - linear mixed effect model of thylakoid surface during the de-etiolation. (A) Total surface of thylakoid membrane (in log2) in function of the time of light exposure. (B) Individual plots for each biological replicate. (C) Values, standard errors, t-Value and P-value of the four parameters (a, b, c and d) used in Equation.4, are shown.

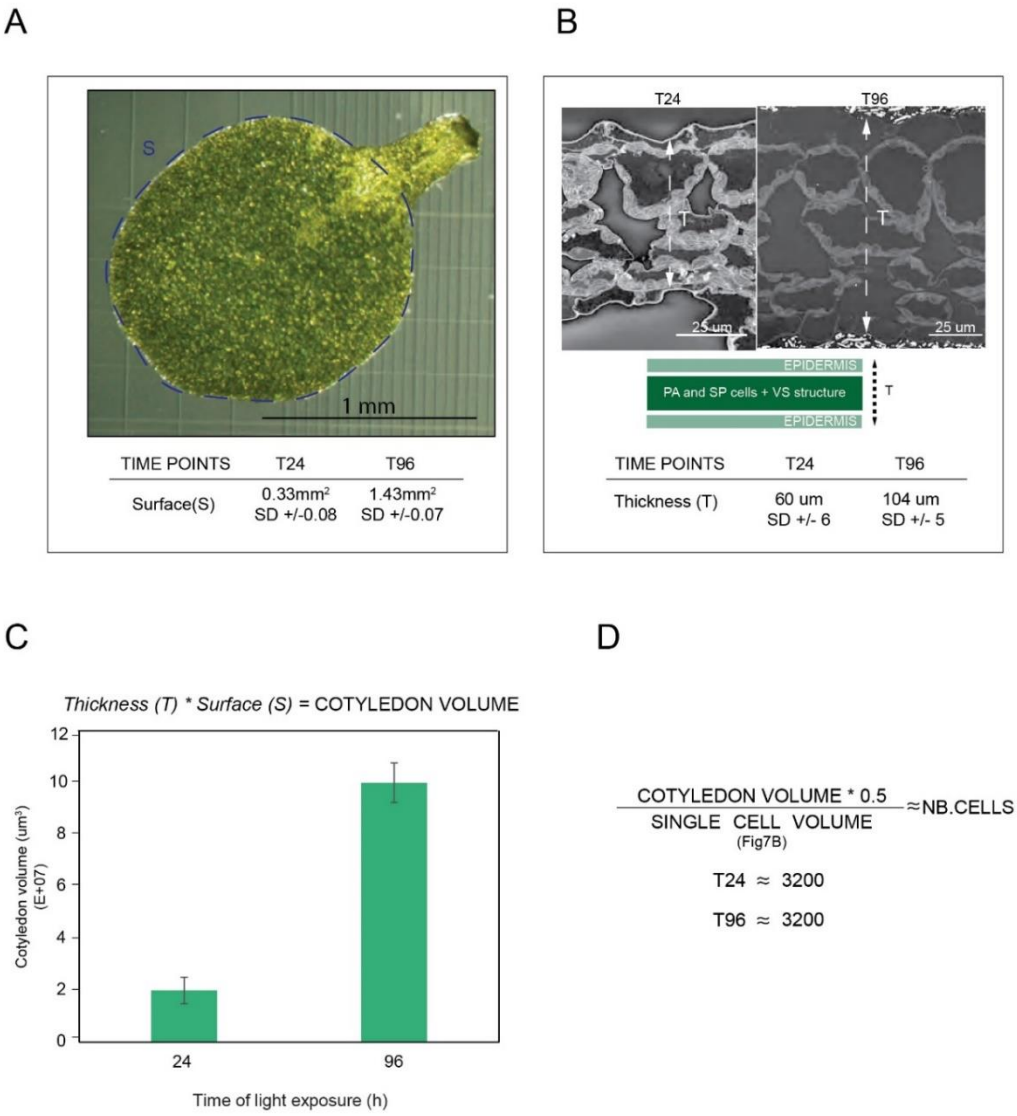

Supplemental Figure 8: Morphometric analysis of cotyledon. (A) Cotyledon surface area of 3 day-old dark grown *Arabidopsis thaliana* (Columbia) seedlings illuminated for 24 and 96 h in continuous white light (40µmol/m^2/s). (B) The thickness (T) of mesophyll tissue constituted of palisade (PA), spongy (SP) cells and vascular system (VS) in addition to the epidermal tissue was measured, ± SD (n=4). (C) Estimation of cotyledon volume. Error bars indicate ± SD (n=3). (D) Estimation of the number of cells per cotyledon (see the Supplemental Dataset 4 for calculations)

	Method	T0	T4	T8	T12	T24	T48	T72	T96
Thylakoid surface (µm²)	SBF-SEM	—	**65.1** (SD = +/ - 24.7)	—	—	**1245** (SD = +/ -94)	—	—	**1658** (SD = +/ - 315)
Thylakoid volume (µm³)	SBF-SEM	—	**1.34** (SD = +/- 0.54)	—	—	**12.70** (SD = +/- 2.66)	—	—	**25.33** (SD = +/- 4.93)
Thylakoid/envelope ratio surface	SBF-SEM	—	**1.5** (SD= +/- 0.18	—	—	**6** (SD= +/- 0.88	—	—	**5.2** (SD= +/- 1.53
Lenght of plastid (µm)	TEM	**2** (SD = +/- 0.90)	**2.8** (SD = +/- 0.90)	—	—	**5.1** (SD = +/- 1.47)			**6** (SD = +/- 1.62)
Chloroplast volume (µm³)	SBF-SEM	**9.5** (SD=+/- 1.5)	**8.2** (SD=+/- 4.4)	—	—	**65.2** (SD=+/-14.5)	—	—	**104.7** (SD=+/- 4.5)
Chloroplast volume (µm³)	confocal	—	—	—	—	**59.8** (SD=+/-13)	**80.1** (SD=+/-16.7)	**83** (SD=+/-10)	**121.1** (SD=+/- 11.2)
Cell Volume (µm³)	SBF-SEM	**1170** (SD= +/- 280)	**1700** (SD= +/- 400)	—	—	**6000** (SD= +/- 1100)	—	—	**47000** (SD= +/- 17000)
Cell Volume (µm³)	confocal	—	—	—	—	**5900** (SD=+/-1200)	**9100** (SD=+/-3300)	**19000** (SD=+/-7000)	**55000** (SD=+/-7400)
Nb.chloroplast/cell	SBF-SEM	**22** (SD = +/- 6.2)	**25** (SD = +/- 7.9)	—	—	**26** (SD =+/- 5.9)	—	—	**112** (SD = +/- 28.6)
Estimation cell number		—	—	—	—	**≈ 3200**	—	—	**≈ 3200**
Protein/GLs ratio surface		**0.36** (SD = +/-0.10)	**0.43** (SD = +/-0.09)	**0.64** (SD = +/-0.06)	**0.98** (SD = +/-0.14)	**1.48** (SD = +/-0.30)	**1.66** (SD = +/-0.41)	**1.75** (SD = +/-0.19)	**1.83** (SD = +/-0.42)
GLs (nmol/seedling)	Lipidomics	**0.12** (SD = +/-0.007)	**0.13** (SD = +/-0.02)	**0.13** (SD = +/-0.02)	**0.21** (SD = +/-0.02)	**0.27** (SD = +/- 0.02)	**0.55** (SD = +/- 0.05)	**0.93** (SD = +/- 0.1)	**1.4** (SD = +/- 0.09)
PsbA (nmol/seedling)	Western blot	**6.9^{E}-06** (SD = +/- 1.8^{E}-06)	**9.2^{E}-06** (SD = +/- 1.8^{E}-06)	**1.5^{E}-05** (SD = +/- 7.1^{E}-07)	**3.3^{E}-05** (SD = +/- 4.3^{E}-06)	**9.3^{E}-05** (SD = +/- 2.2^{E}-05)	**2.0^{E}-04** (SD = +/- 6.2^{E}-05)	**3.9^{E}-04** (SD = +/- 4.0^{E}-05)	**6.2^{E}-04** (SD = +/- 1.7^{E}-04)
PsaC (nmol/seedling)	Western blot	n.d	n.d	n.d	**5^{E}-06** (SD = +/- 2.5^{E}-06)	**7.3^{E}-05** (SD = +/- $2.4.^{E}$05)	**1.2^{E}-04** (SD = +/- $7.2.^{E}$05)	**1.7^{E}-04** (SD = +/- $4.2.^{E}$05)	**2.3^{E}-04** (SD = +/- 1^{E}-04)
PetC (nmol/seedling)	Western blot	**2.7^{E}-05** (SD = +/- 7.8^{E}-06)	**2.8^{E}-05** (SD = +/- 9.8^{E}-06)	**2.5^{E}-05** (SD = +/- 4.5^{E}-06)	**5.3^{E}-05** (SD = +/- 2.2^{E}-05)	**1.2^{E}-04** (SD = +/- 4.1^{E}-05)	**1.8^{E}-04** (SD = +/- 3.4^{E}-05)	**5.7^{E}-04** (SD = +/- 1.8^{E}-04)	**7.9^{E}-04** (SD = +/- 3.7^{E}-04)

Supplemental Table 1: Collection of quantitative data. Morphometric data corresponding to thylakoid surfaces and volumes, thylakoid / envelope surface ratio, chloroplast and cell volumes as well as number of chloroplasts were collected after SBF-SEM analysis. Chloroplast and cell volumes were also quantified by after confocal microscopy analysis, while the length of plastid was measured on TEM images. Molecular data for galactolipids (GLs) were analyzed by lipidomics while PsbA, PsaC and PetC were quantified by quantitative immunodetection.

	surface in nm²	*reference*
MGDG	0.82	*Bottier et al., 2007*
DGDG	0.64	*Bottier et al., 2007*
PSII -LHCII ($C_2S_2M_2$)	494	*Caffarri et al., 2014*
cyt b_6f	49.5	*Kurisu et al., 2003*
PSI	300	*Caffarri et al., 2014*

Supplemental Table 2: Surfaces occupied by lipids and protein complexes retrieved from literature. MGDG and DGDG surface correspond to the minimal molecular area. Surface values of PSII-LHCII, Cyt b_6/f and PSI correspond to the surface exposed to the stroma.

	T0	T4	T8	T12	T24	T48	T72	T96
MGDG	**1.17^{E}+07** SD = +/- 3.84E+05	**1.22^{E}+07** SD = +/- 1.07E+06	**1.17^{E}+07** SD = +/- 1.16E+06	**1.85^{E}+07** SD = +/- 1.91E+06	**4.04^{E}+07** SD = +/- 4.14E+06	**8.39^{E}+07** SD = +/- 5.78E+06	**1.61^{E}+08** SD = +/- 8.52E+06	**2.26^{E}+08** SD = +/- 1.87E+07
DGDG	**3.85^{E}+06** SD = +/- 4.27E+05	**4.47^{E}+06** SD = +/- 5.59E+05	**4.34^{E}+06** SD = +/- 1.39E+05	**6.61^{E}+06** SD = +/- 4.96E+05	**6.68^{E}+06** SD = +/- 2.55E+06	**1.41^{E}+07** SD = +/- 1.11E+06	**2.44^{E}+07** SD = +/- 1.57E+06	**3.36^{E}+07** SD = +/- 2.28E+06
PSII	**2.04^{E}+06** SD = +/- 5.38E+05	**2.74^{E}+06** SD = +/- 5.30E+05	**4.40^{E}+06** SD = +/- 2.12E+05	**9.91^{E}+06** SD = +/- 1.29E+06	**2.75^{E}+07** SD = +/- 6.42E+06	**6.06^{E}+07** SD = +/- 1.85E+07	**1.15^{E}+08** SD = +/- 1.19E+07	**1.83^{E}+08** SD = +/- 5.17E+07
PSI	**0^{E}+00** SD = +/-0E+00	**0^{E}+00** SD = +/- 0E+00	**0^{E}+00** SD = +/- 0E+00	**8.95^{E}+05** SD = +/- 4.49E+05	**1.33^{E}+07** SD = +/- 4.31E+06	**2.10^{E}+07** SD = +/- 1.30E+07	**3.04^{E}+07** SD = +/- 7.55E+06	**4.24^{E}+07** SD = +/- 1.89E+07
Cyt b_6f	**7.99^{E}+05** SD = +/- 2.33E+05	**8.43^{E}+05** SD = +/- 2.91E+05	**7.50^{E}+05** SD = +/- 1.33E+05	**1.57^{E}+06** SD = +/- 6.71E+05	**3.44^{E}+06** SD = +/- 1.22E+06	**5.30^{E}+06** SD = +/- 1.01E+06	**1.69^{E}+07** SD = +/- 5.48E+06	**2.37^{E}+07** SD = +/- 1.11E+07

Supplemental Table 3: Thylakoid surface per seedling. Surface area occupied by the main galactolipids (MGDG and DGDG) and photosynthetic complexes (PSII, cyt *b_6f* and PSI) is shown, at different time points upon illumination of 3-day-old etiolated seedlings. Each value (in bold) indicates the calculated surface area in µm^2 and corresponds to the average of three biological replicates. SD (n=3).

Conclusions and Perspectives

Photosynthetic reactions occur at the internal membrane system of the chloroplast called thylakoids. Galactolipids are the major class of lipids, which constitutes the thylakoid membrane. Photosynthesis-associated proteins and pigments are assembled into photosystems in the thylakoid membrane. Formation of the thylakoids is a central process in chloroplast biogenesis.

The precise mechanisms of thylakoid formation remain largely unknown and represent a key question in how a plant develops into a photosynthetic organism. The novel, integrative approach employed in my PhD thesis contributes to a deeper understanding of chloroplast biogenesis. The combination of morphometric data acquired from 3D reconstruction of chloroplasts and cells with quantitative biochemical data on thylakoid lipids and proteins provide a precise timeline for the onset of photosynthetic activity, protein and lipid composition of the thylakoid membrane in relation to ultrastructural changes. Morphometric data of the entire chloroplast and cellular ultrastructures were collected during the de-etiolation process. 5000 proteins were identified by proteome analysis and provided information not only on plastid development but also on other light-regulated developmental processes. The eukaryotic and prokaryotic galactolipid biosynthesis pathways were involved at distinct stages in the formation of the thylakoid membrane highlighting by the differences in galactolipid composition between prolamellar body and thylakoid membrane.

My study, however, was unable to shed light on the mechanisms of lipid transfer between the envelope (where galactolipid biosynthesis occurs) and the thylakoid membrane. This would be an attractive field for further research in chloroplast biogenesis and thylakoid formation. At the cellular level, the synthesis of chloroplast lipids is coordinated with the endoplasmic reticulum and the possible involvement of further organelles in lipid transport cannot be excluded. Phosphate deprivation induces the transfer of DGDG from chloroplast to mitochondria that would depend on lipid transport between plastids and mitochondria (Jouhet et al., 2004). It has already been shown in diatoms that chloroplasts and mitochondria interact physically to accomplish metabolic processes in the dark (Flori et al., 2017). Serial block face –

scanning electron microscopy in combination with electron tomography and molecular techniques may serve to study the physical interactions between organelles, a research area that would deserve a major investigation.

In addition, my results demonstrated that the expansion of the thylakoid membrane occurred in concomitance with the chloroplast differentiation as well as chloroplast division. However, the factors influencing the increase of chloroplast size and the triggers of chloroplast division are still unknown.

Finally, the mathematical model presented in my thesis, described the thylakoid expansion during chloroplast biogenesis. One of the next challenges could be to test the model under perturbing conditions using mutants affected in chloroplast biogenesis and thylakoid formation (for example lipid biosynthesis (*mgd*), chloroplast protein import (*ppi*) as well as thylakoid architecture mutants (*curt*)) or environmental factors (such as different qualities of light, humidity, salinity etc). The data obtained could potentially be used to develop predictive models for chloroplast biogenesis and thylakoid formation that drive plant growth under specific grown conditions.

Clearly, much remains to be done in this field and there will be plenty of work for future motivated PhD students.

References

Agne B, Kessler F. 2010. Modifications at the A-domain of the chloroplast import receptor Toc159. *Plant Signal Behav* **5**:1513–6. doi:10.1104/pp.110.158048

Amunts A, Nelson N. 2009. Plant Photosystem I Design in the Light of Evolution. *Structure* **17**:637–650. doi:10.1016/j.str.2009.03.006

Armarego-Marriott T, Kowalewska Ł, Burgos A, Fischer A, Thiele W, Erban A, Strand D, Kahlau S, Hertle A, Kopka J, Walther D, Reich Z, Schöttler MA, Bock R. 2019. Highly Resolved Systems Biology to Dissect the Etioplast-to-Chloroplast Transition in Tobacco Leaves. *Plant Physiol* **180**:654–681. doi:10.1104/pp.18.01432

Aronsson H, Schöttler M a, Kelly A a, Sundqvist C, Dörmann P, Karim S, Jarvis P. 2008. Monogalactosyldiacylglycerol deficiency in Arabidopsis affects pigment composition in the prolamellar body and impairs thylakoid membrane energization and photoprotection in leaves. *Plant Physiol* **148**:580–592. doi:10.1104/pp.108.123372

Austin JR, Staehelin LA. 2011. Three-Dimensional Architecture of Grana and Stroma Thylakoids of Higher Plants as Determined by Electron Tomography. *Plant Physiol* **155**:1601–1611. doi:10.1104/pp.110.170647

Bailleul B, Berne N, Murik O, Petroutsos D, Prihoda J, Tanaka A, Villanova V, Bligny R, Flori S, Falconet D, Krieger-Liszkay A, Santabarbara S, Rappaport F, Joliot P, Tirichine L, Falkowski PG, Cardol P, Bowler C, Finazzi G. 2015. Energetic coupling between plastids and mitochondria drives CO2 assimilation in diatoms. *Nature* **524**:366–369. doi:10.1038/nature14599

Bastien O, Botella C, Chevalier F, Block MA, Jouhet J, Breton C, Girard-Egrot A, Maréchal E. 2016. New Insights on Thylakoid Biogenesis in Plant Cells, International Review of Cell and Molecular Biology. Academic Press. doi:10.1016/bs.ircmb.2015.12.001

Bauer J, Chen K, Hiltbunner a, Wehrli E, Eugster M, Schnell D, Kessler F. 2000. The major protein import receptor of plastids is essential for chloroplast biogenesis.

Nature **403**:203–7.
doi:10.1038/35003214

Bischof S, Baerenfaller K, Wildhaber T, Troesch R, Vidi P-A, Roschitzki B, Hirsch-Hoffmann M, Hennig L, Kessler F, Gruissem W, Baginsky S. 2011. Plastid proteome assembly without Toc159: photosynthetic protein import and accumulation of N-acetylated plastid precursor proteins. *Plant Cell* **23**:3911–28.
doi:10.1105/tpc.111.092882

Block MA, Dorne A-J, Joyard J, Douce R. 1983. Preparation and Characterization of Membrane Fractions of Outer and Inner Envelope Membranes from Spinach C. *J Biol Chem* **258**:13281–13286.
doi:10.1007/978-94-017-4973-2_5

Blomqvist LA, Ryberg M, Sundqvist C. 2008. Proteomic analysis of highly purified prolamellar bodies reveals their significance in chloroplast development. *Photosynth Res* **96**:37–50.
doi:10.1007/s11120-007-9281-y

Bottier C, Géan J, Artzner F, Desbat B, Pézolet M, Renault A, Marion D, Vié V. 2007. Galactosyl headgroup interactions control the molecular packing of wheat lipids in Langmuir films and in hydrated liquid-crystalline mesophases. *Biochim Biophys Acta* **1768**:1526–1540.
doi:10.1016/j.bbamem.2007.02.021

Bräutigam A, Weber APM. 2009. Proteomic analysis of the proplastid envelope membrane provides novel insights into small molecule and protein transport across proplastid membranes. *Mol Plant* **2**:1247–1261.
doi:10.1093/mp/ssp070

Caffarri S, Tibiletti T, Jennings R, Santabarbara S. 2014. A Comparison Between Plant Photosystem I and Photosystem II Architecture and Functioning. *Curr Protein Pept Sci* **15**:296–331.
doi:10.2174/1389203715666140327102218

Daum B, Kühlbrandt W. 2011. Electron tomography of plant thylakoid membranes. *J Exp Bot* **62**:2393–2402.
doi:10.1093/jxb/err034

Daum B, Nicastro D, Mcintosh JR, Ku W. 2010. Arrangement of Photosystem II and ATP Synthase in Chloroplast Membranes of Spinach and Pea 1299–1312 .

doi:10.1105/tpc.109.071431

Deerinck TJ, Bushong EA, Thor A, Ellisman MH. 2010. NCMIR methods for 3D EM : a new protocol for preparation of biological specimens for serial block face scanning electron microscopy 6–8.

Demarsy E, Lakshmanan AM, Kessler F. 2014. Border control: selectivity of chloroplast protein import and regulation at the TOC-complex. *Front Plant Sci* **5**:483. doi:10.3389/fpls.2014.00483

Demé B, Cataye C, Block M a, Maréchal E, Jouhet J. 2014. Contribution of galactoglycerolipids to the 3-dimensional architecture of thylakoids. *FASEB J* **28**:3373–83. doi:10.1096/fj.13-247395

Dubreuil C, Jin X, Barajas-lópez JDD, Hewitt TC, Tanz SK, Dobrenel T, Schröder WP, Hanson J, Pesquet E, Grönlund A. 2018. Establishment of Photosynthesis through Chloroplast Development Is Controlled by Two Distinct Regulatory Phases 1 **176**:1199–1214.
doi:10.1104/pp.17.00435

Engel BD, Schaffer M, Cuellar LK, Villa E, Plitzko JM, Baumeister W. 2015. Native architecture of the chlamydomonas chloroplast revealed by in situ cryo-electron tomography. *Elife* **2015**:1–29.
doi:10.7554/eLife.04889

Ferro M, Salvi D, Brugière S, Miras S, Kowalski S, Louwagie M, Garin J, Joyard J, Rolland N. 2003. Proteomics of the chloroplast envelope membranes from Arabidopsis thaliana. *Mol Cell Proteomics* **2**:325–345.
doi:10.1074/mcp.M300030-MCP200

Flori S, Jouneau P-H, Bailleul B, Gallet B, Estrozi LF, Moriscot C, Bastien O, Eicke S, Schober A, Bártulos CR, Maréchal E, Kroth PG, Petroutsos D, Zeeman S, Breyton C, Schoehn G, Falconet D, Finazzi G. 2017. Plastid thylakoid architecture optimizes photosynthesis in diatoms. *Nat Commun* **8**:15885.
doi:10.1038/ncomms15885

Fox J, Weisberg S. 2018. Visualizing fit and lack of fit in complex regression models with predictor effect plots and partial residuals, Journal of Statistical Software. doi:10.18637/jss.v087.i09

Grossmann J, Roschitzki B, Panse C, Fortes C, Barkow-Oesterreicher S, Rutishauser D, Schlapbach R. 2010. Implementation and evaluation of relative and absolute

quantification in shotgun proteomics with label-free methods. *J Proteomics* **73**:1740–1746.
doi:10.1016/j.jprot.2010.05.011

Hashimoto M, Endo T, Peltier G, Tasaka M, Shikanai T. 2003. A nucleus-encoded factor, CRR2, is essential for the expression of chloroplast ndhB in Arabidopsis. *Plant J* **36**:541–549.
doi:10.1046/j.1365-313X.2003.01900.x

Hooper CM, Castleden IR, Tanz SK, Aryamanesh N, Millar AH. 2017. SUBA4: The interactive data analysis centre for Arabidopsis subcellular protein locations. *Nucleic Acids Res* **45**:D1064–D1074.
doi:10.1093/nar/gkw1041

Jouhet J, Maréchal E, Baldan B, Bligny R, Joyard J, Block MA. 2004. Phosphate deprivation induces transfer of DGDG galactolipid from chloroplast to mitochondria. *J Cell Biol* **167**:863–874.
doi:10.1083/jcb.200407022

Jouhet J, Marechal E, Block MA. 2007. Glycerolipid transfer for the building of membranes in plant cells. *Prog Lipid Res* **46**:37–55.
doi:10.1016/j.plipres.2006.06.002

Kato Y, Sakamoto W. 2018. FtsH protease in the thylakoid membrane: Physiological functions and the regulation of protease activity. *Front Plant Sci* **9**:1–8. doi:10.3389/fpls.2018.00855

Kessler F, Schnell DJ. 2006. The function and diversity of plastid protein import pathways: A multilane GTPase highway into plastids. *Traffic* **7**:248–257.
doi:10.1111/j.1600-0854.2005.00382.x

Kimura M, Manabe K, Abe T, Yoshida S, Matsui M, Yamamoto YY. 2003. Analysis of Hydrogen Peroxide–independent Expression of the High-light–inducible ELIP2 Gene with the Aid of the ELIP2 Promoter–Luciferase Fusion¶. *Photochem Photobiol* **77**:668–674.
doi:10.1562/0031-8655(2003)0770668AOHPEO2.0.CO2

Kirchhoff H, Hall C, Wood M, Herbstová M, Tsabari O, Nevo R, Charuvi D, Eyal S, Ziv R. 2011. Dynamic control of protein diffusion within the granal thylakoid lumen **108**:20248–20253. doi:10.1073/pnas.1104141109

Kleffmann T, von Zychlinski A, Russenberger D, Hirsch-Hoffmann M, Gehrig P,

Gruissem W, Baginsky S. 2007. Proteome Dynamics during Plastid Differentiation in Rice. *Plant Physiol* **143**:912 LP – 923. doi:10.1104/pp.106.090738

Kobayashi K. 2016. Role of membrane glycerolipids in photosynthesis, thylakoid biogenesis and chloroplast development. *J Plant Res* **129**:565–580. doi:10.1007/s10265-016-0827-y

Koochak H, Puthiyaveetil S, Mullendore DL, Li M, Kirchhoff H. 2019. The structural and functional domains of plant thylakoid membranes. *Plant J* **97**:412–429. doi:10.1111/tpj.14127

Kowalewska ŁM, Mazur R, Suski S, Garstka M, Mostowska A. 2016. Three-dimensional visualization of the internal plastid membrane network during runner bean chloroplast biogenesis. Dynamic model of the tubular-lamellar transformation. *Plant Cell* **28**:875–891. doi:10.1105/tpc.15.01053

Kubis S, Baldwin A, Patel R, Razzaq A, Dupree P, Lilley K, Kurth J, Leister D, Jarvis P. 2003. The Arabidopsis ppi1 mutant is specifically defective in the expression, chloroplast import, and accumulation of photosynthetic proteins. *Plant Cell* **15**:1859–1871. doi:10.1105/tpc.012955

Kurisu G, Zhang H, Smith JL, Cramer WA. 2003. Structure of the Cytochrome b 6 f Complex of Oxygenic Photosynthesis : Tuning the Cavity **302**:1009–1015. doi:10.1126/science.1090165

Liang Z, Zhu N, Mai KK, Liu Z, Tzeng D, Osteryoung KW. 2018. Thylakoid-Bound Polysomes and a Dynamin-Related Protein , FZL , Mediate Critical Stages of the Linear Chloroplast Biogenesis Program in Greening Arabidopsis Cotyledons **30**:1476–1495. doi:10.1105/tpc.17.00972

Marechal E, Block MA, Dome A, Douce R, Joyard J. 1997. Lipid synthesis and metabolism in the plastid envelope **100**:65–77. doi:10.1111/j.1399-3054.1997.tb03455.x

Martinis J, Kessler F, Glauser G. 2011. A novel method for prenylquinone profiling in plant tissues by ultra-high pressure liquid chromatography-mass spectrometry. *Plant Methods* **7**:1–23. doi:10.1186/1746-4811-7-23

Mazur R, Mostowska A, Szach J, Gieczewska K, Wójtowicz J, Bednarska K, Garstka

M, Kowalewska Ł. 2019. Galactolipid deficiency disturbs spatial arrangement of the thylakoid network in Arabidopsis thaliana plants. *J Exp Bot* **70**:4689–4703. doi:10.1093/jxb/erz219

Mi H, Muruganujan A, Huang X, Ebert D, Mills C, Guo X, Thomas PD. 2019. Protocol Update for large-scale genome and gene function analysis with the PANTHER classification system (v.14.0). *Nat Protoc* **14**:703–721. doi:10.1038/s41596-019-0128-8

Michaud M, Jouhet J. 2019. Lipid Trafficking at Membrane Contact Sites During Plant Development and Stress Response. *Front Plant Sci* **10**:1–10 . doi:10.3389/fpls.2019.00002

Ohlrogge J, Browse J. 1995. Lipid biosynthesis. *Plant Cell* **7**:957–970. doi:10.1105/tpc.7.7.957

Peddie CJ, Collinson LM. 2014. Exploring the third dimension: Volume electron microscopy comes of age. *Micron* **61**:9–19. doi:10.1016/j.micron.2014.01.009

Pinali C, Kitmitto A. 2014. Serial block face scanning electron microscopy for the study of cardiac muscle ultrastructure at nanoscale resolutions. *Curr Ther Res - Clin Exp* **76**:1–11. doi:10.1016/j.yjmcc.2014.08.010

Pinheiro J, Bates M. 2000. Pinheiro - Mixed Effects Models in S & S PLUS. *Springer B*. doi:org/10.1007/b98882

Plöscher M, Reisinger V, Eichacker LA. 2011. Proteomic comparison of etioplast and chloroplast protein complexes. *J Proteomics* **74**:1256–1265. doi:10.1016/j.jprot.2011.03.020

Pyke KA, Leech RM. 1994. A Genetic Analysis of Chloroplast Division and Expansion in Arabidopsis thaliana. *Plant Physiol* **104**:201–207. doi:10.1104/pp.104.1.201

Reiland S, Grossmann J, Baerenfaller K, Gehrig P, Nunes-nesi A. 2011. Integrated proteome and metabolite analysis of the de-etiolation process in plastids from rice (Oryza sativa L .) **11**:1751–1763. doi:10.1002/pmic.201000703

Richardson LGL, Schnell DJ. 2019. Origins, function, and regulation of the TOC–TIC general protein import machinery of plastids. *J Exp Bot* **71**:1226–1238.

doi:10.1093/jxb/erz517

Rudowska L, Gieczewska K, Mazur R, Garstka M, Mostowska A. 2012. Chloroplast biogenesis - correlation between structure and function. *Biochim Biophys Acta* **1817**:1380–7.
doi:10.1016/j.bbabio.2012.03.013

Runge S, Sperling U, Frick G, Apel K, Armstrong GA. 1996. Distinct roles for light-dependent NADPH:protochlorophyllide oxidoreductases (POR) A and B during greening in higher plants. *Plant J* **9**:513–523.
doi:10.1046/j.1365-313X.1996.09040513.x

Scorrano L, De Matteis MA, Emr S, Giordano F, Hajnóczky G, Kornmann B, Lackner LL, Levine TP, Pellegrini L, Reinisch K, Rizzuto R, Simmen T, Stenmark H, Ungermann C, Schuldiner M. 2019. Coming together to define membrane contact sites. *Nat Commun* **10**:1–11.
doi:10.1038/s41467-019-09253-3

Solymosi K, Aronsson H. 2013. Plastid Development in Leaves during Growth and Senescence **36**:39–64.
doi:10.1007/978-94-007-5724-0

Solymosi K, Schoefs B. 2010. Etioplast and etio-chloroplast formation under natural conditions: The dark side of chlorophyll biosynthesis in angiosperms. *Photosynth Res* **105**:143–166.
doi:10.1007/s11120-010-9568-2

Tomizioli M, Lazar C, Brugière S, Burger T, Salvi D, Gatto L, Moyet L, Breckels LM, Hesse A-M, Lilley KS, Seigneurin-Berny D, Finazzi G, Rolland N, Ferro M 2014. Deciphering Thylakoid Sub-compartments using a Mass Spectrometry-based Approach. *Mol Cell Proteomics* **13**:2147–2167.
doi:10.1074/mcp.M114.040923

Van Bezouwen LS, Caffarri S, Kale R, Kouřil R, Thunnissen AMWH, Oostergetel GT, Boekema EJ. 2017. Subunit and chlorophyll organization of the plant photosystem II supercomplex. *Nat Plants* **3**:1–11.
doi:10.1038/nplants.2017.80

Van Wijk KJ, Kessler F. 2017. Plastoglobuli: Plastid Microcompartments with Integrated Functions in Metabolism, Plastid Developmental Transitions, and Environmental Adaptation. *Annu Rev Plant Biol* **68**:253–289.

doi:10.1146/annurev-arplant-043015-111737

Von Wettstein D, Gough S, Kannangara CG. 1995. Chlorophyll Biosynthesis. *Plant Cell* **7**:1039–1057.
doi:10.1105/tpc.7.7.1039

Wang BC, Pan YH, Meng DZ, Zhu YX. 2006. Identification and quantitative analysis of significantly accumulated proteins during the Arabidopsis seedling de-etiolation process. *J Integr Plant Biol* **48**:104–113.
doi:10.1111/j.1744-7909.2006.00215.x

Weier TE, Brown DL. 1970. Formation of the Prolamellar Body in 8-Day, Dark-Grown Seedlings. *Am J Bot* **57**:267–275.
doi:10.2307/2485302

Yoshida Y. 2018. Insights into the mechanisms of chloroplast division. *Int J Mol Sci* **19**:1–13.
doi:10.3390/ijms19030733

Acknowledgements

I would like to thank my thesis director Professor Felix Kessler to give me the opportunity to carry out my PhD thesis in his laboratory. I am very grateful for his scientific support, enthusiasm as well as for all the interesting discussions.

I would like to thank my thesis director Dr. Emilie Demarsy for following and supporting me during my PhD thesis. I am very grateful for her determination, passion and constructive criticism.

I would like to thank Professor Samuel Zeeman, Simona Eicke, Dr. Barbara Pfister and Dr. Denis Falconet for their collaboration.

Thanks to my lovely boyfriend Federico Giacomarra. He supported me in every single moment during these years of my PhD even when a quite few kilometres separated us. Thanks for his love, curiosity, positive spirit and kindness.

I would like to thank my lovely family, my parents Antonino and Maria and my brothers Giovanni and Antonino Roberto.

I would like to thank my colleague and friend Thibaut Pralon for his sincere friendship, for all funny moments and scientific discussions in the laboratory.

Thanks to Professor Samuel Zeeman and Professor Josephus Vermeer for accepting to be members of my thesis committee.

I would like to thank some colleagues and friends for all the kind moments spent together in Neuchatel; Livia Spicher, Susana Bernardo, Carla Coppola, Sonia Accossato, Angelica Candido, Paolo Longoni, Bruno Cabete, Francesco Stefanelli, Véronique Douet, Sarah Rottet, Monica Zufferey and Hamed Sattari as well as all the members of the LPV team.